UNIVERSITÄT BAYREUTH

Lehrstuhl für Anorganische Chemie I

Microporous Organically Pillared Layered Silicates (MOPS) with tunable Functionality

Dissertation

zur Erlangung des akademischen Grades

Doktor der Naturwissenschaften (Dr. rer. nat.)

an der Bayreuther Graduiertenschule für Mathematik und Naturwissenschaften (BayNAT)

vorgelegt von

Markus M. Herling

geboren in Neustadt an der Waldnaab

Bayreuth, 2014

Die vorliegende Arbeit wurde in der Zeit von Oktober 2010 bis August 2014 in Bayreuth am Lehrstuhl für Anorganische Chemie I (AC I) unter der Betreuung von Herrn Prof. Dr. Josef Breu angefertigt.

Vollständiger Abdruck der von der Bayreuther Graduiertenschule für Mathematik und Naturwissenschaften (BayNAT) der Universität Bayreuth genehmigten Dissertation zur Erlangung des akademischen Grades eines Doktors der Naturwissenschaften (Dr.rer.nat.).

Dissertation eingereicht am: 15.09.2014

Zulassung durch Leitungsgremium: 15.10.2014

Wissenschaftliches Kolloquium: 19.12.2014

Amtierender Direktor: Prof. Dr. Franz Xaver Schmid

Prüfungsausschuss:

Prof. Dr. Josef Breu (Erstgutachter)

Prof. Dr. Jürgen Senker (Zweitgutachter)

Prof. Dr. Rainer Schobert (Vorsitz)

JProf. Dr. Markus Retsch

Meiner Familie und Aniela.

Abkürzungsverzeichnis

Å	Angström
BET	Brunauer-Emmet-Teller
bpy	2,2'-Bipyridine
CEC	Cation Exchange Capacity
CF-HP	Continuous Flow Hyperpolarized
DFT	Dichtefunktionaltheorie
diamsar	3,6,10,13,16,19-Hexaazabicyclo[6.6.6]eicosane-1,8-diamine
ee	Enantiomeric excess
EXSY	Exchange Spectroscopy
HETCOR	Heteronuclear Correlation
IUPAC	International Union of Pure and Applied Chemistry
Me_2DABCO^{2+}	1,4-Dimethyl-1,4-diazabicyclo[2.2.2]octandikation
MOF	Metal Organic Framework
MOPS	Microporous Organically Pillared Layered Silicate
NMR	Nuclear Magnetic Resonance
MAS	Magic Angle Spinning
PCP	Porous Coordination Polymer
PILC	Pillared Inter-layered Clay
p.f.u.	per formula unit
PSA	Pressure Swing Adsorption
PXRD	Powder X-Ray Diffraction
REM	Rasterelektronenmikroskop
sep	Sepulchrate (1,3,6,8,10,13,16,19-octaazabicyclo [6.6.6] eicosane)
TMA	Tetramethylammonium

TEA	Tetraethylammonium
VK	Variationskoeffizient
XRD	X-Ray Diffraction

Inhaltsverzeichnis

1. Summary - Zusammenfassung

The aim of this thesis was the synthesis of microporous hybrid materials through pillaring of charge homogeneous, synthetic layered silicates, yielding microprous organically pillared layered silicates (MOPS). On the one hand it was focused on the fine tuning of the pore width of these materials by adjusting the charge density of the silicate host post synthesis and on the other hand on the functionalization of the pore space. This modularity of the pillaring approach offers a unique chance to extend the field of functional microporous materials by a new class of tailorable MOPS.

The term “Pillared Interlayered Clays” (PILCs) unfortunately has been used in the literature for both truly pillared, microporous materials but also for simply intercalated compounds with no proof of interlayer porosity presented. Moreover, by far the largest group of PILCs was obtained by “intercalation” of iso- and heteropolycations like Keggin ions followed by calcinations. The very few papers that have characterized such materials by means of high resolution electron microscopy, however, suggest that indeed the polycations did not enter the interlayer space but rather these materials represent heterocoagulates. The porosity of these materials thus does not originate from the interlayer space but represents purly interparticle porosity generated by the microstructure of coagulated spherical cationic and platy anionic colloids.

In an attempt to clarify the concept of pillaring, a review was written that critically analyzes the usage of the term and its definition given by the IUPAC in 1999 whereat the focus was strictly put on real intercalation compounds. Commencing with the pioneering work by Barrer *et al.* papers reporting pillaring of natural and synthetic clays with organic cations or metal-organic cations were critically reviewed in the light of recent results with far better characterized MOPS obtained from charge homogenous synthetic layered silicates by Breu *et al.*.

To prove the possibility of reducing the layer charge post synthesis, a low charged K-hectorite was synthesized and ion exchanged with Mg^{2+}. The so called Hofman-Klemen-effect was used by subsequent heat treatments at 250 °C to gradually reduce the layer charge. Mg^{2+} is migrating into the octahedral sheet replacing octahedrally coordinated Li^{+} and thus reducing the charge density of the silicate host. These materials were then pillared with Me_2DABCO^{2+} and $Rh(bpy)^{3+}$ to yield microporous hybrid materials with a narrow pore size distribution. Ar-physisorption measurements showed on the one hand an increase in the pore width and on the

other hand a significantly increased pore volume. These results layed the basis for further research allowing for adjusting the pore width in a gradual manner.

In close cooperation with the group of Prof. J. Senker, the pore space of three different charged hectorites pillared with Me_2DABCO^{2+} was studied in more detail by multicore solid state NMR spectroscopy in combination with high resolution ^{129}Xe NMR MAS spectroscopy. Temperature dependent 1D and 2D wide line ^{129}Xe NMR together with Xe- and Ar-physisorption measurements were used to obtain structural information of the pillar inside the interlayer space. The pillar molecule was homogeneously distributed inside the interlayer, which was confirmed by ^{1}H, ^{13}C, ^{19}F and ^{29}Si MAS NMR measurements. With charge reduction an increase of the pore width as well as an increase in the pore volume could be confirmed. By applying the Demarquay-Fraissard-model to the chemical shift of the ^{129}Xe peak, a pore width between 5.9-6.6 Å similar to the DFT calculated pore widths of the Ar-physisorption isotherms were calculated. These results are showing the applicability of the ^{129}Xe-NMR spectroscopy to calculate the pore width and thus characterizing these kinds of materials.

Hectorites with four different charge densities (0.49, 0.44, 0.39, 0.36 p.f.u.) were pillared with enantiopure (+)-$Co(sep)^{3+}$ (sep = $C_{12}H_{30}N_8$ = 1,3,6,8,10,13,16,19-octaazabicyclo[6.6.6]-eicosane) and (-)-$Co(sep)^{3+}$ cations to synthesize new microprous hybrid materials (UBT-1 to UBT-8) with pore widths of 5-7 Å. These materials were tested as potentially stereo- and size selective adsorbents with (±)-But-3-yn-2-ol and 2-Methyl-but-3-yn-2-ol as adsorbates. Depending on the pore width, which can be gradually adjusted by choosing the right layer charge, stereo- and sizeselectivity was observed for the first time for the new class of MOPS. The best values for the enantiomeric excess (ee) were obtained with the smallest pore size (8.24 ± 0.48 % for (-)-$Co(sep)^{3+}$ and 7.45 ± 0.45 % for (+)-$Co(sep)^{3+}$, respectively). Even a slight increase of the pore width resulted in a dramatic decrease of the ee, because the intimate contact with the chiral pillar molecules needed to preferentially adsorb one enantiomer is lost. A similar trend for the separation efficiency for size selectivity as well as for stereo discrimination is observed, resulting in a decrease of resolution by increasing the pore width. By applying this material as a stationary phase in chromatography beds with higher effective plate numbers a complete chiral resolution should be achievable.

In Metal Organic Frameworks (MOFs) a selective “gate opening”-effect depending on the adsorbate is well known. In MOPS with pillars of ellipsoidal geometries a similar phenomenon was expected. By using a ellipsoidally shaped Me_2DABCO^{2+} molecule as pillar

of a synthetic layered silicate (UBT-9) a two dimensional microporous network with narrow pore size distribution (4-6 Å) is generated. The pillar molecule of UBT-9 arranges itself in a regular manner which was confirmed by the occurrence of *10*-band indicative for a hexagonal superstructure reflex. And indeed, as expected, an expansion of the interlayer height upon CO adsorption was observed after reaching a certain threshold pressure. This change resulted in a shift of the *00l*-series and an increase of the basal spacing of 0.6 Å monitored by *in-situ* powder X-ray diffraction measurements. This so called "gate opening" was selective for CO and could not be observed for N_2, which renders this material in general suitable as adsorbent in CO/N_2 separations utilizing pressure swing adsorption.

Das Ziel der vorliegenden Arbeit war es, mikroporöse Hybridmaterialien durch Pillaring ladungshomogener, synthetischer Schichtsilicate herzustellen. Dabei wurde zum einen besonderes Augenmerk auf die Anpassung der Porenweite durch gezielte post-synthetische Ladungsreduktion des Schichtsilikats gelegt und zum anderen auf die Einstellung der chemischen Natur des Porenraums durch die Funktionalitäten des verwendeten Pillarmoleküls. Durch dieses hoch modulare Pillaring-Konzept erweitern diese neuen, individuell anpassbaren Hybridmaterialien, sogenannte „Microporous Organically Pillared Layered Silicates“ (MOPS), die Klasse der mikroporösen Materialien.

Die Bezeichnung „Pillared Interlayered Clays (PILCs)“ wird in der Literatur leider nicht nur für tatsächlich gepillarte, mikroporöse Materialien verwendet, sondern zum Teil auch für normale Einlagerungsverbindungen ohne jeden Nachweis einer Mikroposität. Die weitaus größte Gruppe von PILCs wurde aber durch die „Interkalation“ von Iso- und Heteropolykationen, z.B. Kegginionen, mit anschließender Calcinierung hergestellt. Die wenigen Arbeiten in denen solche Materialien mit moderner hochauflösender Elektronen-mikroskopie charakterisiert wurden legen aber nahe, dass tatsächlich gar keine Interkalation der Polykationen stattgefunden hat, sondern dass die Materialien vielmehr Heterokoagulate darstellen. Die Porosität ist auf das Gefüge aus sphärischen kationischen und plättchenförmigen anionischen Kolloiden zurückzuführen, welche eine reine interpartikuläre Porosität darstellt und keine aus dem Zwischenschichtraum stammende intrapartikuläre Porosität.

Um zur Klärung dieser Begrifflichkeiten beizutragen, wurde in einem Übersichtsartikel die Verwendung und die Definition des Begriffs „PILC“ der IUPAC kritisch beleuchtet, wobei nur auf tatsächliche Interkalationsverbindungen fokussiert wurde. Ausgehend von den ersten Pionierarbeiten von Barrer *et al.* wurden Arbeiten in denen natürliche und synthetische Schichtsilikate mit Organokationen bzw. kationischen Komplexverbindungen gepillart wurden vor dem Hintergrund neuerer Erkenntnisse kritisch beleuchtet. Diese wurden durch die Verwendung von wesentlich besser charakterisierbaren, auf ladungshomogenen synthetischen Schichtsilikaten von Breu *et al.* basierenden, MOPS gewonnen.

Um die Anpassung der Schichtladung post-synthetisch zu untersuchen, wurde ein K-Hectorit ($K_{0.48(2)}[Mg_{2.54(8)}Li_{0.43}]Si_4O_{10}F_2$) mit einer Schichtladung von 0.48 p.f.u. synthetisiert. Das Zwischenschichtkation wurde durch Mg^{2+}-Ionen ersetzt und anschließend post-synthetisch unter bei 250 °C graduell ladungsreduziert. Diesem Ladungsreduktionsprozess liegt der Hofmann-Klemen Effekt zu Grunde. Dabei migrieren die in der Zwischenschicht lokalisierten Mg^{2+}-Ionen durch die hexagonalen Kavitäten der Tetraederschicht in die Oktaederschicht und

ersetzen dabei das niedervalente Li^+-Ionen, welches wiederrum in die Zwischenschicht freigesetzt wird. Sowohl das Ausgangsmaterial mit einer Schichtladung von 0.48 p.f.u. als auch eine Ladungsreduktionsstufe mit einer Schichtladung von 0.39 p.f.u. wurden mit Me_2DABCO^{2+} und $Rh(bpy)_3^{3+}$ gepillart. Argon-Physisorptionsmessungen zeigten sowohl eine Steigerung des Porenvolumens als auch eine Erhöhung des Porendurchmessers. Diese Ergebnisse legten den Grundstein für weitere Untersuchungen bezüglich der individuellen Einstellung der Porenweite.

Der Porenraum dreier, mit Me_2DABCO^{2+} gepillarter, synthetischer K-Hectorite unterschiedlicher Ladungsdichte (0.48, 0.44 und 0.39 p.f.u.) wurde in Kooperation mit der Arbeitsgruppe von Prof. J. Senker NMR-spektroskopisch mit Multikern Festkörper NMR Spektroskopie in Kombination mit hochauflösender ^{129}Xe MAS NMR Spektroskopie untersucht. Weitere temperaturabhängige ein- und zweidimensionale „*wide-line*“ ^{129}Xe NMR Untersuchungen zusammen mit Argon- und Xenon-Physisorptionsmessungen wurden durchgeführt. Eine homogene Verteilung des Me_2DABCO^{2+}-Moleküls in der Zwischenschicht wurde durch ein- und zweidimensionale ^1H, ^{13}C, ^{19}F und ^{29}Si MAS Messungen festgestellt. Es konnte sowohl die Erhöhung des Porendurchmessers als auch des Porenvolumens bestätigt werden. Dabei konnte unter Anwendung des Demarquay-Fraissard-Modells die Verschiebung des ^{129}Xe-Signals unterschiedlicher Poren mit Porendurchmessern zwischen 5.9 und 6.6 Å zugeordnet werden. Diese Porenweiten decken sich mit den aus Physisorptionsmessung ermittelten Porenweiten (4-7 Å). Auch Xenon-Adsorptionsenthalpien, die sowohl durch Xenon-Physisorptionsmessungen als auch durch Anpassung der chemischen Verschiebung des ^{129}Xe-Kerns aus CF-HP ^{129}Xe-Messungen berechnet wurden, stimmten sehr gut überein. Somit kann diese alternative Methode der Porenbestimmung für die genauere Charakterisierung des Porenraums neben der klassischen Physisorptionsmessung herangezogen werden.

Um die Anwendbarkeit von MOPS als gestalt- und stereoselektive Adsorbentien zu untersuchen, wurde ein synthetischer Na-Hectorit ($Na_{0.57(3)}[Mg_{2.59(5)}Li_{0.17(3)}]Si_4O_{10}F_2$) graduell ladungsreduziert und Materialien verschiedener Schichtladung generiert. Anschließend wurden diese mit enantiomerenreinem (+)-$Co(sep)^{3+}$ und (-)-$Co(sep)^{3+}$ gepillart und chirale MOPS (UBT-1 bis UBT-8) mit einer engen Porenweitenverteilung (5-7 Å) erhalten. Anschließend wurden diese Materialien als Adsorbentien für (±)-But-3-yn-2-ol und 2-Methyl-but-3-yn-2-ol getestet. Abhängig von der Porenweite und des verwendeten Pillarmoleküls konnte zum ersten Mal für MOPS eine stereoselektive Adsorption beobachtet werden. Dabei

adsorbierte (-)-$Co(sep)^{3+}$ bevorzugt das *(S)*-Enantiomer mit einem Enantiomerenüberschuss von 8.24 ± 0.48 % und (+)-$Co(sep)^{3+}$ mit einem Enantiomerenüberschuss von 7.45 ± 0.45 % bevorzugt das *(R)*-Enantiomer. Eine Erhöhung des Porendurchmessers resultierte in einem drastischen Abfall der Stereodiskriminierung, da die Adsorbat-Adsorbent-Wechselwirkung nicht mehr ausreichten um eine chirale Induktion hervorzurufen. Verwendet man beide Moleküle in einer äquimolaren Mischung, konnte eine Größenselektivität beobachtet werden, wobei (±)-But-3-yn-2-ol bevorzugt adsorbiert wird. Auch hier konnte ein Abfall der Trennleistung mit steigender Porenweite beobachtet werden. Somit wurde sowohl die Modularität dieser Materialien als auch dessen Trennleistung in Abhängigkeit von der Porengröße bestätigt und eine mögliche Anwendung als größen- und stereo-selektive Adsorbentien aufgezeigt.

Der Effekt des „*gate opening*“ in Abhängigkeit vom Adsorbat ist bei Metal Organic Frameworks (MOFs) bereits bekannt und sollte prinzipiell für MOPS mit Pillarmolekülen bestimmter Geometrie auch beobachtet werden können. Der bereits vorher verwendete Hectorit mit einer Schichtladung von 0.47 p.f.u. wurde mit einem ellipsoiden Me_2DABCO^{2+} Molekül gepillart. In diesem mikroporösen Hybridmaterial (UBT-9) mit einem zwei-dimensionalen Porennetzwerk und einer Porenweite von 4-6 Å, ordnen sich die Pillar-moleküle in einer hexagonalen Überstruktur an. Dies wurde durch das Auftreten einer *10*-Bande im Pulverdiffraktogramm bestätigt. Durch die Geometrie des Pillarmoleküls konnte bei der Adsorption von CO nach dem Erreichen einer Druckschwelle eine Expansion des Zwischenschichtraumes beobachtet werden. Dabei verschiebt sich die *00l*-Serie unter Erhöhung des Basalabstandes um 0.6 Å. Dieser Effekt ist selektiv für CO und konnte im Falle einer N_2-Adsorption nicht beobachtet werden. Ein mögliches Anwendungsfeld dieses Materials ist die CO/N_2-Trennung unter Verwendung der sogenannten „*pressure swing adsorption*“ (PSA).

2. Einleitung

2.1 Etablierte mikroporöse Materialien

Mikroporöse Materialien haben aufgrund ihrer vielseitigen Anwendungen seit jeher das Interesse von Materialwissenschaftlern geweckt. Als erste Klasse kristalliner, mikroporöser Oxide wurden Zeolithe und Aluminophosphate als Katalysatoren für Cracking und der Synthese von Rohchemikalien verwendet.[1-7] Diese eignen sich aufgrund ihrer einheitlichen Porengröße, hoher (Reaktions-)Oberfläche, hoher Stabilität sowohl gegenüber Temperatur und Hydrolyse als auch niedrigem pH-Wert sehr gut für Hochtemperaturanwendungen. Darüber hinaus besitzen Zeolithe (Abb. 1A) eine hohe Wirt-Gast-Wechselwirkung, die sich sowohl in einer Größen- als auch Gestaltselektivität niederschlägt, wodurch sie bevorzugt als Adsorbent, selektiver Katalysator oder in der Separation verwendet werden.[8] Durch die Wahl geeigneter Template konnte eine Vielzahl verschiedener Käfig- und Gerüststrukturen synthetisiert werden, deren Synthesebedingungen und Zusammensetzungen je nach Anwendungsfeld angepasst werden können.[9-13]

Die Klasse der metallorganischen Gerüstverbindungen (*Metal Organic Frameworks* (MOFs) oder *Porous Coordination Polymers* (PCP)) als neue Klasse poröser Hybridmaterialien hat sich seit den 1990er Jahren entwickelt.[14] Diese Gerüststrukturen werden durch anorganische Knotenpunkte („*nodes*“) und organische Linker („*linkers*“) aufgebaut (Abb. 1B), dessen Modularität während der Synthese den Weg zur Herstellung einer großen Anzahl verschiedener Poren- und Netzwerktopologien ebnete. Darüber hinaus können durch die Wahl von geeigneten *linker-node*-Paaren zum einen die Gestalt und Größe der Poren und zum anderen verschiedene chemische Funktionalitäten eingestellt werden.[15]

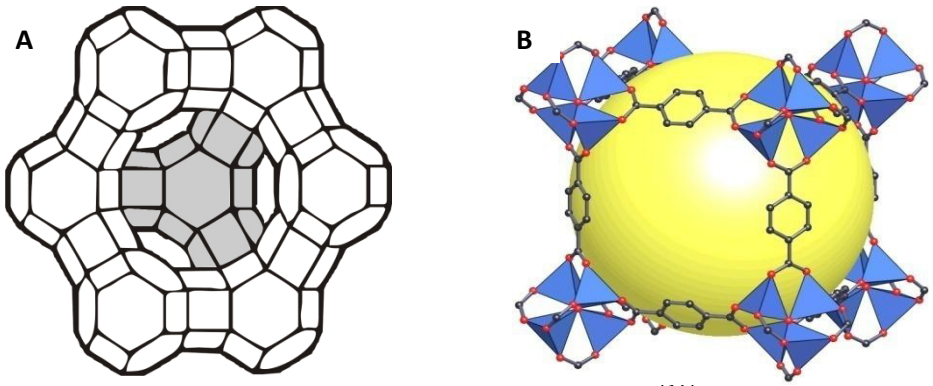

Abb. 1: A) Struktur eines Zeolith Y; B) Struktur eines MOFs.[16]

MOFs sind zwar in Bezug auf thermische und chemische Stabilität den Zeolithen unterlegen, jedoch verlagerte sich in den letzten Jahren der Forschungs- und Anwendungsfokus auf Anwendungen bei niedriger Temperatur ≤ 200 °C. Beispiele hierfür sind die Anwendungen sowohl in der Gasaufreinigung und –trennung als auch in der enantioselektiven Katalyse und Stereodiskrimination.[17-20] Die Klasse der PCP's wurde von Kitagawa 1998 in drei Generationen mit unterschiedlichen Merkmalen unterteilt.[21] Die erste Generation besitzt keine permanente Mikroporosität, da deren Netzwerkstruktur nach Entfernung der Solvensmoleküle kollabiert. Die zweite Generation kann als den Zeolithen am nächsten angesehen werden, wobei hier nach der Entfernung des adsorbierten Lösungsmittels ein stabiles Porensystem generiert wird. Die dritte Generation besitzt eine flexible Netzwerkstruktur, wodurch ein reversibles und dynamisches Adsorptionsverhalten des porösen Netzwerkes festgestellt wurde. Darüber hinaus zeigt dieses System das Phänomen der Atmung („*breathing effect*“) und des „*gate opening*“-Effekts, welches in den letzten Jahren sehr intensiv untersucht wurde.[22] „*Gate Opening*“ beschreibt den Vorgang, bei dem sich ab einem gewissen Druck die Orientierung des Linkers in der MOF-Struktur so ändert, dass eine Zugänglichkeit der Gasmoleküle für eine Adsorption innerhalb der Porenstruktur ermöglicht wird.

Neben der beiden etablierten Klassen mikroporöser Materialien, der Zeolithe und MOFs, wurden seit 1950 schichtartige Strukturen, vor allem 2:1-Schichtsilikate durch das Einbringen molekularer Abstandshalter, sowohl organisch, metallorganisch als auch rein anorganisch (PILCs), in die Zwischenschicht („*Pillaring*“), als alternative, unabhängige Route zu mikroporösen Materialien untersucht.[23-33]

2.2 Synthese der Microporous Organically Pillared Layered Silicates (MOPS)

2.2.1 Aufbau eines Schichtsilikats

Als anorganische Gerüststruktur werden in dieser Arbeit für die Herstellung von mikroporösen, organisch gepillarten Hybridmaterialien ladungshomogene, synthetische Schichtsilikate verwendet. Diese sind durch die Arbeiten von Breu *et al.* nun in größerem Maßstab verfügbar.[34-37]

Die Struktur der Schichtsilikate (Abb. 2) lässt sich im Wesentlichen durch miteinander eckenverknüpfte Polyeder der Tetraederschichten (T) und kantenverknüpften Polyedern der Oktaederschichten (O) beschreiben.[38]

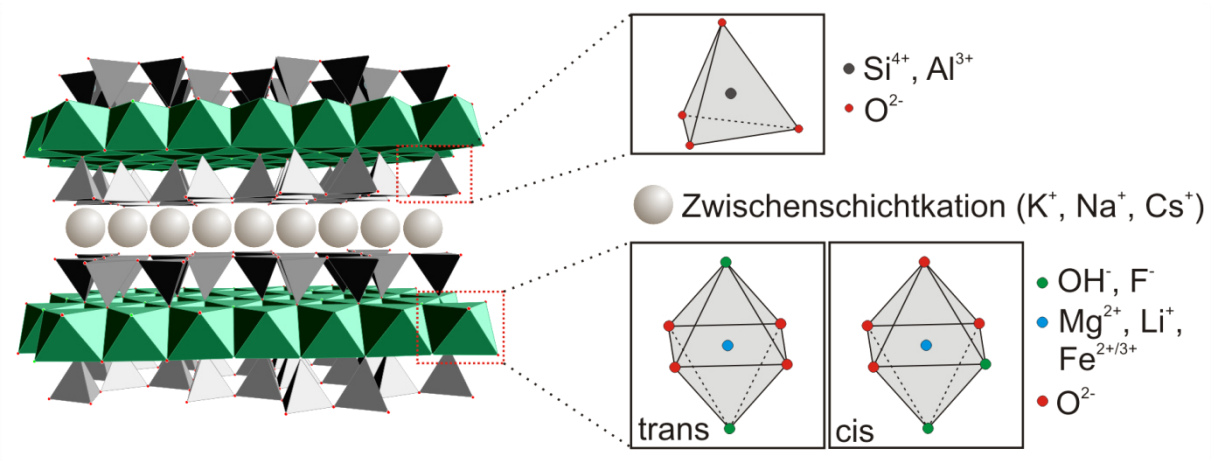

Abb. 2: Aufbau eines 2:1 Schichtsilikats.[23]

Im Fall der 1:1 Schichtsilikate besteht die Struktur aus einer Tetraeder- und einer Oktaederschicht, wohingegen die Oktaederschicht der 2:1 Schichtsilikate von zwei Tetraederschichten umgeben ist. (Abb. 2).[39] Die Tetraederschicht besteht aus SiO_4^{4-}-Tetraedern, welche durch drei basale Sauerstoffe innerhalb einer Ebene miteinander verknüpft sind. Dabei wird ein Netzwerk aus Sechsringen (Kavitäten) gebildet, welches auch als Kagomé-Netz bekannt ist (Abb. 3)

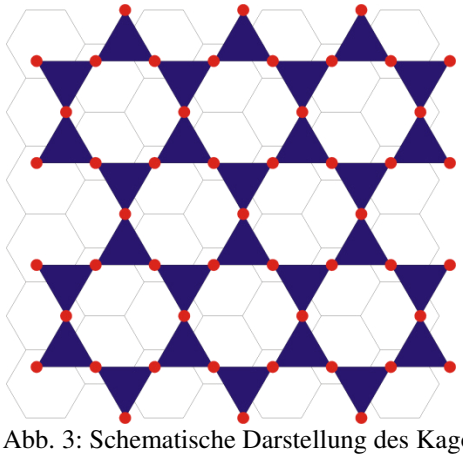

Abb. 3: Schematische Darstellung des Kagomé-Netzes

Der apikale Sauerstoff bildet die Verbindung zwischen Tetraeder und Oktaederschicht. Diese Schicht besteht aus verschiedenwertigen Kationen (z.B. Mg^{2+}, Li^{+}, $Fe^{2+/3+}$, Co^{2+}), die oktaedrisch von den apikalen Sauerstoffatomen der Tetraederschicht und zusätzlichen OH^{-}. O^{2-} oder F^{-} koordiniert sind. In einem dioktaedrischen Schichtsilikat sind 2/3 der Oktaederlücken besetzt, wobei eine volle Besetzung ein trioktaedrisches Schichtsilikat bezeichnet. Eine isomorphe Substitution der Oktaeder- oder Tetraederschichtkationen mit niedriger geladenen Kationen resultiert in einer negativen Gesamtladung der Schicht, die durch nicht hydratisierte oder hydratisierte Kationen (z.B. Cs^{+}, K^{+}, Na^{+}) in der Zwischenschicht kompensiert wird.[38] Schichtsilikate mit hoher Schichtladung weisen in der Regel keine intrakristalline Reaktivität auf, wodurch weder eine Zugänglichkeit der Zwischenschicht für einen Kationenaustausch noch ein Quellungsverhalten beobachtet werden können.[40;41] Im Hinblick auf die Synthese mikroporöser Hybridmaterialien spielt die intrakristalline Reaktivität eine sehr wichtige Rolle, weswegen für Kationenaustauschreaktionen hauptsächlich Schichtsilikate niedriger Schichtladung (≤ 0.5 p.f.u.) verwendet werden.

2.2.2. Definition Pillaring

„*Pillaring*“ beschreibt gemäß des 1999 veröffentlichten Berichts der IUPAC den Prozess, bei dem eine schichtartige Verbindung unter Erhalt der Schichtstruktur in ein thermisch stabiles mikro- oder mesoporöses Material überführt wird („a process by which a layered compound is transformed in a thermally stable micro- and/or mesoporous material with retention of the layer structure.“).[42] Dabei hat das gepillarte Material folgende Eigenschaften:

a) Expandierte Zwischenschichten, die nach Entfernung des Lösungsmittels nicht kollabieren
b) Die minimale Änderung des Basalabstandes ist größer als der Durchmesser eines Stickstoffmoleküls, welches normalerweise zur Oberflächen- und Porenvolumenbestimmung verwendet wird
c) Das Pillaring Agens ist in der Zwischenschicht und hat die Abmessungen eines Moleküls (molecular dimensions)
d) Der Zwischenschichtraum ist porös und zugänglich für Moleküle, die größer sind als Stickstoff; dabei gibt es weder eine Einschränkung in der Größe der Poren noch in dem Mechanismus der Interkalation und dem verwendeten Interkalationsagens.

Bedauerlicherweise setzte der Bericht weder eine regelmäßige Schichtabfolge noch eine eindimensionale Kristallinität (Translationssymmetrie) voraus, sondern nur das Vorhandensein

einer Interferenz, die im weitesten Sinne als Schichtabstand interpretiert werden kann. Diese Ungenauigkeiten in der Definition lassen einen sehr weiten Interpretations- und Spekulationsspielraum der resultierenden Diffraktogramme von „gepillarten“ Verbindungen zu.

Die Bezeichnung „Pillared Interlayered Clays (PILCs)“ wird in der Literatur in der Folge leider nicht nur für tatsächlich gepillarte, mikroporöse Materialien verwendet. Zum Teil werden auch normale Einlagerungsverbindungen ohne jeden Nachweis einer Mikroposität so bezeichnet. Die weitaus größte Gruppe von PILCs wurde aber durch die „Interkalation“ von Iso- und Heteropolykationen, z.B. Kegginionen, mit anschließender Calcinierung hergestellt. Die wenigen Arbeiten in denen solche Materialien mit modernen hochauflösender Eleketronenmikroskopie charakterisiert wurden legen aber nahe, dass tatsächlich gar keine Interkalation der Polykationen stattgefunden hat, sondern dass die Materialien vielmehr Heterokoagulate darstellen, deren Porosität auf das Gefüge aus sphärischen kationischen und plättchenförmigen anionischen Kolloiden zurückzuführen ist, also reine Interpartikelporosität darstellt und nicht in einem mikroporösen Zwischenschichtraum beruht.

Die in dieser Arbeit gepillarten Hybridmaterialien basieren auf dem Pillaring synthetischer Schichtsilikate mit organischen oder metallorganischen Abstandshaltern und weisen eine integrale Serie der *00l*–Reflexe mit erhöhtem Basalabstand, eine Zugänglichkeit des Zwischenschichtraums für Adsorbate und zugleich eine thermische Stabilität auf. Um diese Materialien auch begrifflich klar von den heterocoagulierten PILCs abzusetzen, wurde der Begriff MOPS eingeführt. Die Klasse der MOPS kann eindeutig als gepillarte Hybdridmaterialien gemäß der IUPAC-Definition bezeichnet werden, deren Porosität alleinig im Zwischenschichtraum lokalisiert ist.

2.3 Abhängigkeit der Porengröße eines MOPS

Beim Pillaring eines ladungshomogenen 2:1 Schichtsilikats, wird durch einen Kationenaustausch das Zwischenschichtkation (z. B. Mg^{2+}, K+ oder Na^{+}) durch den molekularen Abstandshalter (Pillar) ersetzt und somit eine permanente Mikroporosität generiert. Die Mikroporosität besteht nach dem Bericht der IUPAC aus Poren mit Durchmessern ≤ 2 nm.[43] Bei den neuen mikroporösen, organisch gepillarten Schichtsilikaten kann die Mikroporosität höchst modular eingestellt werden.

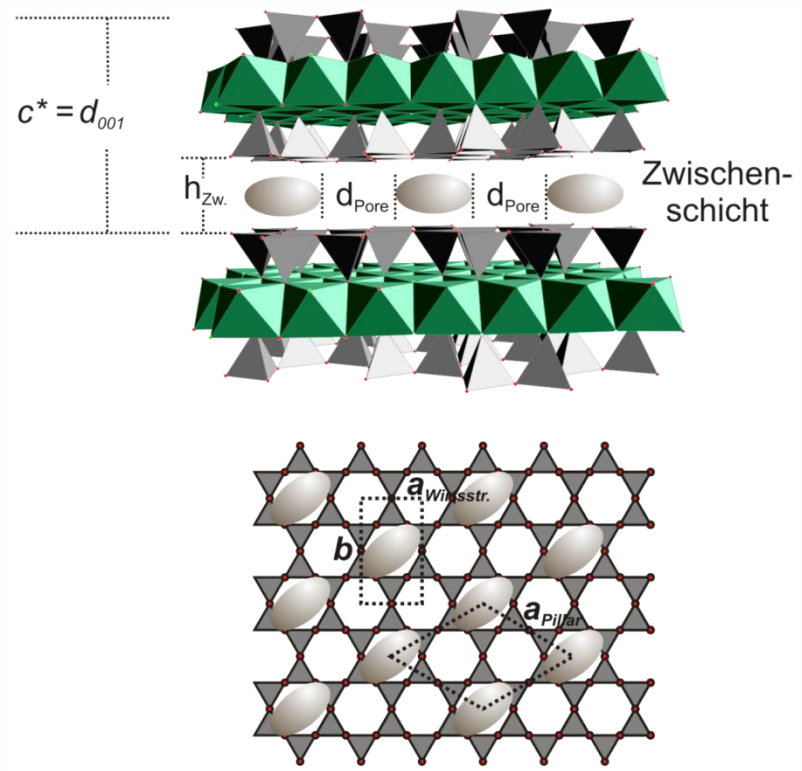

Abb. 4: Schematische Darstellung der Abhängigkeit des Porendurchmessers und der Pillarordnung im Zwischenschichtraum (Seitenansicht und Draufsicht).[23]

Die zylindrischen oder schlitzartigen Poren werden zum einen durch den Abstand der Pillar d_{pore} und zum anderen durch die Höhe $h_{int.}$ der Zwischenschicht, welcher abhängig von der Pillargeometrie und Orientierung in der Zwischenschicht ist, begrenzt (Abb. 4).

Um nun eine Gasdiffusion von z.B. Stickstoff zu ermöglichen, muss die Pore einen Durchmesser besitzen, der größer als der kinetische Radius des Stickstoffmoleküls (ca. 3.2 Å) ist. Daraus ergibt sich ein minimaler Basalabstand von 12.8 Å (9.6 Å Schichtdicke) und somit einer Zwischenschichthöhe von 3.2 Å ergibt.[39]

Der laterale Pillarabstand d_{Pore} kann unter bestimmten Annahmen berechnet werden. Dabei wird angenommen, dass die Pillarmoleküle aufgrund ihrer elektrostatischen Abstoßung eine hexagonale Anordnung im Zwischenschichtraum annehmen. Aus der Differenz von Zellparameter a_{Pillar} mit dem Durchmesser des Pillarmoleküls d_{Pillar} wird der Durchmesser der

Mikropore erhalten. Um eine Zugänglichkeit des Porensystems zu erreichen, muss dieser Durchmesser größer als der kinetische Radius eines Stickstoffmoleküls sein.[44]

Dabei ist die resultierende Porenweite und somit das zugängliche mikroporöse, zweidimensionale Netzwerk in der Zwischenschicht von drei Faktoren abhängig (Abb. 4):

a) Schichtladung (Ladungshomogenität) des synthetischen Schichtsilikates
b) Größe und Geometrie des verwendeten Pillarmoleküls
c) Valenz des Pillarmoleküls

Wie bereits in Kapitel 2.2.1 erwähnt, resultiert die Schichtladung der 2:1 Schichtsilikate aus der isomorphen Substitution in der Tetraeder und/oder Oktaederschicht. Diese Substitution muss aber strikt statistisch erfolgen, um eine homogene Ladungsdichte zu gewährleisten.

Diese Ladungsdichte kann durch zwei unterschiedliche Ansätze post-synthetisch genau eingestellt werden. Im ersten Ansatz wird durch Oxidation von strukturellem Fe^{2+} in der Oktaederschicht eines synthetischen Eisentänioliths ($Cs_{0.98}[Fe^{2+}_{1.93}Li_{1.01}]Si_4O_{10}F_2$) die Schichtladung signifikant reduziert.[45] Dabei wurde durch die oxidativen Interkalationsbedinungen während des hydrothermalen Kationentausches bei 120 °C mit Me_2DABCO^{2+} 43 % des strukturellen Fe^{2+} oxidiert, wobei die Schichtladung von 0.98 p.f.u. auf 0.46 p.f.u. reduziert wurde.[46] Verwendet man nun während der Interkalation stärkere Oxidationbedingungen durch die Zugabe von Br_2, werden 97 % des strukturellen Fe^{2+} oxidiert. Dabei wurde weder eine Verringerung der Pillardichte im Zwischenschichtraum, noch eine Reduktion der Schichtladung unter 0.46 p.f.u. erhalten. Diese Ladungsdichte stellt somit eine natürliche Untergrenze für die Ladungsreduktion unter oxidativen Bedingungen dar. Dabei weicht das System durch Freisetzung oktaedrisch koordinierter Li^+-Ionen in die Zwischenschicht aus, wobei somit trotz weiterer Oxidation die CEC (*cation exchange capacity*) konstant bleibt. Dieser Mechanismus wurde als Anti-Hofmann-Klemen-Effekt bezeichnet.[47;48]

Der Hofman-Klemen-Effekt hingegen beschreibt die Migration von kleinen Ionen wie Li^+-Ionen aus der Zwischenschicht in Lücken der Oktaederschicht. Dort werden z.B. bei natürlichen dioktaedrischen Schichtsilikaten Leerstellen im Oktaedergitter besetzt und somit die Schichtladung reduziert.[48] Jaynes *et al.* modifizierte diese Ladungsreduktionsmethode dahingehend, dass die in der Zwischenschicht enthaltenen Na^+ und Ca^{2+} Ionen eines Ca^{2+}-Hectorits durch Mg^{2+}-Ionen ersetzt werden.[49;50] Anschließend wurde bei 250 °C eine Migration der Mg^{2+}-Ionen auf Lithiumpositionen im Oktaedergitter beobachtet. Dadurch werden die Li^+-Ionen in die Zwischenschicht abgegeben und die Schichtladung durch das Ersetzten eines monovaltenten Kations durch ein divalentes Kation folglich reduziert. Dieser

zweite Ansatz der Ladungsreduktion kann nun auf trioktaedrische synthetische Na^+- und K^+-Hectorite angewendet werden, um die Schichtladung graduell einzustellen (Abb. 5).

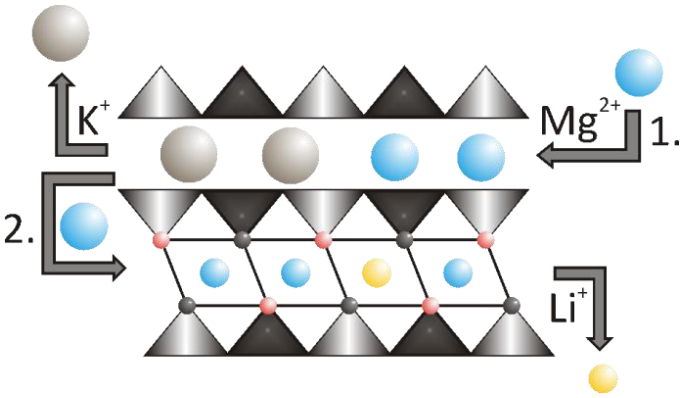

Abb. 5: Schematische Darstellung des angepassten Hofman-Klemen-Ladungsreduktionsmechanismus. Reprinted with permission from M. M. Herling, H. Kalo, S. Seibt, R. Schobert, J. Breu, *Langmuir* **2012**, *28*, 14713-14719. Copyright 2012 American Chemical Society.

Neben der Schichtladung ist die Größe und Geometrie des Pillarmoleküls entscheidend für die resultierende Mikroporosität.

Die Orientierung des organischen Abstandshalters wird in Abhängigkeit von seiner Geometrie durch die elektrostatische Anziehung zwischen der negativ geladenen Silikatschicht und dem positiv geladenen Pillar vorgegeben. Durch diese Coulomb-Wechselwirkung minimiert das System den Basalabstand, wobei ellipsoidale und lineare Pillarmoleküle sich mit ihrer Längsachse senkrecht zur Silikatschicht orientieren. Sphärische Pillar besitzen aufgrund ihrer Gestalt keine Möglichkeit sich in der Zwischenschicht in unterschiedlichen Orientierungen zu positionieren.

Baumgartner *et al.* konnte durch die Interkalation von Me_2DABCO^{2+} in einen eisenhaltigen Täniolith mit anschließender Einkristallverfeinerung die Orientierung des Pillars in der Zwischenschicht bestimmen. Dabei realisierte Me_2DABCO^{2+} im Zwischenschichtraum einen Winkel von 24° zur Tetraederschicht.[46] Die Anzahl der Pillarmoleküle und somit deren Pillardichte ist aufgrund der Ladungsneutralität zum einen durch die Ladungsdichte des verwendeten Schichtsilikats und zum anderen durch die Valenz des Pillars definiert. Wird nun ein höher valentes Pillarmolekül verwendet, verringert sich folglich die Pillardichte unter Erhöhung des Pillarabstandes (d_{Pillar}) im Zwischenschichtraum. Die Dichte des Pillars im Zwischenschichtraum wird neben der Valenz und Geometrie des molekularen Abstandshalters hauptsächlich durch die Höhe der negativen Schichtladung bestimmt. Durch die Auswahlmöglichkeiten an Schichtladung und Pillarmolekül resultiert eine sehr hohe Modularität in Bezug auf Funktionalitäten und Einstellbarkeit des Porenraums (Abb. 6).

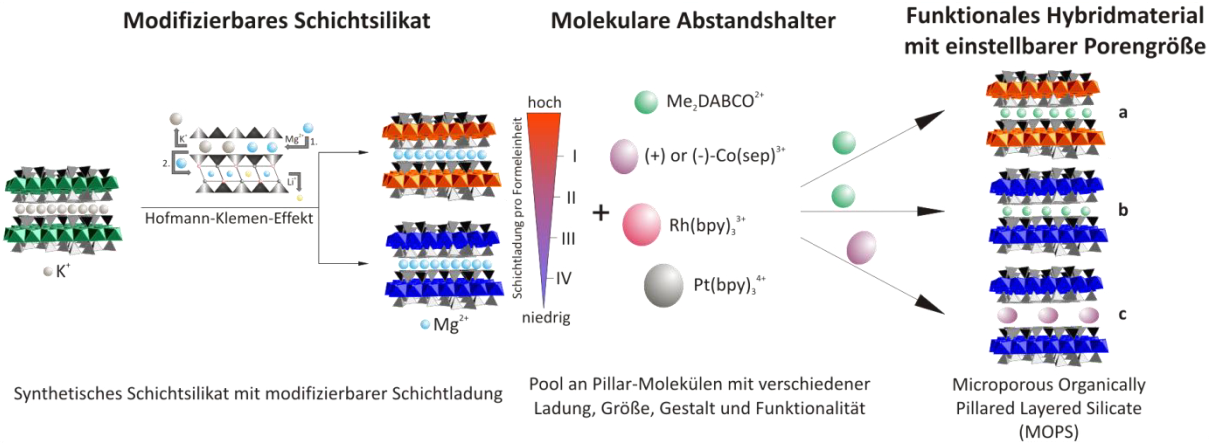

Abb. 6: Schematische Darstellung des Pillaring-Konzepts

2.4 Alternative Bestimmung des Porendurchmessers mittels hyperpolarisierter ^{129}Xe-NMR Spektroskopie

Neben den klassischen Physisorptionsmessungen mit Ar oder N_2 zur Bestimmung des Porendurchmessers und –volumens kann die ^{129}Xe-NMR Spektroskopie weiterführende strukturelle Informationen in Bezug auf die Porenstruktur liefern. Anfangs wurde thermisch polarisiertes Xenon verwendet, jedoch konnte nur eine geringe Hyperpolarisation erreicht werden. Bei hyperpolarisiertem ^{129}Xe oder *spin exchange optical pumping*-^{129}Xe wird durch optisches Pumpen von Alkalimetallatomen mit anschließendem Spinaustausch eine Hyperpolarisation erreicht. Durch diese kann nun das hyperpolarisierte ^{129}Xe als Adsorbat für die zweidimensionale Porensstruktur von MOPS verwendet werden. Die polarisierte Elektronenhülle des ^{129}Xe-Kerns reagiert darüber hinaus sehr sensibel auf Umgebungsveränderungen und ermöglicht dadurch eine signifikant reduzierte Messdauer. Während des Adsorptionsprozesses von Xenon in den Zwischenschichtraum zeigt sich eine Änderung der chemischen Verschiebung. Das von Demarquay und Fraissard 1987 entwickelte Modell für Zeolithe kann angewendet werden, um den Porendurchmesser zu bestimmen.[51] Dabei wird die isotrope chemische Verschiebung des ^{129}Xe-Signals mit einem Porendurchmesser bekannter Geometrie verglichen. Einflüsse wie magnetische oder elektrische Felder im Falle von geladenen Systemen werden hier vernachlässigt. Diese neue Charakterisierungsmethode in Kombination mit klassischen Physisorptionsmessungen erlaubt eine realistischere Abschätzung des Porenraumes und dessen Geometrie für mikroporöse, silicatbasierte und niedrig geladene Hybridmaterialien.

2.5 Pillaring nanoskaliger Schichtsilikate

Pillaring eines natürlichen Montmorillonits mit organischen Molekülen (Tetramethyl (TMA)- und Tetraethylammonium (TEA)) wurde von Barrer und MacLeod in den 1950ern berichtet.[24] Dabei wurde ein Basalabstand von 13.5 Å und 13.9 Å erreicht. Darüber hinaus zeigte der TEA-gepillarte Montmorillonit aufgrund des verringerten Pillar-Pillar-Abstandes (d_{Pillar}) in der Zwischenschicht. ein deutlich reduziertes Porenvolumen im Vergleich zum TMA gepillarten Material bei gleicher Ladungsdichte. Die N_2-Isothermen beider Materialien zeigen aufgrund ihres nanoskaligen Charakters sowohl Mikro- als auch Mesoporosität. Letztere resultiert hauptsächlich durch interpartikuläre Agglomeration durch die Keilporen generiert werden. Barrer begann folgerichtig den Einfluss der äußeren Oberfläche auf die Sorptionsmessungen durch die Einführung einer Inklusions-Isotherme des Typs I zu korrigieren.[25]

Anschließend wurden weitere Kationen, wie z.B. Alkylammonium und –diammonium sowie $[Co(en)_3]^{3+}$-Kationen als Pillarmoleküle verwendet. In einer darauffolgenden Veröffentlichung von Barrer wurde die Abhängigkeit des Mikroporenvolumens und der Adsorptionskapazität von der Äquivalentfläche des Pillars und der Ladungsdichte des Schichtsilikats behandelt.[52] Darüber hinaus wurden theoretische Berechnungen anhand Pillargeometrien, Pillardichten und Basalabstand zur Abschätzung des Porenvolumens durchgeführt.[26;51;53] Mortland und Berkheiser verwendeten 2H-DABCO^{2+} als Pillaringagens und konnten damit ein deutlich erhöhtes Porenvolumen als mit TEA erreichen, wobei diese Materialien darüber hinaus in der Lage sind, Moleküle wie 2,4-Dimethylpentan im Zwischenschichtraum anzureichern.[54] 1994 beschrieben Lao und Detellier die Trennung linearer Kohlenwasserstoffe mit TMA gepillartem Montmorillonit und Hectorit, wobei diese mit Tetraphenylphosphonium und quaternisierten Polyammonium-gepillarten Materialien verglichen wurden.[55] Die Trennleistung konnte mit der Größe und Geometrie des Porenraumes korreliert werden, wobei dieses Material als stationäre Phase in der Gaschromatographie zur Trennung leichter Kohlenwasserstoffe etabliert wurde.

Neben der Charaktersierung der Mikroporen mit Hilfe von Physisorptionsmessungen kann, wie bereits erwähnt, durch die Anwendung hyperpolarisierter ^{129}Xe-NMR-Spektroskopie die Mikroporenstruktur untersucht werden. Sozzani untersuchte einen mit TEA gepillarten Hectorit ($Ex_{0.66}[Mg_{5.34}Li_{0.66}]Si_8O_{20}(OH,F)_4$), dessen Zwischenschichtkation bereits während der Synthese mit TEA als Kristallisationsagens ausgetauscht wurde.[56] Dabei konnte durch die Verschiebung des ^{129}Xe-Signals unter Anwendung des semi-empirischen Demarquay-

Fraissard-Modells[51] der Porendurchmesser von 7 Å bestimmt werden. Dieser wurde bei N_2-Physisorptionmessungen durch die Horvath-Kavazoe-Methode von 6 Å bestimmt. Die Physisorptionsisotherme zeigte ein Typ IV-Verhalten, was auf interpartikuläre Porosität und Kapillarkondensation schließen lässt. Bei der Interpretation von Physisorptionsmessungen gepillarter Schichtsilikate ist sehr darauf zu achten, ob es sich um inter- oder intrapartikuläre Porosität handelt. Die Verwendung eines natürlichen, nanoskaligen Schichtsilikats als Wirtsmaterial führt in den meisten Fällen zu einem signifikanten Beitrag der interpartikulären Porosität zum Gesamtporenvolumen. Wird bei gleicher Ladungsdichte und Pillarmolekül ein synthetisches Schichtsilikat verwendet, beträgt der Beitrag von Agglomeraten und äußeren Oberflächen maximal 5 %. Die aus Physisorptionsmessungen resultierende Isotherme ist von Typ I, charakteristisch für ein rein mikroporöses Material. Bei natürlichen Materialien wird eine Typ IV-Isotherme realisiert, deren Adsorptionsverhalten bei hohen Relativdrücken aus der Adsorption in interpartikulären Keilporen resultiert (Abb. 7).[23]

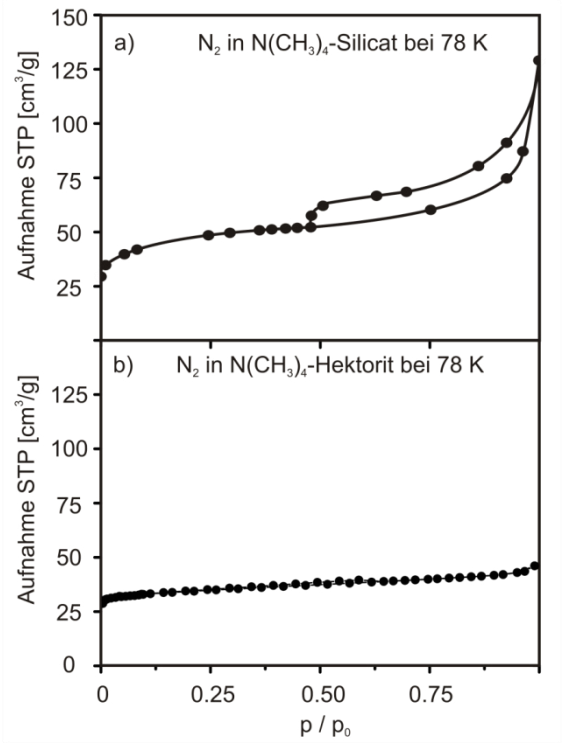

Abb. 7: a) N_2-Physisorptionsisotherme eines mit TMA gepillarten Montmorillonits; b) N_2-Physisorptionsisotherme eines mit TEA gepillarten synthetischen Hectorits.[23]

2.6 Pillaring synthetischer, grobkörniger Schichtsilikate

Wie bereits erwähnt, besitzen natürliche Schichtsilikate keine homogene Ladungsdichte und zeigen somit eine Anfälligkeit für Defekte, wie z.B. Ladungsinhomogenitäten, Stapel- und Rotationsfehlordnungen. Werden nun geordnete, synthetische Schichtsilikate mit homogener Ladungsdichte für die rationale Synthese mikroporöser Hybridmaterialien verwendet, umgeht man diese Probleme.

Durch diese neu entwickelte und hochskalierbare Synthese ladungshomogener, geordneter Schichtsilikate mit hohem Aspektverhältnis können diese Schichtsilikate als Ausgangsmaterial für mikroporöse Hybridmaterialien dienen.[37;57] Die Struktur eines Ein- und Zweischichthydrats eines hoch geladenen, quellfähigen Na-Hectorits konnte durch Einkristallstrukturverfeinerung gelöst werden und bestätigte somit indirekt die sehr homogene Ladungsdichte des synthetischen Schichtsilikats.[58] Darüber hinaus konnte durch die richtige Größe des Zwischenschichtkations, z.B. Cs^+, die Stapelordnung der Schicht erhöht werden und somit auch als Ausgangmaterial für dreidimensional geordnete mikroporöse Hybridmaterialien dienen.[39]

Die Position des Pillars TMA^+ in der Zwischenschicht eines synthetischen Hectorits konnte durch die Verwendung eines geordneten Ausgansmaterial bestimmt werden.[59] Dabei liegen zwei Methylgruppen in der *ab*-Ebene, wobei zwei weitere, die Zwischenschicht mit den Silikatschichten verknüpfende, Methylgruppen in den hexagonalen Kavitäten zu finden sind.[59] Die Interkalation eines elliptischen Me_2DABCO^{2+}-Moleküls in die Zwischenschicht eines Cs-Fluorohectorits folgt dem gleichen Prinzip. Abweichend von den Ergebnissen von Shabtai *et al.* orientiert sich gemäß Einkristallstrukturverfeinerung das Pillarmolekül mit seiner C_3-Längachse aus elektrostatischen Gründen parallel zur Silikatschicht.[60] Eine ähnliche Struktur wurde bei Baumgartner *et al.* durch oxidatives Pillaring eines synthetischen Cs-Täniolith ($Cs_{0.98}Fe^{2+}_{1.93}Li_{1.01}Si_4O_{10}F_2$) mit Me_2DABCO^{2+} erhalten. Dabei orientiert sich das Pillarmolekül in der Zwischenschicht mit seiner C_3-Längsachse in einem Winkel von ca. 24 ° gegen die *ab*-Ebene. Basierend auf der Einkristallstrukturverfeinerung und der Zusammensetzung des gepillarten Materials wurde die theoretische Porenweite abgeschätzt. Die Berechnung berücksichtigte sowohl die Schichtladung als auch die Ladung des Pillars und dessen van der Waals-Radius (Abb. 8).[46] Das mit Me_2DABCO^{2+} gepillarte, mikroporöse Material zeigte eine enge Porenverteilung (5 – 7 Å), die mit den Abschätzungen (3.7 – 6.1 Å) nahezu übereinstimmt.

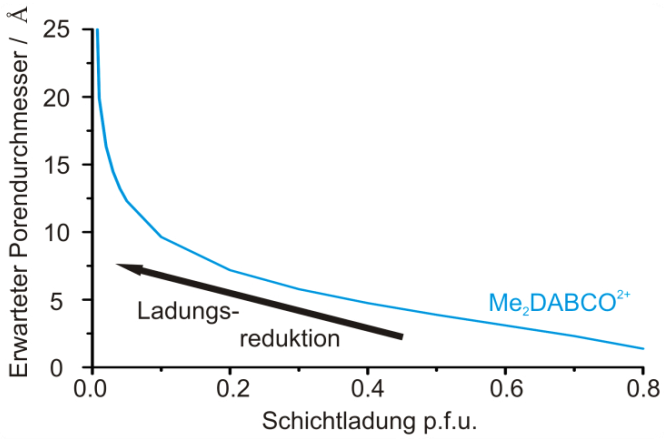

Abb.8: Theoretische Berechnung des Porendurchmessers eines Me_2DABCO^{2+}-gepillarten Schichtsilikats in Abhängigkeit von der Schichtladung.

Neben diesen Erkenntnissen, konnte in wenigen Fällen eine langreichweitige Ordnung des Pillarmoleküls in der Zwischenschicht beobachtet werden. Tsvetkov und White interkalierten verschiedene Komplexkationen ($Ir(diamsar)^{3+}$ (diamsar: 1,8-diamino-3,6,10,13,16,19-hexa-azabicyclo[6.6.6]eicosan), $Hg(diamsarH_2)^{4+}$ und $Hg(diamsar)^{2+}$) in einen Na-Montmorillonit und einen hoch geladenen synthetischen Fluorohectorit.[61] Im Falle des synthetischen Materials konnte eine zweidimensionale langreichweitige Ordnung beobachtet werden. Bei der Interkalation eines $[Ru(bpy)_3]^{2+}$-Komplexes in einen Na-Fluorohectorit wurden schwache λ-geformte Reflexe beobachten, die durch die zweidimensionale Streuung für *hk*-Banden sprechen.[62] Auch Stöcker *et al.* konnte beim Pillaring eines synthetischen Cs-Hectorits mit 2H-$DABCO^{2+}$ Reflexe einer 3 $a \times b$ Überzelle indizieren, was wiederum für eine zwei-dimensionale Ordnung des Pillars in der Zwischenschicht spricht. (Abb. 9)

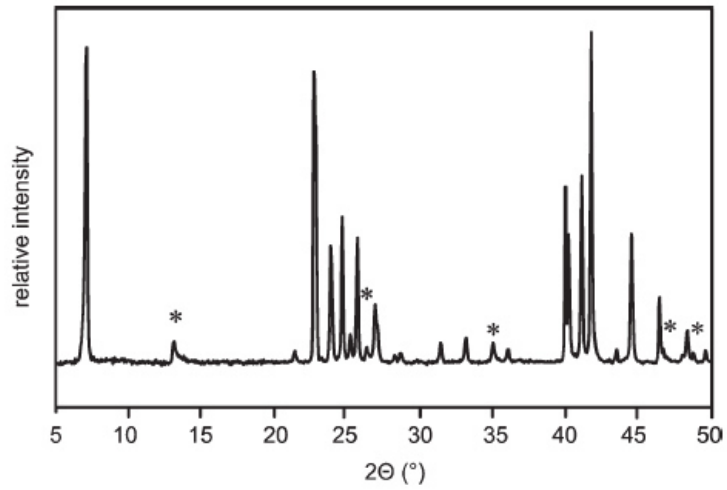

Abb. 9: Pulverdiffraktogramm eines 2H-$DABCO^{2+}$-Hectorits. * markieren die Überstrukturreflexe der 3 $a \times b$ Zelle. M. Stöcker, W. Seidl, L. Seyfarth, J. Senker and J. Breu, *Chem. Commun.*, **2008**, 629 – Reproduced by the permission of the Royal Society of Chemistry.

Es kann somit davon ausgegangen werden, dass es sich um eine zweidimensionale Ordnung des Pillars in der Zwischenschicht neben der dreidimensionalen Ordnung der Silikatschicht

handelt, welche stark von den Pillar-Silicat-Wechselwirkungen und das Hineinreichen der Pillarmoleküle in die hexagonalen Kavitäten abhängt. Auch dieses gepillarte Material wies eine enge Mikroporenverteilung (4-7 Å) auf.[63]

In dieser Arbeit wurde das Pillaring-Konzept um mikroporöse Hybridmaterialien zu synthetisieren erweitert und die Klasse der „Microporous Organically Pillared Layered Silicates (MOPS)“ eingeführt. Diese Materialien basieren auf der Kombination synthetischer, ladungshomogener Schichtsilikate mit metallorganischen und organischen molekularen Abstandshaltern („Pillar“), die durch die elektrostatischen Kräfte zwischen den Silicatlamellen und dem Pillar stabilisiert werden.

Während MOFs und Zeolithe aus kovalent gebundenen Netzwerken bestehen, besitzen MOPS die Möglichkeit der post-synthetischen Anpassung der Porenweite. Diese Modularität spiegelt die Attraktivität dieser neuen mikroporösen Materialklasse wider, welche eine hohe thermische Stabilität, Funktionalität und Flexibilität aufweist. Folglich können MOPS in bestimmten Anwendungsfeldern, wie z.B. selektive Adsorbentien, mit etablierten mikroporösen Systemen konkurrieren.

3. Problemstellung

Das Ziel dieser Arbeit war nun die Synthese und Charakterisierung funktionaler und anpassbarer mikroporöser Materialien durch Anwendung des Pillaring-Konzeptes weiter zu entwickeln. Die Entwicklung des Pillaring-Konzeptes mit anorganischen und organischen Pillarmolekülen soll dabei kritisch beleuchtet werden. Die gezielte Modifizierung der Ladungsdichte des synthetischen Schichtsilikats und die Verwendung funktionaler Abstandshalter soll untersucht werden, um mögliche Anwendungen dieser Materialien in der Größen- und Stereoselektivität zu evaluieren.

Auf Basis der Ergebnisse aus dem oxidativen Pillaring eines Cs-Täniolith mit Me_2DABCO^{2+} und dessen beobachtete Untergrenze der Ladungsreduktion soll nach alternativen Ladungsreduktionsmechanismen gesucht werden, die es erlauben, diese Untergrenze zu überwinden. Gelingt nun diese graduelle Einstellung der Schichtladung, kann durch Pillaring mit unterschiedlich geladenen Pillarmolekülen ein mikroporöses Hybridmaterial synthetisiert werden. Mit Hilfe von Argon-Physisorptionsmessungen kann dieses hinsichtlich Porenweite und –volumen untersucht werden.

Als alternative Charakterisierungsmethode soll die Porositätsbestimmung mittel ^{129}Xe-NMR-Spektroskopie unter Anwendung des Demarquay-Fraissard-Modells an verschieden gepillarten Schichtsilikaten unterschiedlicher Ladungsdichten getestet werden.

Um nun Funktionalitäten, wie z.B. Chiralität, in die generierten Mikroporen der Zwischenschicht einzubringen, sollen enantiomerenreine Kationen verwendet werden. Nach erfolgreicher Synthese dieser chiralen MOPS soll eine mögliche Enantiodiskriminierung kleiner volatiler, organischer Moleküle, wie z.B. (±)-But-3-yn-2-ol, untersucht werden. Darüber hinaus soll durch die Verwendung des größeren 2-Methyl-but-3-yn-2-ols als Adsorbat eine mögliche Größenselektivität untersucht werden.

Aufgrund der elektrostatischen Wechselwirkung des molekularen Abstandshalters mit den Silicatschichten kann sich das Pillarmolekül prinzipiell in der Zwischenschicht in Abhängigkeit vom Adsorbat umorientieren und somit eine Expansion des Zwischenschichtraumes hervorrufen. Diese Expansion des Porenvolumens ist bei MOFs unter den Effekten des „*breathings*“ und des „*gate openings*“ bereits bekannt. Das mögliche Auftreten dieser Effekte bei MOPS soll durch das Einbringen eines ellipsoidalen Pillarmoleküls in die Zwischenschicht eines synthetischen Schichtsilikats in Abhängigkeit von der Adsorption

unterschiedlicher Gase (z.B. CO, $N_{2)}$ untersucht und eine mögliche Anwendung in der Gasseparation evaluiert werden.

4. Synopsis

Die vorgelegte kumulative Dissertation enthält fünf Publikationen bzw. Manuskripte mit dem Ziel der Synthese und Charakterisierung mikroporöser, funktionaler Hybridmaterialien auf Basis von synthetischen Schichtsilikaten. Diese wurden teilweise sowohl in Kooperationen mit dem Lehrstuhl für Organische Chemie I und Anorganische Chemie III der Universität Bayreuth, sowie mit dem Institute for Integrated Cell-Material Sciences der Kyoto University erarbeitet. Die Einordnung der Veröffentlichungen bzw. Manuskripte in das Pillaring-Konzept ist in Abb. 10 schematisch dargestellt.

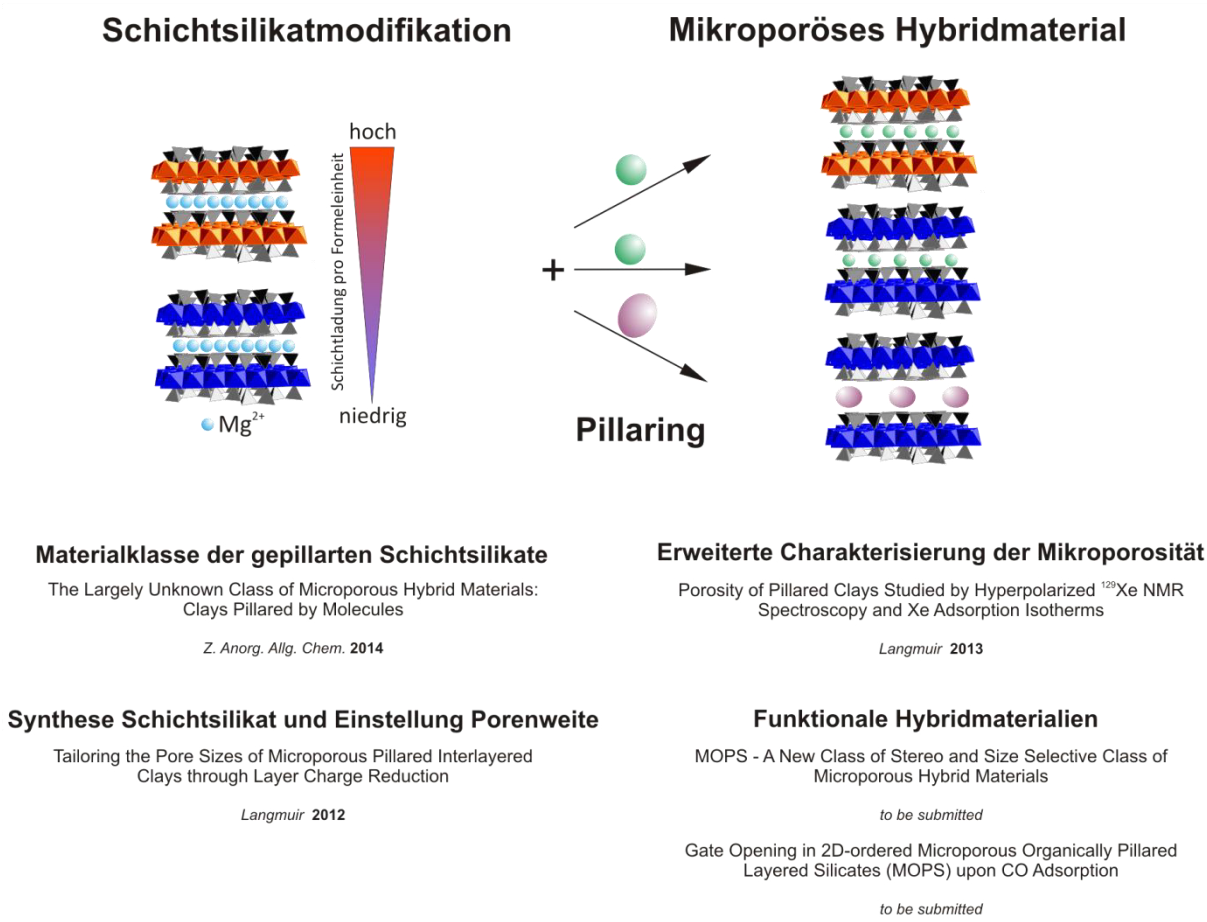

Abb. 10: Schematische Darstellung der Synopsis.

Einen Überblick über die Materialklasse der gepillarten Schichtsilikate behandelt sowohl *Pillared Interlayered Clays* mit anorganischen Abstandshaltern als auch organisch gepillarter Schichtsilikate. (Kap. 4.1.). Anschließend wird auf die Einstellung der Schichtladung und somit der Mikroporosität (Kap. 4.2) und dessen Charakterisierung mit ^{129}Xe-NMR-Spektroskopie (Kap. 4.3) eingegangen. Mögliche Applikationsuntersuchungen der MOPS als funktionales Hybridmaterial wird in Kap. 4.4 und 4.5 untersucht.

4.1 Mikoporöse Hybridmaterialien auf Basis von organisch-gepillarten synthetischen Schichtsilikaten

In diesem Übersichtsartikel werden Entwicklung, Fortschritt und Charakterisierungsmethoden im Feld der interkalierten und gepillarten Materialien (*Pillared Interlayered Clays*) auf Basis von natürlichen und synthetischen Schichtsilikate kritisch reflektiert. Zunächst werden hierbei Schwachstellen von PILC-Charakterisierungsmethoden analysiert und die Auslegung der IUPAC-Definition für gepillarte Materialien kritisch hinterfragt.

Wird als Ausgangsmaterialein natürliches, nanoskaligen Schichtsilikat verwendet, besitzt dies Defekte, wie z.B. Ladungsinhomogenitäten, Stapel- und Rotationsfehlordnungen und hohe Einflüsse externer Oberflächen zur Gesamtoberfläche. Diese Schwachstellen spiegeln sich in einem breiten Interpretationsspielraum analytischer Ergebnisse wider. Durch die Verwendung eines grobkörnigen, synthetischen Schichtsilikats als Ausgangsmaterial werden Fehlordnungen und Ladungsinhomogenitäten vermieden und verlässliche Analyseergebnisse erhalten. Um den Einfluss des Ausgangsmaterials zu untersuchen, wurde sowohl ein natürliches als auch synthetisches Schichtsilikat vergleichbarer Schichtladung mit Tetramethylammonium gepillart und mit Hilfe von Stickstoff-Physisorptionsmessungen charakterisiert. (Kapitel 2.5, Abb. 7) Im Falle des natürlichen Schichtsilikats ist der Einfluss der interpartikulären Porosität im erhöhten Relativdruckbereich erkennbar. Das synthetische Schichtsilikat hingegen zeigt eine rein intrapartikuläre Mikroporosität, die nur im Zwischenschichtraum lokalisiert ist und sich in einer klassischen Typ I-Isotherme widerspiegelt.

Zusammenfassend wurde die Attraktivität des Pillaring-Konzepts zusammen mit der Verwendung ladungshomogener, synthetischer Schichtsilikate dargestellt. Dabei können mikroporöse Materialien unter Größen-, Gestalt- und Funktionalitätskontrolle des Porenraums designt werden. Dies spiegelt die Stärke und das große Potential des Pillaring-Konzepts wider, welches aufgrund des möglichen Feintunings der Poren im Bereich $\leq$ 0.2 Å mikroporösen Materialien, wie z.B. MOFs, überlegen ist.

Details und weitere Diskussion:

The Largely Unknown Class of Microporous Hybrid Materials: Clays Pillared by Molecules

Markus M. Herling and Josef Breu, *Z. Anorg. Allg. Chem.*, **2014**, *640*, 547-560.

4.2 Einstellung der Porengröße mikroporöser, gepillarter Schichtsilikate durch gezielte Schichtladungsreduktion

Um die oben genannte Untergrenze der Schichtladungsreduktion zu überwinden, wurde ein synthetischer Kalium-Hectorit mit einer Schichtladung von 0.48 p.f.u. hergestellt. Die Ladungsreduktion gelang dann unter Verwendung des Hofmann-Klemen-Effekts.[48] Dabei wurde das K^+-Ion in der Zwischenschicht durch Mg^{2+} ausgetauscht und anschließend bei 250 °C behandelt. Bei dieser Temperatur migrieren die in der Zwischenschicht lokalisierten Mg^{2+}-Ionen durch hexagonale Kavitäten der Tetraederschicht in die Oktaederschicht und ersetzten dort Li^+-Ionen, die wiederum in die Zwischenschicht freigegeben werden. Dadurch kann mit jedem 12 h – Temperschritt eine mittlere Schichtladungsreduktion von je 0.016 p.f.u. realisiert werden. Die Schichtladung konnte nach sechsfacher Reduktion zu 0.39 p.f.u. bestimmt werden. Dies konnte sowohl durch CEC-Bestimmungen nach DIN ISO 11260 als auch durch Li^+-AAS-Messungen der Waschlösung verfolgt werden (Abb. 11).

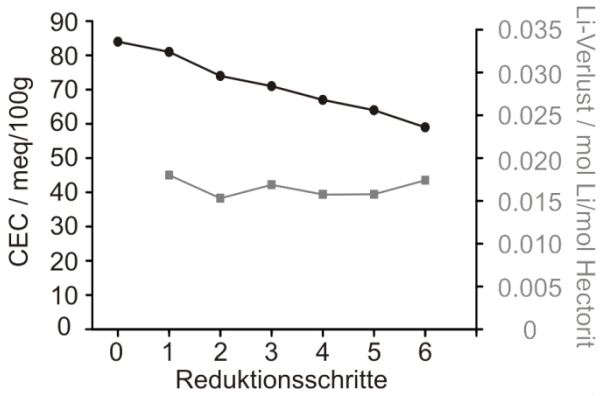

Abb. 11:Verlauf der CEC und des Li-Verlustes bei steigenden Reduktionsschritten. Reprinted (adapted) with permission from M. M. Herling, H. Kalo, S. Seibt, R. Schobert, J. Breu, *Langmuir* **2012**, *28*, 14713-14719. Copyright 2012 American Chemical Society

Die Schichtladungsbestimmung nach Lagaly bestätigte, dass die Ladungshomogenität weitestgehend erhalten wurde.[44] Durch eine nicht perfekt statistische Substitution von Li^+ durch Mg^{2+} kann es jedoch zu einer geringen Einbuße in der Ladungshomogenität kommen.

Die hier verwendete graduelle Anpassung der Schichtladung stellt eine attraktive Methode zur post-synthetischen Einstellung der Porenweite und somit für die Anwendung dieser neuartigen organisch gepillarten, mikroporösen Schichtsilikate dar, die weder für MOFs noch für Zeolithe zugänglich ist.

Durch die Verwendung zweier Pillar (Me_2DABCO^{2+} und $Rh(bpy)_3^{3+}$) wurde die Abhängigkeit der Porenweite sowohl von der Schicht- als auch der Pillarladung und Pillargeometrie untersucht. Hierfür wurden jeweils von dem nicht und sechsfach ladungsreduzierten,

gepillarten Hectorit Argonadsorptionsisothermen bei 87.3 K aufgenommen. Dabei ergaben sich signifikante Unterschiede sowohl im Porenvolumen als auch in der Porenverteilung (Abb. 12). Die röntgenographischen Analysen zeigten dabei keinerlei Unterschied im Basalabstand, die bei 43% rH für Me_2DABCO^{2+} 14.4 Å und für $Rh(bpy)_3^{3+}$ 17.5 Å betragen.

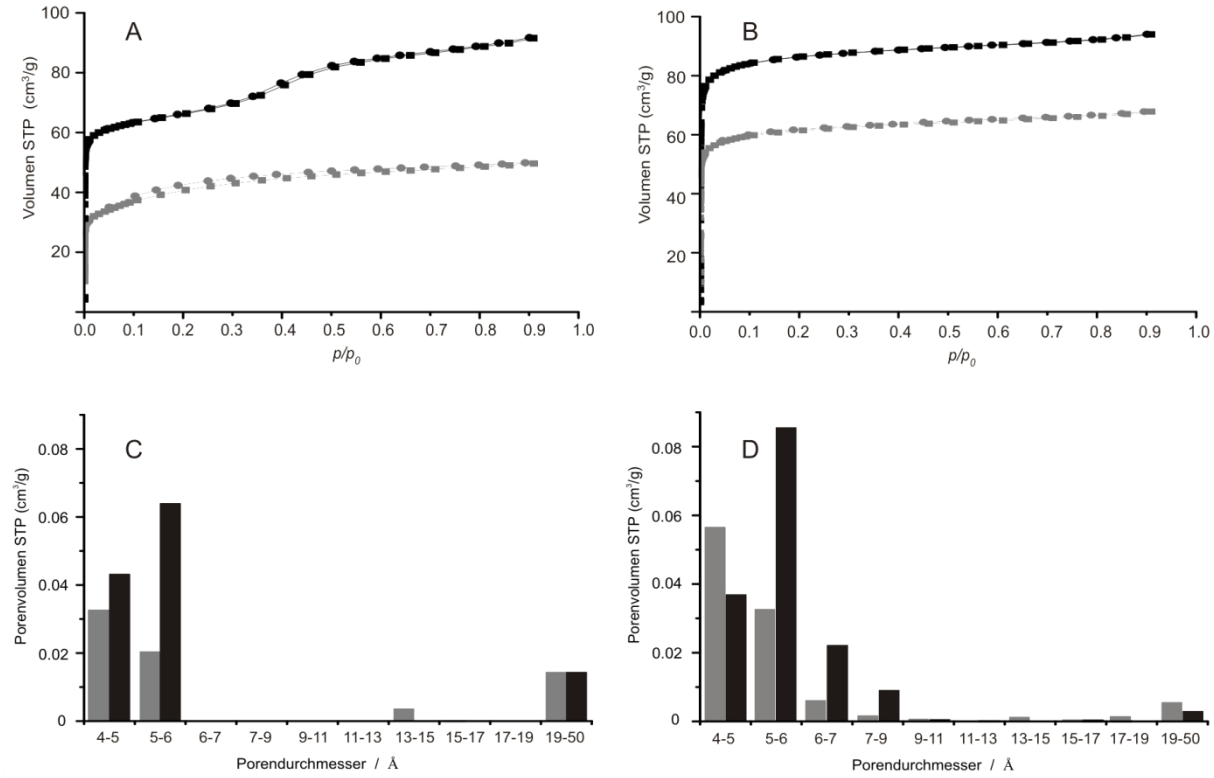

Abb. 12: Argon-Physisorptionsisothermen von Me_2DABCO^{2+}-Hectorit (A) und $Rh(bpy)^{3+}$-Hectorit (B) und die Porenverteilung von Me_2DABCO^{2+}-Hectorit (C) und $Rh(bpy)^{3+}$-Hectorit (D). Reprinted (adapted) with permission from M. M. Herling, H. Kalo, S. Seibt, R. Schobert, J. Breu, *Langmuir* **2012**, *28*, 14713-14719. Copyright 2012 American Chemical Society

$Rh(bpy)_3^{3+}$-gepillarter Hectorit mit einer Schichtladung von 0.39 p.f.u. zeigte im Vergleich zur Schichtladung 0.48 p.f.u. eine Erhöhung des Porenvolumens um 46 %, während die Erhöhung des Me_2DABCO^{2+} gepillarten Hectorits 95 % betrug. Die Porenweite konnte in beiden Fällen um 1-2 Å erhöht werden (Abb. 12). Mit Hilfe dieser Methode kann die Grenze von 0.44 p.f.u., die bisher mittels oxidativer Schichtladungsreduktion realisiert werden konnte, überwunden werden. Dies ermöglicht somit eine effiziente post-synthetische Anpassung der Schichtladung und bewirkt somit eine Steigerung der Modularität des Pillaring-Konzepts.

Details und weitere Diskussion:

Tailoring the Pore Sizes of Microporous Pillared Interlayered Clays through Layer Charge Reduction.

Markus M. Herling, Hussein Kalo, Sebastian Seibt, Rainer Schobert, and Josef Breu, *Langmuir*, **2012**, *28*, 14713-14719.

4.3 Charakterisierung der Porengrößenverteilung gepillarter Schichtsilikate mit hyperpolarisierter ^{129}Xe MAS NMR-Spektroskopie

Um nun den Einfluss der Schichtladungsreduktion auf die Mikroporosität im Detail zu untersuchen, wurden drei mit Me_2DABCO^{2+} gepillarte Hectorite unterschiedlicher Schichtladung (p (0.48 p.f.u.), r_3 (0.44 p.f.u.) und r_6 (0.39 p.f.u.)) NMR spektroskopisch untersucht. Die lokale Anordnung der Me_2DABCO^{2+}-Pillarmoleküle im Zwischenschichtraum der drei Materialien wurde mit Hilfe von 1D ^{1}H, ^{13}C, ^{19}F und ^{29}Si und 2D ^{19}F(^{1}H) sowie ^{1}H(^{13}C) „*heteronuclear correlation*“ HETCOR NMR Experimenten charakterisiert.

Durch den Austausch von strukturellem Li^+ durch Mg^{2+} während des Ladungsreduktionsprozesses ändert sich die Verschiebung des ^{19}F Kerns, sodass dieser Austauschprozess durch ^{19}F MAS Messungen verfolgt werden kann.

Bei der spektralen Dekonvolution konnte das relative Mg/Li-Verhältnis bestimmt werden, welches mit dem aus AAS erhaltenen Verhältnis übereinstimmt und mit zunehmenden Ladungsreduktionszyklen von 5.9(1):1 auf 7.9(1):1 ansteigt. ^{1}H(^{19}F) und ^{13}C(^{1}H) HETCOR Messungen zeigten, dass der Me_2DABCO^{2+}-Pillargehalt mit dem Mg^{2+}- und Li^+-Gehalt in der Oktaederschicht und somit der Schichtladung korreliert. Darüber hinaus zeigte Me_2DABCO^{2+} eine homogene Verteilung im Zwischenschichtraum und bestätigt somit die homogene Schichtladung des Hectorits.

Um nun Unterschiede im Xenonadsorptionsprozess zu untersuchen, wurden 2D EXSY Spektren bei niedriger und hoher Xenonbeladung sowie bei 295 K und 195 K mit Hilfe von CF-HP ^{129}Xe NMR Spektroskopie aufgenommen. Dabei stellte sich heraus, dass bei niedriger Beladung inter- und intrakristalline Austauschprozesse ablaufen. Bei hoher Beladung und niedriger Temperatur adsorbiert Xenon im Mikroporensystem des gepillarten Materials und besitzt eine dichtere Packung als in der Gasphase.

Das Mikroporensystem zeigt somit sowohl eine hohe als auch schnelle Zugänglichkeit des offenen Porensystem für das Gasmolekül, wobei die Xe-Diffusion innerhalb weniger 100 ms stattfindet. Hochauflösende CF-HP ^{129}Xe MAS-Spektren zeigten sehr kleine Rotationsseitenbanden, die durch die nahezu vollständige Ausmittelung der CSA-Verbreiterung für alle Proben hervorgerufen werden (Abb. 13).

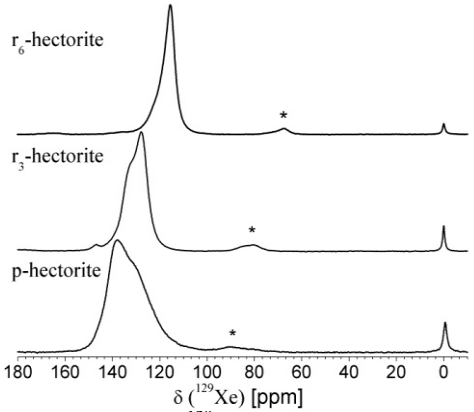

Abb. 13: CF-HP ^{129}Xe MAS Spektrum von adsorbiertem Xenon bei 298K in p-, r_3 und r_6-Hectorit. Seitenbanden sind mit * markiert. Reprinted with permission from C. D. Keenan, M. M. Herling, R. Siegel, N. Petzold, C. R. Bowers, E. A. Rössler, J. Breu, J. Senker, *Langmuir* **2013**, *29*, 643-652. Copyright 2013 American Chemical Society

Anhand dieser Messung und unter Anwendung des Demarquay-Fraissard-Modells kann ein effektiver Porendurchmesser berechnet werden. Dabei wird die chemische Verschiebung des ^{129}Xe-Signals mit einer freien Weglänge λ des Xenonmoleküls im Porenraum korreliert, unter der Annahme, dass keine ladungsinduzierte Verschiebung des Signals vorhanden ist. Es wurden sowohl das Hauptsignal, als auch die Schulter für die Berechnung berücksichtig. Die erhaltenen Porendurchmesser von 5.9-6.7 Å korrelieren gut mit den erhaltenen Porendurchmessern aus Ar/Ar(l)-Physisorptionsmessungen von 5-7 Å. Darüber hinaus wurde die Xe-Adsorptionsenthalpie aus der chemischen Verschiebung von VT ^{129}Xe-Spektren berechnet und mit den Enthalpien aus Xenon-Physisorptionsmessungen verglichen. Dabei wurde festgestellt, dass die Adsorbat-Adsorbat-Wechselwirkungen bei hoher Beladung dominieren und somit die Enthalpie verringern. Bei hoher Ladung stimmen die erhaltenen Werte -14(1) kJ/mol bei Schichtladung 0.48 p.f.u. und -17(1) kJ/mol für eine Schichtladung von 0.39 p.f.u.) aus beiden Methoden überein. Um nun diese Adsorbat-Adsorbat-Wechselwirkungen zu verringern, sind geringe Beladungen nötig, welche nur bei einer Steigerung der ^{129}Xe-Polarisation auf über 30 % erreicht werden können. Zusammenfassend wurde in diesem Manuskript gezeigt, dass die CF-HP ^{129}Xe Festkörper-NMR-Spektroskopie gut geeignet ist um Struktur- und Oberflächenänderungen mikropröser, gepillarter Schichtsilikate zu untersuchen.

Details und weitere Diskussion:

Characterizing the Micropore Size Distribution of Pillared Interlayered Clays by Hyperpolarized ^{129}Xe MAS NMR

Caroline D. Keenan, Markus M. Herling, Reneé Siegel, Ernst A. Rössler, Josef Breuand Jürgen Senker, *Langmuir*, **2013**, *29*, 642-652.

4.4 MOPS – Eine neue Klasse mikroporöser, stereo- und größenselektiver Hybridmaterialien

Die in Kapitel 4.2 diskutierte Ladungsreduktionsmethode wurde mit einem Na-Hectorit ($Na_{0.47(3)}[Mg_{2.59(5)}Li_{0.17(3)}]Si_4O_{10}F_2$) durchgeführt, wobei in diesem Fall Mg^{2+} in die Lücken der Oktaederschicht migriert und somit die Reduktionsdauer signifikant verkürzt.

Zur Untersuchung möglicher Trenneigenschaften chiral gepillarter Schichtsilikate, wurden vier Hectorite unterschiedlicher Schichtladung (0.47, 0.44, 0.39 und 0.36 p.f.u.) jeweils mit enantiomerenreinem (-)- und (+)-$Co(sep)^{3+}$-Komplex (sep = $C_{12}H_{30}N_8$ = 1,3,6,8,10,13,16,19-octaazabicyclo[6.6.6]-eicosane) gepillart. Die erhaltenen mikroporösen Hybridmaterialien UBT-1 bis UBT-8 weisen einen Zwischenschichtabstand von 16.1(1)Å und somit eine Porenhöhe von 6.5(1)Å auf. Aufgrund der unterschiedlichen Ladungsdichten der Wirtsstrukturen konnte die Porenweite mit sinkender Ladungsdichte graduell erhöht werden. Dies ist durch die Verschiebung in der Porenverteilung zu erkennen (Abb. 14).

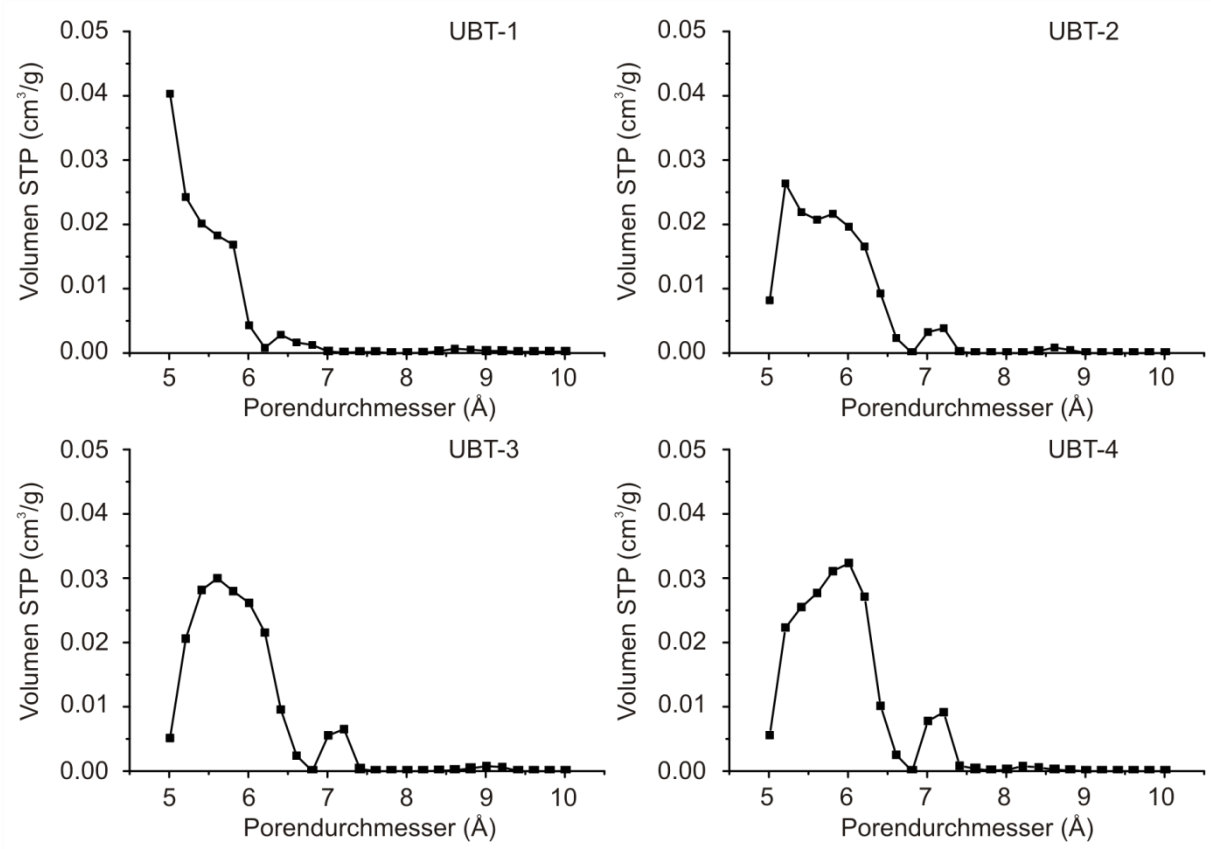

Abb. 14: Porenverteilung aus Argon-Physisorptionsmessungen von UBT-1 bis UBT-4.

Diese graduelle Erhöhung der Porenweite von insgesamt ca. 0.5 Å mit 0.1-0.2 Å Schritten je Reduktionsstufe ist weder bei Zeolithen noch bei MOFs realisierbar und steigert somit die Attraktivität der neuen mikroporösen Materialien (MOPS). Diese genaue Einstellung ermöglicht die Anpassung der Mikroporen auf ein gewünschtes Substrat um somit die Wirt-

Gast-Wechselwirkung zu optimieren und folglich die Effektivität von Trennprozessen zu maximieren.

Eine mögliche Größenselektivität wurde durch Adsorptionsversuche von 2-Methyl-but-3-yn-2-ol und (±)-But-3-yn-2-ol bestätigt. Dabei konnte das Applikationsmischungsverhältnis 2-Methyl-but-3-yn-2-ol/(±)-But-3-yn-2-ol von 1.05 auf 0.36 (UBT-1) verändert werden. Das kleinere Adsorbatmolekül ((±)-But-3-yn-2-ol) wird durch stärkere Wechselwirkungen mit dem Porenraum bevorzugt adsorbiert. Mit steigender Porenweite verändert sich das Verhältnis auf 0.46 (UBT-2), 0.50 (UBT-3) und 0.57 (UBT-4), was die Signifikanz der Anpassung des Porenraums widerspiegelt.

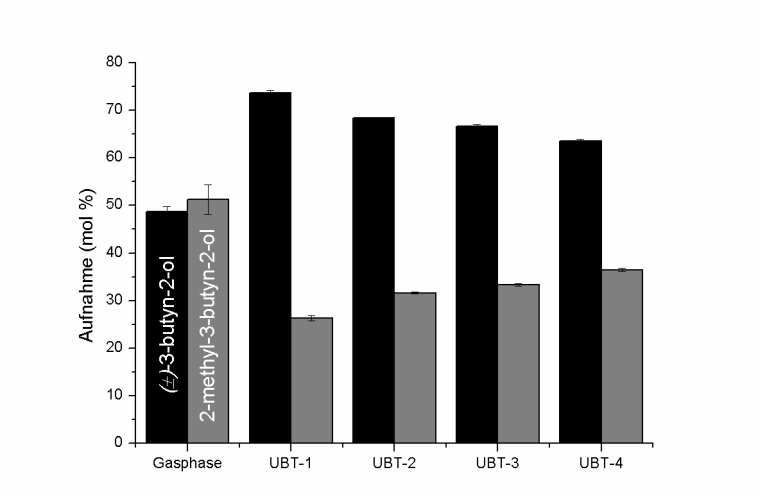

Abb. 15: Molare Verhältnisse der Adsorption einer Mischung (±)-But-3-yn-2-ol/-Methyl-but-3-yn-2-ol von UBT-1 bis UBT-4.

Neben der Größenselektivität wurde bei der Adsorption von *(±)*-But-3-yn-2-ol eine Enantiodiskriminierung beobachtet. Die chirale Information des enantiomerenreinen $Co(sep)^{3+}$-Komplexes kann bei hoher Passgenauigkeit der Porenweite mit dem Substrat auf das Adsorbent ((±)-But-3-yn-2-ol) übertragen werden (Abb. 16).

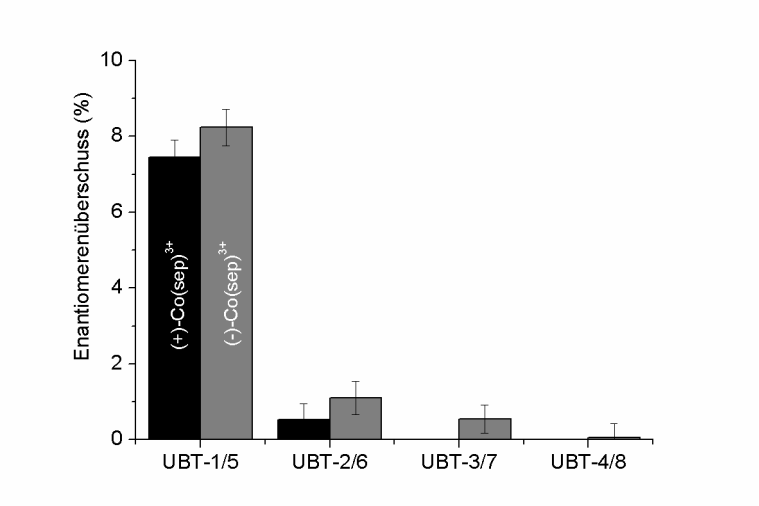

Abb. 16: Enantiomerenüberschuss der Stereoselektivität von UBT-1 bis UBT-8 bei Adsorption von *(±)*-But-3-yn-2-ol

Im Falle des (+)-Co(sep)$^{3+}$-Komplexes als molekularer Abstandshalter wird bevorzugt *(R)*-But-3-yn-ol, im Falle des (-)-Co(sep)$^{3+}$-Komplexes bevorzugt *(S)*-But-3-yn-ol adsorbiert. Dabei konnte ein Enantiomerenüberschuss von 7.45±0.45 % ((+)-Co(sep)$^{3+}$) und 8.24±0.48 % ((-)-Co(sep)$^{3+}$) erreicht werden. Bei steigender Porenweite wurde eine Verringerung der Enantiodiskriminierung auf 0 % festgestellt, was auch hier darauf zurückzuführen ist, dass die Stärke der Gast-Pillar-Wechselwirkung nicht mehr ausreicht um ein Enantiomer bevorzugt zu adsorbieren. Dies ermöglicht die zukünftige Verwendung des Hybridmaterials als stationäre Phase mit höherer Bodenanzahl in der Chromatographie, um die vollständige Trennung des Racemats zu erreichen.

Mit Hilfe von chiralen MOPS konnte in dieser Arbeit weltweit zum ersten Mal die Enantiodiskriminierung in Abhängigkeit der Ladungsdichte des Silikats und somit der Pillardichte im Zwischenschichtraum erreicht werden. Die graduelle Anpassung der Porenweite, kombiniert mit möglichen funktionalen Pillarmolekülen spiegelt die Vorteile der Modularität dieser neuen Materialklasse wider und legt den Grundstein für weitere Untersuchungen.

Details und weitere Diskussion:

MOPS – A New Class of Stereo and Size Selective Class of Microporous Hybrid Materials

Markus M. Herling, Mathias Schwedes, Sebastian Seibt, Hussein Kalo, Ulrike Lacher, Rainer Schobert and Josef Breu, *to be submitted.*

4.5 „Gate Opening“ in zweidimensional geordneten MOPS durch CO-Adsorption

Das ellipsoidale Me_2DABCO^{2+}-Molekül besitzt aufgrund seiner Geometrie die Möglichkeit in Abhängigkeit des Gastmoleküls seine Orientierung im Zwischenschichtraum responsiv zu verändern. Dabei wurde in diesem Manuskript das unterschiedliche Adsorptionsverhalten von N_2 und CO in Zusammenarbeit mit Dr. Ryotaro Matsuda an der Kyoto University untersucht.

Der verwendete Hectorit ($Na_{0.47(3)}[Mg_{2.59(5)}Li_{0.17(3)}]Si_4O_{10}F_2$) mit einer Schichtladung von 0.47(3) p.f.u. wurde mit Me_2DABCO^{2+}gepillart und so ein mikroporöses Hybridmaterial (UBT-9) mit einer Porenweite von 4-6 Å erhalten. Der molekulare Abstandshalter (Me_2DABCO^{2+}) ordnete sich in einer $2a \times 2a$ Überzelle im Zwischenschichtraum an. Diese geordnete Verteilung konnte durch das Auftreten einer *10*-Bande im Pulverdiffraktogramm bestätigt werden. Die Ladungsdichte der Einheitszelle (50.52 $Å^2$/+) des Wirtsgitters mit einer Schichtladung von 0.94 stimmt mit der Ladungsdichte der Pillarmoleküle in der hexagonalen Überzelle überein (47.38 $Å^2$/+).

Die elektrostatische Anziehung der negativ geladenen Wirtsstruktur und der positiv geladenen Zwischenschicht minimiert den Basalabstand, welcher durch die Gestalt des Me_2DABCO^{2+} bestimmt wird. Das Pillarmolekül orientiert sich mit seiner Längsachse parallel zur Schichtstruktur, sodass ein Basalabstand im trockenen Zustand von 13.9(1) $Å^2$ realisiert wurde. Im Gegensatz zur Adsorptionsisotherme von N_2 bei 77 K, zeigte die Adsorption von CO bei 82 K keinen für rein mikroporöse Materialien charakteristischen Typ I-Isothermenverlauf (Abb. 17).

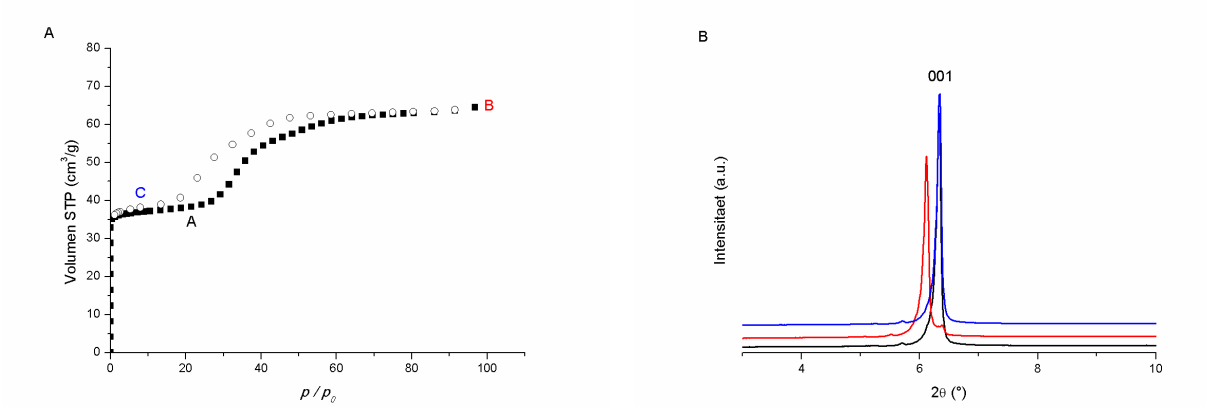

Abb. 17: CO-Phyisorptionsisotherme (A) und Röntendiffraktogramm des *001*-Reflexes von UBT-9.

Im Niederdruckbereich (bis ca. 35 kPa) wurde das zur Verfügung stehende Mikroporenvolumen mit CO gefüllt. Bei steigendem Druck wird der Grenzwert überschritten, bei dem die Adsorptionsenthalpie ausreicht um die elektrostatische Anziehung der negativen Schicht mit

der positiven Zwischenschicht zu überwinden. Dies bewirkt eine Erhöhung des Basalabstandes um 0.6 Å, woraus eine zusätzliche Adsorption von CO in Höhe von ca. 70 % resultiert, was auf eine Reorientierung des ellipsoidalen Pillarmoleküls zurückzuführen ist.

Im Falle des N_2-Moleküls ist die Adsorption auf die Füllung des ursprünglichen Porenvolumens beschränkt, da die Adsorptionsenthalpie des N_2-Moleküls nicht ausreicht um die elektrostatischen Wechselwirkungen im Material zu überwinden. Aufgrund des sehr unterschiedlichen Adsorptionsverhaltens beider Gase zusammen mit dem Auftreten des „*gate opening*"-Effekts könnte dieses Material für die CO/N_2-Trennung verwendet werden.

In diesem Manuskript wurden zum ersten Mal MOPS mit atmenden Netzwerkstrukturen und selektivem „*gate opening*"-Effekt in Abhängigkeit von den verwendeten Gasmolekülen gezeigt. Dieses Verhalten wurde bereits mit der Materialklasse der PCP's erfolgreich in Gasseparationsprozessen etabliert und kann nun auch für MOPS intensiv untersucht werden.

Details und weitere Diskussion:

Gate Opening in 2-D-ordered Microporous Organically Pillared Layered Silicates (MOPS) upon CO Adsorption

Markus M. Herling, Hiroshi Sato, Liangchun Li, Hussein Kalo, Ryotaro Matsuda, Susumu Kitagawa and Josef Breu, *to be submitted.*

5. Verwendete Literatur

[1] C. Martinez, A. Corma, *Coordination Chemistry Reviews* **2011**, *255*, 1558-1580.

[2] A. Corma, A. Martinez, *Advanced Materials* **1995**, *7*, 137-144.

[3] N. Rahimi, R. Karimzadeh, *Applied Catalysis A – General* **2011**, *398*, 1-17.

[4] G. W. Huber, A. Corma, *Angewandte Chemie – International Edition* **2007**, *46*, 7184-7201.

[5] W. O. Haag, Catalysis by Zeolites – *Science and Technology, Elsevier, Amsterdam* **1994**, 1375-1394.

[6] W. Vermeiren, J. P. Gilson, *Topics in Catalysis* **2009**, *52*, 1131-1161.

[7] A. K. Cheetham, G. Ferey, T. Loiseau, *Angewandte Chemie – International Edition* **1999**, *38*, 3268-3292

[8] J. Caro, M. Noack, P. Kolsch, R. Schafer, *Microporous and Mesoporous Materials* **2000**, *38*, 3-24.

[9] S. Zones, *Microporous and Mesoporous Materials* **2011**, *144*, 1-8.

[10] W. Schmidt, *Chemcatchem* **2009**, *1*, 53-67.

[11] F. Schüth, *Annual Review of Materials Research* **2005**, *35*, 209-238.

[12] J. Weitkamp, *Solid State Ionics* **2000**, *131*, 175-188.

[13] A. Corma, *Journal of Catalysis* **2003**, *216*, 298-312.

[14] S. Kitagawa, R. Kitaura, S. Noro, *Angewandte Chemie – International Edition* **2004**, *43*, 2334-2375.

[15] O. M. Yaghi, M. O'Keeffe, N. W. Ockwig, H. K. Chae, M. Eddaoudi, J. Kim, *Nature* **2003**, *423*, 705-714.

[16] H. Li, M. Eddauodi, M. O'Keeffe, O. M. Yaghi, *Nature* **1999**, *402*, 276-279.

[17] A. U. Czaja, N. Trukhan, U. Mueller, *Chemical Society Reviews* **2009**, *38*, 1284-1293.

[18] J. R. Li, R. J. Kuppler, H. C. Zhou, *Chemical Society Reviews* **2009**, *38*, 1477-1504.

[19] L. Ma, C. Abney, W. Lin, *Chemical Society Reviews* **2009**, *38*, 1248-1256.

[20] Y. Liu, W. Xuan, Y. Cui, *Advanced Materials* **2010**, *22*, 4112-4135.

[21] S. Kitagawa, M. Kondo, *Bulletin of the Chemical Society of Japan* **1998**, *71*, 1739-1753.

[22] G. Ferey, C. Serre, *Chemical Society Reviews* **2009**, *38*, 1380-1399.

[23] M. M. Herling, J. Breu, *Zeitschrift für Anorganische und Allgemeine Chemie* **2014**, *640*, 547-560.

[24] R. M. Barrer, D. M. Macleod, *Transactions of the Faraday Society* **1955**, *51*, 1290-1300.

[25] R. M. Barrer, *Clays and Clay Minerals* **1989**, *37*, 385-395.

[26] R. M. Barrer, *Pure and Applied Chemistry* **1989**, *61*, 1903-1912.

[27] G. W. Brindley, R. E. Sempels, *Clay Minerals* **1977**, *12*, 229-237.

[28] A. Gil, L. M. Gandia, M. A. Vicente, *Catalysis Reviews-Science and Engineering* **2000**, *42*, 145-212.

[29] A. Gil, S. Korili, M. Vicente, *Catalysis Reviews-Science and Engineering* **2008**, *50*, 153-221.

[30] J. T. Kloprogge, *Journal of Porous Materials* **1998**, *5*, 5-41.

[31] Z. Ding, J. T. Kloprogge, R. L. Frost, G. Q. Lu, H. Y. Zhu, *Journal of Porous Materials* **2001**, *8*, 273-293.

[32] A. Gil, S. A. Korili, R. Trujilano, M. A. Vicente, *Pillared Clays and Related Catalysts*, Springer, New York **2010**.

[33] M. A. Vicente, A. Gil, F. Bergaya, in *Handbook of Clay Science* ,Vol. 5A, (Eds.: F. Bergaya, G. Lagaly), Elsevier, Amsterdam **2013**, 523-557.

[34] H. Kalo, M. W. Moeller, D. A. Kunz, J. Breu, *Nanoscale* **2012**, *4*, 5633-5639.

[35] J. Breu, W. Seidl, A. J. Stoll, K. G. Lange, T. U. Probst, *Chemistry of Materials* **2001**, *13*, 4213-4220.

[36] M. Stöter, D. A. Kunz, M. Schmidt, D. Hirsemann, H. Kalo, B. Putz, J. Senker, J. Breu, *Langmuir* **2013**, *29*, 1280-1285.

[37] H. Kalo, M. W. Möller, M. Ziadeh, D. Dolejs, J. Breu, *Applied Clay Science* **2010**, *48*, 39-45.

[38] F. Bergaya, G. Lagaly, in *Handbook of Clay Science* ,Vol. 1, (Eds.: F. Bergaya, B. K. G. Theng, G. Lagaly), Elsevier, Amsterdam **2006**.

[39] J. Breu, W. Seidl, A. Stoll, *Zeitschrift fur Anorganische und Allgemeine Chemie* **2003**, *629*, 503-515.

[40] I. Berend, J. M. Cases, M. Francois, J. P. Uriot, L. Michot, A. Masion, F. Thomas, *Clays and Clay Minerals* **1995**, *43*, 324-336.

[41] J. M. Cases, I. Berend, M. Francois, J. P. Uriot, L. J. Michot, F. Thomas, *Clays and Clay Minerals* **1997**, *45*, 8-22.

[42] R. A. Schoonheydt, T. Pinnavaia, G. Lagaly, N. Gangas, *Pure and Applied Chemistry* **1999**, *71*, 2367-2371.

[43] K. S. W. Sing, *Pure and Applied Chemistry* **1982**, *54*, 2201-2218.

[44] G. Lagaly, *Clay Minerals* **1981**, *16*, 1-21.

[45] R. Mariychuk, A. Baumgartner, F. E. Wagner, A. Lerf, A. Dubbe, R. Moos, J. Breu, *Chemistry of Materials* **2007**, *19*, 5377-5387.

[46] A. Baumgartner, K. Sattler, J. Thun, J. Breu, *Angewandte Chemie - International Edition* **2008**, *47*, 1640-1644.

[47] A. Baumgartner, F. E. Wagner, M. Herling, J. Breu, *Microporous and Mesoporous Materials* **2009**, *123*, 253-259.

[48] U. Hofmann, R. Klemen, Zeitschrift für *Anorganische und Allgemeine Chemie* **1950**, *262*, 95-99.

[49] W. F. Jaynes, J. M. Bigham, *Clays and Clay Minerals* **1987**, *35*, 440-448.

[50] W. F. Jaynes, S. J. Traina, J. M. Bigham, C. T. Johnston, *Clays and Clay Minerals* **1992**, *40*, 397-404.

[51] J. Demarquay, J. Fraissard, *Chemical Physics Letters* **1987**, *136*, 314-318.

[52] R. M. Barrer, R. J. B. Craven, *Journal of the Chemical Society-Faraday Transactions* **1992**, *88*, 645-651.

[53] R. M. Barrer, D. L. Jones, *Journal of the Chemical Society A -Inorganic Physical Theoretical* **1971**, 2594-2603.

[54] S. M. Thomas, J. A. Bertrand, M. L. Occelli, J. M. Stencel, S. A. C. Gould, Chemistry *of Materials* **1999**, *11*, 1153-1164.

[55] H. B. Lao, C. Detellier, *Clays and Clay Minerals* **1994**, *42*, 477-481.

[56] P. Sozzani, S. Bracco, A. Comotti, M. Mauri, R. Simonutti, P. Valsesia, C*hemical Communications* **2006**, *18*, 1921-1923.

[57] H. Kalo, M. W. Moller, D. A. Kunz, J. Breu, *Nanoscale* **2012**, *4*, 5633-5639.

[58] H. Kalo, W. Milius, J. Breu, *RSC Advances* **2012**, *2*, 8452-8459.

[59] W. Seidl, J. Breu, *Zeitschrift fur Kristallographie* **2005**, *220*, 169-176.

[60] J. Breu, W. Seidl, J. Senker, *Zeitschrift fur Anorganische und Allgemeine Chemie* **2004**, *630*, 80-90.

[61] F. Tsvetkov, J. White, *Journal of the American Chemical Society* **1988**, *110*, 3183-3187.

[62] J. Breu, A. Stoll, K. G. Lange, T. Probst, *Physical Chemistry Chemical Physics* **2001**, *3*, 1232-1235.

[63] M. Stöcker, L. Seyfarth, D. Hirsemann, J. Senker, J. Breu, *Applied Clay Science* **2010**, *48*, 146-153.

6. Publikationen und Manuskripte

6.1 Darstellung des Eigenanteils

Die in dieser Dissertation vorgestellten Ergebnisse wurden in Zusammenarbeit mit Kooperationspartnern erhalten und bei den unten aufgeführten Magazinen eingereicht oder bereits veröffentlicht. Nachfolgend wird der Anteil aller Co-Autoren an den Veröffentlichungen genau dargestellt.

6.2 Mikoporöse Hybridmaterialien auf Basis von organisch-gepillarten synthetischen Schichtsilikaten (Appendix 1)

Diese Arbeit wurde im Journal *Zeitschrift für anorganische und allgemeine Chemie* unter dem Titel

"The Largely Unknown Class of Microporous Hybrid Materials: Clays Pillared by Molecules"

von Markus M. Herling und Josef Breu

veröffentlicht.

Mein Eigenanteil an dieser Veröffentlichung war die Literaturrecherche, die Durchführung und Charaktersierung der Experimente und das Verfassen des Manuskripts zusammen mit Josef Breu.

Mein geschätzter Eigenanteil: ca. 80 %

6.3 Einstellung der Porengröße mikroporöser, gepillarter Schichtsilikate durch gezielte Schichtladungsreduktion (Appendix 2)

Diese Arbeit wurde im Journal *Langmuir* unter dem Titel

"Tailoring the Pore Sizes of Microporous Pillared Interlayered Clays through Layer Charge Reduction"

von Markus M. Herling, Hussein Kalo, Sebastian Seibt, Rainer Schobert und Josef Breu

veröffentlicht. Die Arbeit wurde in Zusammenarbeit mit dem Lehrstuhl Organische Chemie I durchgeführt.

Mein Eigenanteil an dieser Veröffentlichung war die Synthese der PILCs und deren Charakterisierung.

Des Weiteren habe ich die Messungen und Auswertung der Diffraktogramme und Physisorptionsmessungen selbst durchgeführt. Die WDX Messung wurde in Zusammenarbeit mit Herrn Detlef Krausse (BGI Bayreuth) durchgeführt. Darüber hinaus verfasste ich das Manuskript und war an der Diskussion und Korrektur beteiligt.

- Hussein Kalo unterstütze mich bei der Synthese des K-Hectorits
- Sebastian Seibt stand für Diskussionen bezüglich der Pillarsynthese zur Verfügung
- Josef Breu und Rainer Schobert standen für Diskussionen und Korrekturen des Manuskripts zur Verfügung.

Mein geschätzter Eigenanteil: ca. 90 %

6.4 Charakterisierung der Porengrößenverteilung gepillarter Schichtsilikate mit hyperpolarisierter ^{129}Xe MAS NMR-Spektroskopie (Appendix 3)

Diese Arbeit wurde im Journal *Langmuir* unter dem Titel

"The Porosity of Pillared Clays Studied by Hyperpolarized Xe NMR Spectroscopy and Xe Adsorption Isotherms"

von Caroline D. Keenan, Markus M. Herling, Renée Siegel, Nikolaus Petzold, Clifford R Bowers, Ernst A. Rössler, Josef Breu und Jürgen Senker

veröffentlicht. Die Arbeit wurde in Zusammenarbeit mit dem Lehrstuhl Anorganische Chemie III, Experimentalphysik II der Universität Bayreuth und dem Department of Chemistry der University of Florida durchgeführt.

Mein Eigenanteil an dieser Veröffentlichung war die Synthese der PILCs und deren Charakterisierung bezüglich des Adsorptionsverhaltens. Dabei habe ich die Argon und Xenon-Adsorptionsisothermen sowie die Diffraktogramme der PILCs selbst gemessen und ausgewertet. Darüber hinaus habe ich die betreffenden Teile des Manuskripts verfasst und war an der Diskussion und Korrektur beteiligt.

- Caroline D. Keenan führte die NMR spektroskopischen Messungen und Auswertungen durch, verfasste das Manuskript und war an der Diskussion und Korrektur beteiligt.
- Renée Siegel unterstützte bei den NMR spektroskopischen Untersuchungen…
- Clifford R. Bowers und Nikolaus Petzold waren am Aufbau der ^{129}Xe-Apparatur beteiligt
- Josef Breu, Ernst A. Rössler und Jürgen Senker standen für Diskussionen und Korrekturen des Manuskripts zur Verfügung.

Mein geschätzter Eigenanteil: ca. 50 %

6.5 MOPS – Eine neue Klasse mikroporöser, stereo- und größenselektiver Hybridmaterialien (Appendix 4)

Dieses Manuskript mit dem Titel

MOPS – A New Class of Stereo and Size Selective Class of Microporous Hybrid Materials

von Markus M. Herling, Mathias Schwedes, Sebastian Seibt, Hussein Kalo, Ulrike Lacher, Rainer Schobert und Josef Breu

wurde zur Veröffentlichung vorbereitet. Die Arbeit wurde in Zusammenarbeit mit dem Lehrstuhl Organische Chemie I durchgeführt.

Mein Eigenanteil an dieser Veröffentlichung war die Synthese und Charakterisierung der MOPS.

Des Weiteren habe ich die Messungen und Auswertung der Diffraktogramme und Physisorptionsmessungen selbst durchgeführt. Die WDX-Messung wurde in Zusammenarbeit mit Herrn Detlef Krausse (BGI Bayreuth) durchgeführt. Darüber hinaus verfasste ich das Manuskript und war an der Diskussion und Korrektur beteiligt.

- Mathias Schwedes und Sebastian Seibt assistierten bei den Gasphasen Experimenten
- Mathias Schwedes und Ulrike Lacher führten die GC-Messungen und Eichungen durch
- Hussein Kalo unterstütze mich bei der Synthese des Schichtsilikates
- Josef Breu und Rainer Schobert standen für Diskussionen und Korrekturen des Manuskripts zur Verfügung.

Mein geschätzter Eigenanteil: ca. 80 %

6.6 „Gate Opening“ in zweidimensional geordneten MOPS durch CO Adsorption (Appendix 5)

Dieses Manuskript mit dem Titel

Gate Opening in 2-D-ordered Microporous Organically Pillared Layered Silicates (MOPS) upon CO Adsorption

von Markus M. Herling, Hiroshi Sato, Liangchun Li, Hussein Kalo, Ryotaro Matsuda, Susumu Kitagawa und Josef Breu

wurde zur Veröffentlichung vorbereitet. Die Arbeit wurde in Zusammenarbeit mit dem Institute for Integrated Cell-Material Sciences der Kyoto University in Japan durchgeführt.

Mein Eigenanteil an dieser Veröffentlichung war die Synthese und Charakterisierung der MOPS.

Des Weiteren habe ich die Messungen und Auswertung der Diffraktogramme und Ar-Physisorptionsmessungen sowie die Auswertung der CO und N_2 Physisorptionsmessungen selbst durchgeführt. Die WDX Messung wurde in Zusammenarbeit mit Herrn Detlef Krausse (BGI Bayreuth) durchgeführt. Darüber hinaus verfasste ich das Manuskript und war an der Diskussion und Korrektur beteiligt.

- Hiroshi Sato führte die in-situ PXRD Messungen der CO und N_2 Physisorptionsmessung durch und stand für Diskussionen zur Verfügung
- Liangchun Li führte CO und N_2 Messungen durch und stand für Diskussionen zur Verfügung
- Hussein Kalo unterstütze mich bei der Synthese des Schichtsilikates
- Ryotaro Matsuda, Susumu Kitagawa und Josef Breu standen für Diskussionen und Korrekturen des Manuskripts zur Verfügung.

Mein geschätzter Eigenanteil: ca. 75 %

Appendix 1

The Largely Unknown Class of Microporous Hybrid Materials: Clays Pillared by Molecules

Markus M. Herling[1] and Josef Breu[1,*]

[1]Lehrstuhl für Anorganische Chemie I, Universität Bayreuth, Universitätsstr. 30, 95440 Bayreuth, Germany

*e-mail: josef.breu@uni-bayreuth.de

Z. Anorg. Allg. Chem. **2014**, *640*, *(3-4)*, 547-560.

DOI: 10.1002/zaac.201300540

The Largely Unknown Class of Microporous Hybrid Materials: Clays Pillared by Molecules

Markus M. Herling[a] and Josef Breu*[a]

Keywords: Pillared Interlayered Clay; PILC; Clays; Microporous materials; Hybrid materials

Abstract. The review summarizes recent progress in the field of synthetic clay minerals pillared with organic or metal complex cations (PILCs). We briefly introduce the field of such PILCs and discuss the weaknesses of the state of the art characterization chart of PILCs. When PILCs are made from nanoscopic host materials like natural clay minerals, charge heterogeneity accompanied by interstratification, the turbostratic disorder in the stacking and the influence of the large external surface weaken essential analytical results. Turning to coarse-grained, well ordered clay minerals synthesized from the melt at temperatures above 1000 K removes all these obstacles and allows to present consistent data underlining the validity of the appealing pillaring concept: Refinement of PILC structures gives information on the pillar-host interaction and the orientation of pillars in the interlayer space. Two-dimensional superstructure reflections give direct evidence of the well-ordered lateral arrangement of pillars. And most importantly, analysis of chemical composition and physisorption isotherms are not corrupted by contributions of large external surfaces and this allows for predicting micropore volume and widths from pillar/host ratios in combination with pillar size/shape. Moreover, recent progress allows fine-tuning the charge density of the host lattice *post-synthesis*. Such deliberate and fine-graded alteration of the pillar density in turn permits adjusting the pore size in steps as small as 0.1 Å to a given adsorbate and thus will pave the way to maximize adsorption enthalpies and to improve selectivity. This feature is unique to PILCs and is not available to MOFs whose porosity can be adjusted only in steps no smaller than the order of chemical bond lengths. Rational design of microporous hybrid materials with full control over size, shape, and chemical nature of micropores certainly represents the strength and great potential of the pillaring approach.

1. Introduction

Crystalline microporous oxides offer size- and shape-selectivity in adsorptivity and are well-known for their ability to control reaction pathways via reactant or transition state selectivity. In particular alumosilicate zeolites and aluminophophates are long-established catalysts for fuel cracking and the synthesis of a variety of commodity chemicals. Besides the narrow pore size distribution and large surface area, zeolites stand out for their stability in respect to temperature, hydrolysis and low pH. Over time by adjusting synthesis regimes and varying molecular templates a plethora of framework-topologies could be realized.[1–5]

* Prof. Dr. J. Breu
Fax: +49-921-55-2788
E-Mail: josef.breu@uni-bayreuth.de
[a] Lehrstuhl für Anorganische Chemie I
Universität Bayreuth
Universitätsstr. 30
95440 Bayreuth, Germany

Josef Breu was born in 1961 and received his Ph.D. in Chemistry at the University of Regensburg in 1992. Following a Postdoc with A.C.R. Catlow at the Royal Institution of Great Britain he returned to Regensburg for his Habilitation. In 2003 he went to the University of Bayreuth for a Full Professor holding the Chair of Inorganic Chemistry I. Josef Breús research priliminarily focuses on layered materials, PILCs, nanocomposites, mesostrucuring of inorganic colloids, and all aspects of polymorph screening.

Markus M. Herling was born in 1985 and received his B.Sc. in Chemistry (2008) and M.Sc. in Materials Science and Catalysis (2010) from the University of Bayreuth. Since 2010 he has been pursuing his PhD in the group of Josef Breu at the University of Bayreuth. His interest is in the synthesis of porous hybrid materials through pillaring and their possible application.

Since the early 1990's Metal Organic Frameworks (MOFs), also called porous coordination polymers (PCPs), have been established as new class of microporous, organic-inorganic hybrid materials.[6] The inorganic metal acts as a node for the organic linkers, which are building a uniform framework.

Again many different framework topologies could be realized over the years by combining various inorganic nodes with an almost unlimited pool of organic linkers. Using different node-linker combinations not only allows for tuning shape and size of the micropores but also their chemical nature.[7] While in respect to thermal and chemical stability MOFs are inferior to zeolites the modular character of MOF-assembly allows for shifting the focus from high temperature reactions to improving the selectivity of adsorption. Separation and purification of gases and even stereodiscrimination have become the main issues in potential applications of MOFs.[8–11] PCPs can be classified into three different generations as proposed by *Kitagawa* et al. 1998.[12] The first generation materials have no permanent porosity, because the porosity collapsed irreversible after solvent removal. The porosity of second generation materials may be regarded most analogous to zeolites and show interesting adsorption behavior. The third generation materials are of flexible nature and inherit a reversibly dynamic, porous framework.

In contrast to the rigid framework of zeolites, PCP's exhibiting such a gate opening or breathing effect have attracted much interest with materials researchers.[13]

Solids thrive for dense packings and microporous materials do not represent a thermodynamic equilibrium. The metastability of these non-dense solids therefore can only be assured by strong covalently linked (sub-)structures and synthesis follows two principle routes: 1. Initially densely packed intermediates are obtained where the micropores are filled by guests and templates that are subsequently removed. 2. Topotactic reactions are applied that leave a rigid (sub-) structure, for instance layers, unchanged, while generating porosity by moving them apart ("pillaring").

Largely unnoticed by both, the zeolite and the MOF-communities, since the early 50's pillaring of layered materials, in particular 2:1 layered silicates (clay minerals), has been explored as a completely independent route to microporous materials. While for both, zeolites and MOFs, the framework topology due to the covalent character of the links may not be altered *post-synthesis*, for these Pillared Interlayered Clays (PILCs) there is no rigid linkage between the two-dimensional interlayer surfaces of the clay host and the pillars which are held in place only by non-directional electrostatic interactions. As a consequence, the porosity of PILCs depends, apart from the nature of the pillars, solely on the homogeneity and magnitude of the negative layer charge of the silicate. *Breu* et al. have recently developed methods to fully control these two properties. Layered silicates with homogeneous charge densities were made accessible on a large scale by an expeditious melt synthesis.[14–17] When intercalated with appropriate cations, microporous PILCs result, that are characterized by narrow pore size distributions and a high degree of long-range order of the pillar arrays.[18–20] By tuning the layer charge, functional PILCs with continuously adjustable microporosity are now available for the first time and in large quantities.[21–23] The option to model their interlayer cavities on the shape of particular guest molecules is a unique feature not available to MOFs whose porosity can be adjusted only in steps no smaller than the order of chemical bond lengths.

We start this review with an in depth discussion of the peculiarities of the pillaring concept followed by a brief non-comprehensive overview of the history of PILCs. In the last section, the sustainability, variability, and consistency of the pillaring concept will be underlined by summarizing recent results obtained by applying synthetic clay minerals as two-dimensional host structures.

2. Pillaring Concept

2.1 Definition

A technical report of the IUPAC in 1999 defines pillaring as "a process by which a layered compound is transformed in a thermally stable micro- and/or mesoporous material with retention of the layer structure. ··· A pillared compound has the following characteristics: (i) the layers are propped apart vertically and do not collapse upon removal of the solvent; (ii) the minimum increase in basal spacing is the diameter of the N_2 molecule, commonly used to measure surface areas and pore volumes: 0.315–0.353 nm; (iii) the pillaring agent has molecular dimensions and is laterally spaced in the interlamellar space on a molecular length scale; (iv) the interlamellar space is porous and at least accessible to molecules as large as N_2; there is no upper limit to the size of the pores. ··· There is no restriction on the nature of the intercalating agent or on the mechanism of intercalation."[24]

This IUPAC definition thus clearly requires that the microporosity is located in the interlayer space and classifies PILCs as porous subgroup of intercalation compounds. "The final criterion is accessibility of the interlayer region by molecules at least as large as N_2." As a consequence of the regular stacking of host layers and mono-sized pillars in the interlayer space, a layer spacing must be observed. Unfortunately, the technical report does not insist on a perfect one-dimensional crystallinity (translational symmetry) along the stacking direction. Only a "certain" order in the stacking is required: "The XRD pattern must show clearly the d_{001} line, but a rational series of d_{001} lines is not required." As will be discussed in some more detail later, this is the Achilles' heel of the IUPAC definition as the non-Bragg-nature of the *00l*-series gives plenty of room for speculation und interpretation. In any case a pillared material is translationally homogeneous and must be regarded a single phase. Nanocomposites of any type may not be called a pillared compound. Probing this single phase nature might not by trivial. In cases where one of the components of a composite material is amorphous sophisticated solid state NMR methods might be required. For instance, the single phase character of a pillared material may be cross-checked by solid state NMR techniques applying double quantum excitation.[25]

While earlier definitions asked for a minimum thermal stability of 200 °C, the temperature limit for a compound to be

Zeitschrift für anorganische und allgemeine Chemie ZAAC Journal of Inorganic and General Chemistry

regarded "thermally" stable is only indirectly defined in the technical report of the IUPAC as it is stated: "…after removal of the solvent, e.g. heating at 120 °C in air or N_2 (Ar, He) for the removal of water."[26]

2.2 Pecularities of Micropores Encountered in PILCs

By pillaring 2:1-layered silicates, microporosity is generated *post-synthesis* of the host by a topotactic incorporation of the pillaring agent in the interlayer region in a cation exchange reaction. The number of pillars is determined by the charge neutrality condition and thus is defined by the valency of the pillar and the charge density of the layered silicate. The electrostatic attraction between negative host and positive interlayer represents a strong driving force that without any doubt will minimize the basal spacing.[27] Elliptical pillars will therefore always arrange with their longer principal axis oriented in the plane of the interlayer space (Figure 1, top).

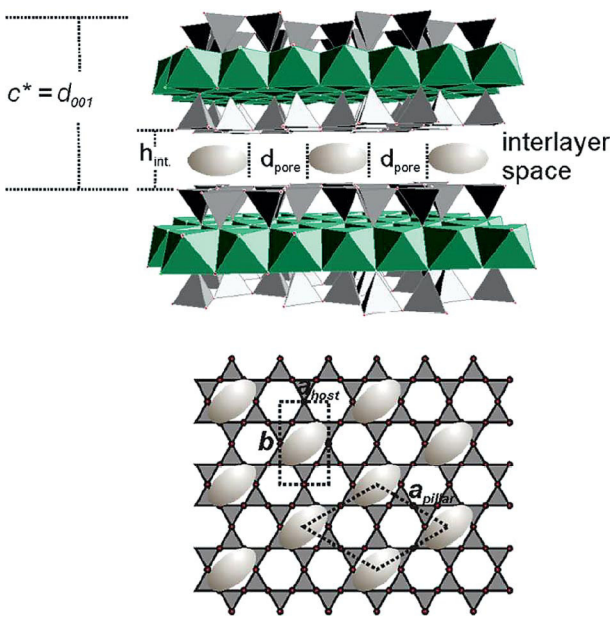

Figure 1. top: Structure of a pillared 2:1 layered silicate with the pore distance d_{pore}, the interlayer height h_{int} and c* as derived from *00l*-series; bottom: top view of the silicate sheet with hexagonal arrangement of pillar molecules. The distance between the pillars is larger than the *a*-axis of the silicate host.

In summary, the size and the shape of the micropores of PILCs is dependent on the following features:

a) Size and shape of the intercalated pillar

b) Valence/charge of the pillar

c) Layer charge (and charge homogeneity) of the layered silicate host

The micropores of PILCs are of slit shape (Figure 1, top). While the width of the slits is defined by the free volume between the pillars (d_{pore}), the height is defined by the shorter principal axis of the pillar which is related to the height of the interlayer space ($h_{int.}$). In order to allow N_2 to enter the interlayer space both these principle dimensions have to be larger than 3.2 Å. Actually, both pore widths have to be significantly bigger than this because the kinetic diameter of N_2 is known to be larger than 3.2 Å. The basal spacing as determined by X-ray diffraction measurements is the sum of the height of the interlayer space (h_{int}) and the thickness of the layer (9.6 Å).[15] Thus the lower limit for the basal spacing that still might allow access to the interlayer space may be estimated as being 12.8 Å.

The distance d_{pore} between the pillars is much more complex to be estimated. As a first approximation it may be assumed that the electrostatic repulsion between the cationic pillars in the interlamellar space will induce a hexagonal arrangement of the pillars (Figure 1, bottom). For a microporous material the distance between the pillars in any case will be greater than the *a*-axis (≈5.3 Å) of the layered silicate host (a_{host}). The two-dimensional lattice of the pillars therefore must be a superlattice (a_{pillar}) that for the moment may be assumed to be incommensurate to the host lattice. The lattice parameter a_{pillar} is determined by the valency of the pillar and the charge density of the host lattice. Subtracting the diameter of the pillar in the plane of the interlamellar space from a_{pillar} yields d_{pore}. For any given pillar there will be an upper limit for the charge density of the pillars where d_{pore} = 3.2 Å (see also Figure 12). Higher charge densities will result in higher pillar densities and d_{pore} will be too low to allow N_2 to enter the interlayer space. For any given charge density of the host layer, increasing the equivalent area (area occupied by the pillar in the plane of the interlayer space divided by its valence) of the pillars by either decreasing the valence or increasing the lateral dimension, will eventually also reduce d_{pore} to the limit where the interlayer space is no longer accessible.[28]

These considerations are of course only valid if the charge density of the host is strictly homogeneous.

The charge density of 2:1 layered silicates originates from isomorphous substitutions in the octahedral and/or tetrahedral layers (Figure 2).

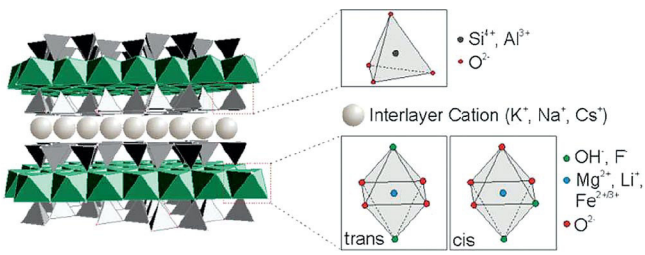

Figure 2. Structure of 2:1 layered silicates.

In order to produce a homogeneous charge density, this isomorphous substitution must thus be strictly statistical. Monte Carlo simulations of the order-disorder behavior of octahedral sheets of phyllosilicate layers suggest that for most compositions, the octahedral cations are segregating, that is, the layers exhibit charge inhomogeneities at low temperatures.[29] Although the degree of segregation has been found to be highly dependent on the nature of the cation, temperatures often exceeding 1000 K are necessary to achieve a disordered solid solution with a homogeneous charge density. At lower temperatures the different cations begin to cluster resulting in do-

Special Issue

mains of higher and lower charge density. Genesis of natural clay minerals like montmorillonite (dioctahedral 2:1 phyllosilicate of the smectite group[30]) typically takes place at low to moderate temperatures (< 400 K). Consequently, when determining the charge density applying the so-called alkylammonium method broad, sometimes bi-modal, charge density distributions are found.[31] Most likely, the charge density of natural and also synthetic clay minerals that were obtained at temperatures much below approx. 1000 K, varies spatially between different layers as well as within domains in a single layer.

The Coulomb interaction between host and pillars has been shown in computer simulations to be the structure determining interaction. The rather mobile cationic pillars in the interlayer space will therefore follow the clustering of isomorphous substitution.[32] The pillars will pack densely between host domains of higher charge density. Consequently, the micropore volume will be highly non-uniform. Charge homogeneity of the host lattice is thus a prerequisite for the pillaring concept to work.

The pillaring concept requires a permanent interlayer micropore volume. As already noticed by *Barrer*, the height of the interlayer gallery, h_{int}, is, however, not necessarily fixed.[33] Much similar to third generation PCPs, the basal spacing may expand further upon inclusion of appropriate sorbate molecules into the micropores. Most likely this breathing of micropores will be accompanied by a reorientation of the pillars. Ordinary non-porous intercalation compounds may, however, also incorporate guest molecules by a "swelling mechanism", which basically represents a thermodynamically favored solvation of interlayer cations and lacks selectivity. X-ray diffraction is incapable to distinguish between sorption into permanent but breathing micropores and swelling. Again, physisorption is the analytical method of choice to distinguish the two distinct cases of sorption.

2.3 Disorder in PILCs

Retrieving structural information on PILCs, or intercalation compounds in general, is inherently difficult because the anisotropic bonding situation in these layered compounds renders them prone to two distinct types of disorder: First statistical interstratification of different basal spacings along the stacking direction and second, stacking faults meaning that the phase relationship, the relative orientation and/or position of adjacent layers, is not strictly defined.

2.3.1. Interstratification

If the charge density, as discussed before, varies from layer to layer, the number of interlayer cations will fluctuate in adjacent interlayer regions and consequently the intracrystalline reactivity of interlayers within a stack of layers will be different. Since such a stack of parallel arranged layers may not necessarily be three-dimensionally ordered, it is commonly not referred to as crystal but as tactoid. The intracrystalline reactivity of clay minerals with inorganic interlayer cations like Na^+ may most easily be tested for by a simple hydration experiment referred to by "swelling with water". Given a homogeneous charge density, all interlayers would realize well defined hydration states of zero (0 WL, 9.6 Å), one (1 WL, 12.4 Å), and two layer hydrate (2 WL, 15.5 Å) as a function of increasing relative humidity with a stepwise change of hydration at well-defined levels. For all hydration states rational *00l* series are observed meaning that the translational symmetry along the stacking direction is strictly obeyed and a one-dimensional Bragg-type diffraction is observed. For clay minerals obtained by melt synthesis at temperatures > 1000 K little to no signs of interstratifications of differently hydrated interlayers within the same tactoid were seen and this unusual uniform intracrystalline reactivity, in turn again indicates a superb homogeneous charge density.[34–40] Contrary to this, for smectites (group name for 2:1 phyllosilicates, di- or trioctahedral, with hydrated exchangeable cations and a layer charge x = 0.2–0.6[30]) obtained at low temperatures at any intermediate relative humidity random interstratifications of 0, 1, 2, and 3 WL are realized.[41;42] The X-ray beam averages over all different basal spacings in a volume weighted manner and while these real basal spacings are well-defined and fixed, as a function of relative humidity, the ratio of different hydration varies and an apparent, artificial basal reflection is observed. Clear signs of interstratification are weak absolute intensities of the basal reflections, large full widths at half maximum with a dependency diverging from the usual 2θ-dependency, and most evident, the *00l*-series becomes irrational, meaning that the basal spacing calculated from different *00l* reflections varies according to *Mering*'s principles[43]. These principles suggest that for random interstratifications of two different basal spacings, the basal reflections are observed between the nominal positions of the *00l*-reflections of both end-members and the exact positions are fixed by the proportions of the end-member incorporated into the interstratification. Furthermore, the full width of half maximum, in addition to size/strain effects, is dominated by broadening caused by interstratifications. The broadening effect is most pronounced if the end-member reflections surrounding the basal reflection of the interstratifications are far apart. In the limiting case with very pronounced disorder in the stacking regularity, only a single broad hump may be observed in the diffraction pattern that despite its non-Bragg nature is nevertheless in many cases erroneously referred to as d_{001} in the literature. Even a composite material where approximately coplanar arranged 10 nm thick tactoids are interstratified with more or less mono-modal nanoparticles of let's say 3 nm will yield such a broad reflection with an apparent d-spacing of the maximum related to the volume weighted average of for instance 12 Å distances within the tactoid and 13 nm distances in the "composite stacking" (Figure 3).

Clearly, the occurrence of such a single maximum as defined as minimum requirement in the technical report of the IUPAC is not sufficient to prove intercalation of a pillaring agent and to distinguish between composite and single phase materials.

Nevertheless, even with heterogeneous charge density and thus varying pillar density, a rational *00l*-series is expected and will be realized as long as the pillars are arranged with the

Zeitschrift für anorganische und allgemeine Chemie ZAAC Journal of Inorganic and General Chemistry

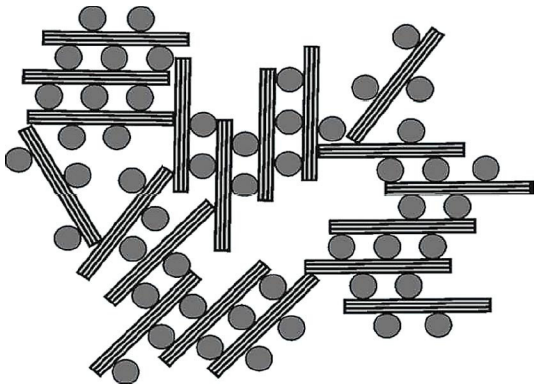

Figure 3. Texture of a semi-ordered nanocomposites resulting from the stacking of clay tactoids and mono-modal nanoparticles.

same orientation in monolayers in every interlayer space: When starting with a natural montmorillonite (MMT) that shows a strongly irrational *00l*-series in its hydrated state upon pillaring with Me_2DABCO^{2+} (Me_2DABCO^{2+} = *N*,*N*-dimethyl-1,4-diazabicyclo[2.2.2]octane-dication) a more rational *00l*-series evolves (Figure 4 and Table 1). The significantly reduced coefficient of variation (CV)[44] of the *00l*-series of the pillared MMT as compared to the hydrated MMT, suggests that as long as the size of the pillar is well-defined and its equivalent area is small enough to be able to satisfy charge neutrality in a monolayer, translational symmetry along the stacking direction will be realized. There is definitely little reason to accept irrational *00l*-series for truly PILCs. For comparison, the *00l*-series of Me_2DABCO^{2+} -pillared tainiolite with perfect translational symmetry, as indicated by a CV as low as 0.06, is included in Table 1.

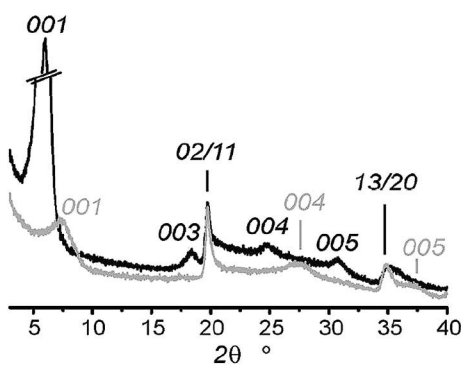

Figure 4. Diffraction pattern of hydrated montmorillonite (black) and Me_2DABCO^{2+} -pillared montmorillonite (gray). Indices of hk-bands are explained in the text..

2.3.2 Stacking Faults

The surface of 2:1 layered silicates is corrugated and exposes a high hexagonal pseudo-symmetry to interlayer species (Figure 5). Hexagonal cavities are arranged in a pseudo-hexagonal pattern. Due to this high pseudo-symmetry even with all cavities occupied as in micas (group name for 2:1 phyllosilicates, di- or trioctahedral, with non-hydrated monovalent cations and a layer charge x = 0.6–1.0[30]), polytypes and/or n × 60° rotational faults are frequently encountered because the first coordination sphere for the interlayer cations is the same and the rotational faults are energetically degenerate in a first approximation.[45,46] If the charge density and thus the number of interlayer cations is reduced into the regime of smectites even rotations differing from n × 60° might still give a decent fit to the fewer interlayer cations. Moreover, with decreasing size of the interlayer cations adjacent layers in the stack experience repulsion from the oxygen atoms forming the base of the tetrahedral layer which may trigger a slipage of adjacent layers, the most prominent slippage observed is by *b*/3. Since the slippage along the +*b* and –*b*-direction are again energetically degenerate, instead of lowering the symmetry to triclinic, stacking faults are generated in a statistical manner.[45] Upon hydration efficient additional slippage planes are introduced into the interlayer space by interlayer water and the phase relationship between adjacent layers is completely lost. Such materials are called turbostratic and in the diffraction patterns only few reflections are observed: The *00l*-series and usually up to three *hk*-bands (*11*-band, *13*-band, and *06*-band).

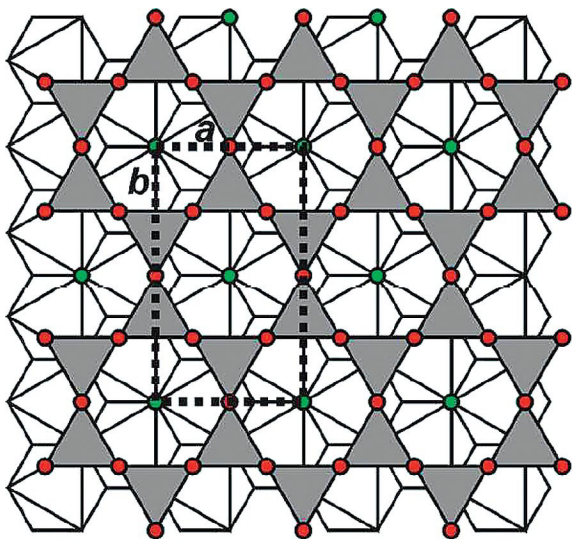

Figure 5. Top view of the 2:1 layered silicate structure showing the pseudo-hexagonal arrangement of the interface to the interlayer.

Table 1. d-values of hydrated montmorillonite, Me_2DABCO^{2+} -pillared montmorillonite, and Me_2DABCO^{2+} -pillared tainiolite

Sample	d_{001} /Å	d_{003} /Å	d_{004} /Å]	d_{005} /Å]	$\bar{d}_{00l}$ /Å	CV[44]
Hydrated MMT	11.91	–	3.25	2.42	12.32 ±0.60	4.9
Me_2DABCO-MMT	14.69	4.84	3.59	2.88	14.53 ±0.14	0.94
Me_2DABCO-tainiolite[19]	14.41	4.80	3.60	2.88	14.41 ±0.01	0.06

The *hk*-bands reflect the two-dimensional translation symmetry of the silicate layers and therefore are not affected by any changes in the basal spacing triggered by pillaring (Figure 4).

The likelihood of the described stacking fault increases with diminishing layer charge. Nevertheless, with large interlayer cations like Cs^+, three-dimensionally ordered 2:1 layered silicates with a layer charge of $x \approx 0.5$ are accessible by melt synthesis that still display sufficient intracrystalline reactivity to allow for pillaring.[45] When pillaring a material with three-dimensional order the stacking order may be preserved even though the interlayer space is expanded dramatically. Contrary to this, when starting with a turbostratically disordered material, a coordinated movement of a all layers in the tactoid would be required to heal the stacking faults and restore a "crystal" which is of course is very unlikely and was never observed.

2.3.3 Structure of the Interlayer Space

As already mentioned the different types and degrees of disorder in PILCs make it inherently difficult to derive structural information on the interlayer space from diffraction experiments.

A one-dimensional Fourier transformation of a rational *00l*-series will at maximum give information on the *z*-coordinates of strongly scattering atoms in the interlayer space. For very special cases and pillaring agents this might then allow deriving the orientation of the pillar.

Even if sufficiently large single crystals of three-dimensionally ordered PILCs are available, gaining information on the structure of the interlayer is still seriously hampered by the different *ab*-dimensions of the host and pillar lattices (Figure 1, bottom). The orientation and the position of the pillars relative to the corrugated surface of the host are defined by the confinement of the pillars between the two layers encompassing the interlayer space. The origin of the superlattice of pillars is, however, not fixed relative to the origin of the host lattice. Consequently, alternatives exist for the relative positioning of pillars in consecutive interlayer spaces. The ordering of the interlayer species therefore at best is only two-dimensional and unfortunately no interference is observed between different interlayers.

2.4 External vs. Internal Surface

Only very few PILCs were made from microscopic synthetic clay minerals, whereas most studies applied nanoscopic natural montmorillonite.[47] While the turbostratic disorder of montmorillonites and related materials already spares few hard experimental facts based on X-ray diffraction, some features inherent to nanoscopic materials cause additional trouble that weaken other essential analytical results and give more space for handwaving. Typical montmorillonite tactoids are 200 nm in diameter and 10 nm in height and consequently the external surface area may not be neglected for these materials.[48] Since the composition, as determined by chemical analysis, is severely influenced by the contribution of external basal and edge surfaces, neither determination of the cation exchange capacity of the interlayer nor of the chemical formula of the host material is straight forward and assumptions need to be built in. Therefore, empirical formulas of pillared compounds that are meant to provide information on the pillar/host ratio suffer from great uncertainty. And consequently they can hardly be used to estimate interlayer micropore volume by taking into account pillar densities and shapes/sizes.

Moreover, the anisotropic particle shape (aspect ratio ≈ 20) in combination with the small particle size induces loosely packed microstructures. These so-called "house of cards"-microstructures contain many wedge-like pores where two tactoids meet at a small angle (Figure 6).

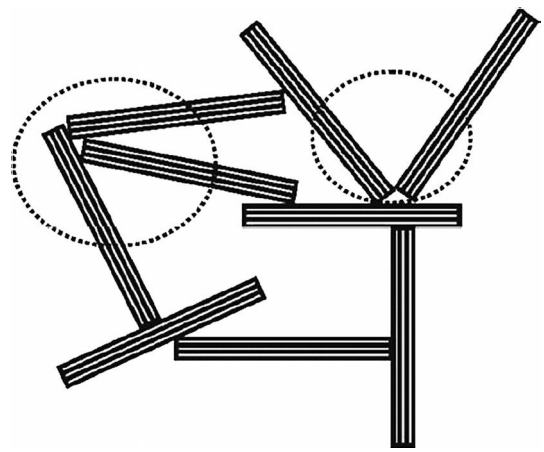

Figure 6. Wedge-like pores between tactoids.

Capillary condensation in such wedge-like pores will cover the full range of relative pressures in physisorption experiments. Thus not only a very broad pore distribution all the way up to mesopores will be observed but the wedge-like pores also contribute to the micropore regime. Therefore, even if N_2 adsorption-desorption isotherms are measured and analyzed via *t*- and α-plots as recommended by the technical report of the IUPAC, the desired pore size distributions of well-defined interlayer micropores generated by pillaring are always masked by the unspecific contribution of the interparticle pores. For this very reason, the technical report states: "Care must be taken to ensure that the observed porosity is the result of pillaring and not simply a consequence of interparticle texture." This request is of course anything but trivial if analytics are dominated by the large external surface area as mentioned above.

For instance, *Yamagishi* et al. in a series of papers described the intercalation of different enantiomerically pure metal complexes (e.g. $[Ru(bpy)_3]^{2+}$ and $[Ru(phen)_3]^{2+}$ with bpy = 2,2'-bipyridine and phen = 1,10-phenanthroline) and found enantioselective autocatalyis and stereodiscrimination when applying these materials in chiral chromatography columns.[49–52] *Yamagishi* et al., however, failed to report N_2-physisorption isotherms to prove interlayer microporosity. Judging from the equivalent areas of the metal complex cations applied, it seems, however, unlikely that the materials would have been

truly porous. At least when pillaring a microscopic synthetic hectorite $Na_{0.4}Mg_{2.6}Li_{0.4}Si_4O_{10}F_2$ (trioctahedral 2:1 phyllosilicate of the smectite group[30]) with $[Ru(bpy)_3]^{2+}$ no appreciable microporosity is observed (Figure 7). Only when the equivalent area of the pillar is significantly reduced by switching to $[Rh(bpy)_3]^{3+}$ interlayer microporosity could be observed. This would suggest that the very interesting stereodiscrimination phenomena reported by *Yamagishi* et al., most likely may be attributed to external surface area rather than to interlayer porosity.

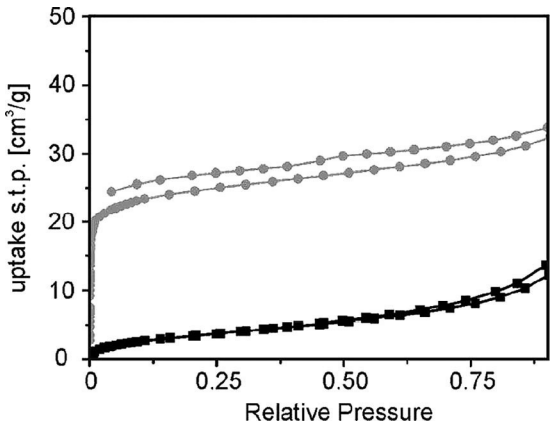

Figure 7. Physisorption isotherm (Ar/Ar(l) at 87 K) of $[Ru(bpy)_3]^{2+}$ -pillared hectorite (black) and $[Rh(bpy)_3]^{3+}$-pillared hectorite (gray).

3. A Brief History of PILCs

The concept of pillaring was first introduced by *Barrer* in the 1950's, when he described that the interlayer space of montmorillonites may be permanently opened up by intercalation of for instance $[N(CH_3)_4]^+$.[53] As pointed out by *Pinnavaia*, *Barrer*'s idea was unfortunately not followed up for two decades because the concomitant advent of synthetic zeolites with superior thermal stability absorbed literally all interest in microporous materials at that time.[47] Much later in 1977, when people were thriving for ever increased pore diameters, *Brindley* et al. finally picked up the idea but used purely inorganic pillaring agents like polyhydroxyaluminum to be able to compete with the thermal stability of zeolites.[54] This high-temperature part of the pillaring activity persists up to today with great momentum and has been reviewed extensively and recently.[55–60]

The great success of MOFs has, however, demonstrated that due to the impact of the greenhouse effect and the renewable energy discussion, catalysis at elevated temperature paled in comparison to molecular sieving, gas separation, and gas storage at temperatures below 200 °C. In this type of applications hybrid structures are more attractive than pure inorganic molecular sieves because they allow for fine-tuning the chemistry of the micropores and not just their size and shape.

For this renewed interest in microporous hybrid materials, we will focus on what used to be called expanded layered clays, meaning PILCs that have been pillared with organic molecules or coordination compounds and which therefore are hybrids by definition. Special attention will be paid to the consistency of the experimental data with the pillaring concept in a strict sense. Expansion of basal spacing by intercalation of the "pillaring agents" is not regarded sufficient if no evidence is presented for porosity originating from the interlayer space. A significant micropore volume as determined by physisorption measurements and which cannot be attributed to interparticle porosity is regarded essential.

4. Pillaring Nanoscopic Clay Minerals

Barrer and *MacLeod* in their pioneering work pillared a montmorillonite (Cation Exchange Capacity (CEC) about 100 meq/100 g) with tetramethyl- (TMA) and tetraethyl-ammonium (TEA) and after removal of the solvent observed a d-spacing of 13.5 Å and 13.9 Å, respectively.[53] Keeping the charge density constant and increasing the size of the pillar reduces d_{pore}. In agreement with this expectation they found a significantly reduced micropore volume for TEA-pillared as compared to TMA-pillared montmorillonite.

Due to the nanoscopic size of the natural montmorillonite used and a texture involving wedge-like pores, in addition to microporosity, mesoporosity is generally found in the N_2-physisorption experiments as evidenced by capillary condensation at 78 K and relative pressures > 0.50 (Figure 8a). It would therefore be expected that some undetermined part of the micropore volume most likely might also be attributed to these wedge-like pores and is not related to interlayer microporosity. Later *Barrer* started to correct uptakes for sorption upon exter-

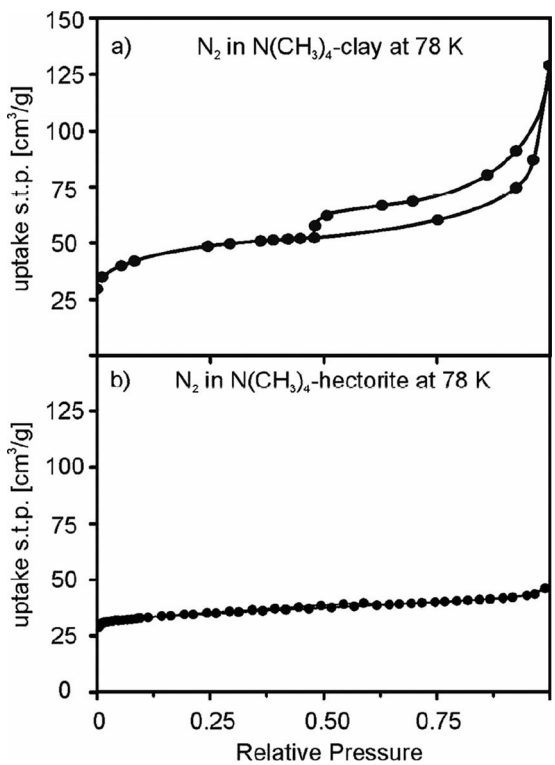

Figure 8. N_2 physisorption isotherms of a) TMA-montmorillonite (adapted from [53]) and b) TMA-hectorite.

nal surfaces and this way obtained so-called inclusion isotherms of type I.[33]

In any case when applying a synthetic hectorite of microscopic size and comparable layer charge, we found a similar micropore volume but no signs of capillary condensation (Figure 8b). Due to the coarse-grained nature of the synthetic clay mineral no appreciable wedge-like pore volume is produced.

In 1994, *Lao* and *Detellier* described the application of TMA-pillared montmorillonites and hectorites for separation of linear hydrocarbons and compared these PILCs with tetraphenylphosphonium- and quaternarized polyammonium-pillared materials.[61] The separation efficiency could be related to the size and shape of the pore space. Moreover, they succeeded to apply these porous PILCs as packing materials for gas chromatography columns separating light hydrocarbons.

Instead of N_2-adsorption, more recently the micropore structure of a hectorite ($Ex_{0.66}(Mg_{5.34}Li_{0.66}]Si_8O_{20}(OH,F)_4$) pillared with TEA was characterized by hyperpolarized ^{129}Xe-NMR spectroscopy.[62] The hectorite was not pillared *post-synthesis* by cation exchange but rather was directly obtained adding TEA as a crystallization agent in the hydrothermal synthesis. The observed ^{129}Xe-shift was evaluated applying a semi-empirical model proposed by *Demarquay* and *Fraissard*[63] and a pore diameter of 7 Å could be derived. N_2-physisorption isotherms were of type IV, which again may be attributed to capillary condensation of interparticle pores produced by the texture because of the limited particles sizes obtained by hydrothermal synthesis. The micropore size was additionally determined from the physisorption isotherm applying the Horvath-Kavazoe method and a slit-pore model to be 6 Å. The pillared hectorite was capable of incorporating different neutral adsorbents. Isotherms of CH_4 at 195 K, benzene at 298 K, and CO_2 at 195 K and 273 K were measured, and the isotherms were found to have different shapes. In the light of the earlier discussion presented in 2.4 this distinct shapes of isotherms might indeed relate to adsorption into (dynamic) micropores vs. swelling mechanisms.

Barrer followed up his initial 1955 publication over subsequent years with a series of papers applying different alkylammonium and –diammonium cations and $[Co(en)_3]^{3+}$ (en = ethylendiammine) as pillars.[64] In a compulsory review of this systematic study he concluded that the adsorption capacities and micropore volumes observed can be consistently explained by the factors already mentioned in chapter 2.2: The equivalent area of the pillars and the charge density of the layered host.[65] He even estimated interlayer pore volumes from pillar shapes and densities and the basal spacing.[66]

Thomas et al. intercalated trinuclear Cobalt complexes, but unfortunately failed to evidence microporosity by N_2-isotherms and consequently these materials should therefore only be considered as ordinary intercalation compounds.[67]

In line with *Barrer*'s finding, *Mortland* and *Berkheiser*, by turning to diprotonated H_2DABCO^{2+} as pillaring agent were able to produce significantly larger pore volumes as compared to TEA-pillared materials and this way PILCs were obtained that were capable to accommodate molecules as large as 2,4-dimethylpentane.[68] Applying a solid solution of a laterally small $[Cr(en)_3]^{3+}$ pillar and a laterally larger, ligand dissociated $[Co(en)_2$ -en$]^{3+}$ pillar, *Chen* et al. were able to tailor the size of the interlayer micropores and to study the adsorptive and diffusive properties of the these PILCs.[69]

Meier et al. investigated Volclay and hectorites "pillared" with a variety of alkylammonium cations and applied them for adsorption of 2-chlorophenol.[70] Although these authors claimed their compounds to be pillared, no N_2-physisorption measurement is presented and thus the materials should rather be regarded as intercalation compounds that due to organophilization swell with 2-chlorophenol, a phenomenon well known for organoclays.

5. Pillaring Coarse Grained Clay Minerals

As pointed out in chapter 2.4, charge heterogeneity accompanied by interstratification, the turbostratic disorder in the stacking and the influence of the external surface in nanoscopic materials as found with natural clay minerals and those synthesized hydrothermally at low temperatures weaken essential analytical results and give space for hand waving. Turning to well-ordered and microscopic synthetic clay minerals removes all these obstacles and allows to present consistent data underlining the validity of concepts proposed in the literature beyond any doubt. Therefore, in the following we will demonstrate the power of the pillaring approach for a rational design of microporous hybrid materials that have the potential to become on par with MOFs.

5.1 Structure of Interlayer Space

The anisotropic bonding situation in layered silicates renders them prone to stacking faults. Only very few deposits of natural vermiculites (group name for 2:1 phyllosilicates, di- or trioctahedral, with hydrated exchangeable cations and a layer charge x = 0.6–0.9[30]) are known that, due to special genesis and high layer charge, show a semi-ordered stacking and consequently less diffuse scattering.

Some of these vermiculite deposits (e.g. Santa Ollala, Spain or Carl Moss Ranch, Llano County, Texas) contain crystals large enough and with greatly diminished stacking faults so that for selected crystals even an ordinary single crystal data collection is possible. The contribution of diffuse scattering is low enough to be neglected and a standard refinement can be performed yielding structural details although with comparatively high reliability factors. This way, even structural models of 2 WL hydrates of vermiculites could be proposed.[71] Unfortunately, the supply of these extraordinarily ordered natural vermiculites seems to be exhausted.

Recently we have published the synthesis of a Na-hectorite with a high layer charge in the range of vermiculites that swells with water vapor and allowed to refine the structure of both 2 WL and, for the first time ever, also 1WL hydrates.[72] This synthetic material could certainly replace the depleted stock of well-ordered natural vermiculites.

Zeitschrift für anorganische und allgemeine Chemie ZAAC Journal of Inorganic and General Chemistry

Alternatively, instead of increasing the layer charge, the size of the interlayer cation may be increased to improve the stacking order. Melt synthesis of Cs-fluorohectorite ($(Cs_{0.5})^{inter}[Mg_{2.5}Li_{0.5}]^{oct}[Si_4]^{tet}O_{10}F_2$) with layer charge of x = 0.5 yields microscopically large single crystals with little stacking faults.[44] Due to the much lower hydration enthalpy of Cs^+ as compared to Na^+ the material does not swell spontaneously in water despite its smectitic charge density. Its intracrystalline reactivity, however, is fully sufficient to allow for a complete cation exchange with organic cations. Moreover, whenever these organic interlayer cations have a shape that allows for penetrating into the corrugated silicate layer surface on both sides of the interlayer space, the stacking order may be preserved despite the large expansion of the interlayer space (typically $>$ 30 %). This readily available Cs-fluorohectorite now allows to routinely synthesizing three-dimensionally ordered PILCs paving the way for experimentally determined structures of PILCs.

5.1.1 Three-dimensionally Ordered PILCs

With three-dimensionally ordered single crystals available, indexing is straight forward and from c and β immediately the relative position of adjacent silicate layers can be derived. In all polytyps of micas the hexagonal cavities of the layers encompassing the interlayer space are arranged opposite of each other. This is true for Cs-fluorohectorite as well. All ordered PILCs derived from this Cs-fluorohectorite preserve this phase relationship between adjacent silicate layers. This particular well-defined phase relationship of adjacent silicate layers is a consequence of thermodynamics and not kinetics. The pillars protrude into the hexagonal cavities and thus a smaller basal spacing leading to a maximized Coulomb-attraction can be realized. Contrary to this, the transition from 1 WL to 2 WL mentioned before involves a concerted slippage of adjacent layers and in the 1 WL structure the hexagonal cavities are not arranged opposite to each other.[45] In all cases of threedimensionally ordered structures of layered compounds, however, the interlayer space is bridged in a well-defined mode that is thermodynamically favored by interlayer (complex) cations interacting on both sides with the silicate layers and that preserves stacking order.

As mentioned before, even for three-dimensionally ordered PILCs, the origin of the superlattice of the pillar is, not fixed. The ordering of the interlayer species thus at best is two-dimensional and no interference is observed between different interlayers. While position and orientation of the pillars relative to the host lattice are defined by the specific interaction mode, the lack of a three-dimensional long-range order of interlayer species, renders the electron density in the interlayer space very diffuse. The Bragg reflections contain only the averaged information on the in-plane arrangement and the orientation of interlayer cations relatively to the silicate layers. The problem might even be worsened by the pseudo-symmetry of the surface of the silicate layers that usually allows for energetically degenerate alternative orientations of pillars. Because of this diffuse nature, identification (through difference fourier maps) and refinement of individual interlayer atoms is risky even when applying massive constraints or restraints and may easily lead into false minima. Refining interlayer cations as complete rigid bodies is clearly advantageous. When the pillars are refined as rigid bodies, however, physically and chemically sensible structural models of the interlayer space are obtained.

For TMA-pillared synthetic hectorite, the TMA-molecules are positioned in the middle of the interlayer space. Two of the methyl groups lie in the *ab*-plane, whereas the remaining two methyl groups point into the hexagonal cavities of the two silicate layers and cross-link the interlamellar space. As the pillars are shifted from the center of the hexagonal cavity these two methyl groups are positioned exactly in the middle of the hexagonal cavities (Figure 9).[73]

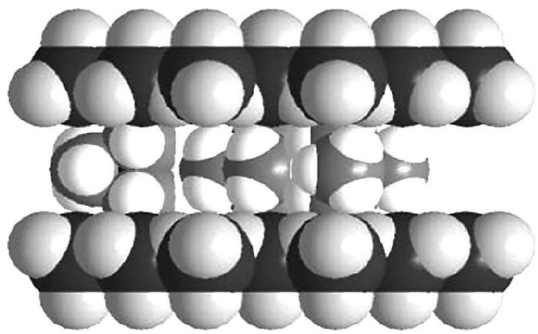

Figure 9. Space filling model of TMA in the interlayer space viewed along c*.[73]

The interlayer structure of Cs-fluorohectorite pillared with Me_2DABCO^{2+} follows the same "rules". Me_2DABCO^{2+} is slightly ellipsoidal. Contrary to what has been proposed by *Shabtai* et al. and as expected from electrostic reasons, the structure refined with single crystal data show the C_3-axis, which is the long principal axis of the molecule, to be oriented parallel to the silicate layers.[74;75] The organic pillars bridge the interlamellar space in a defined way by penetrating into the hollows on the corrugated silicate surfaces on both sides of the interlamellar space. This way the hexagonal cavities are forced to be arranged opposite of each other.

A similar structure is found when Cs-tainiolite ($Cs_{0.98}Fe^{2+}_{1.93}Li_{1.01}Si_4O_{10}F_2$) is oxidatively pillared with Me_2DABCO^{2+}.[19;76] A structurally well ordered, coarse grained PILC with a charge density in the regime of smectites ($(Me_2DABCO^{2+})_{0.22}Fe^{2+/3+}_{1.85}Li_{0.90}Si_4O_{10}F_2$) is obtained by oxidation of structural Fe^{2+} and it displays well defined micropores. The three-dimensional periodic structure of the pristine mica can be maintained during the topotactical intercalation reaction. The hexagonal cavities of the two layers enclosing the interlamellar space are arranged exactly opposite of each other by the cross-linking pillar. The pillar is oriented with its C_3-axis tilted by approximately 24° against the *ab*-plane. While two of the C_2H_4-handles protrude into the silicate layers the third one is in the plane of the interlamellar space (Figure 10).

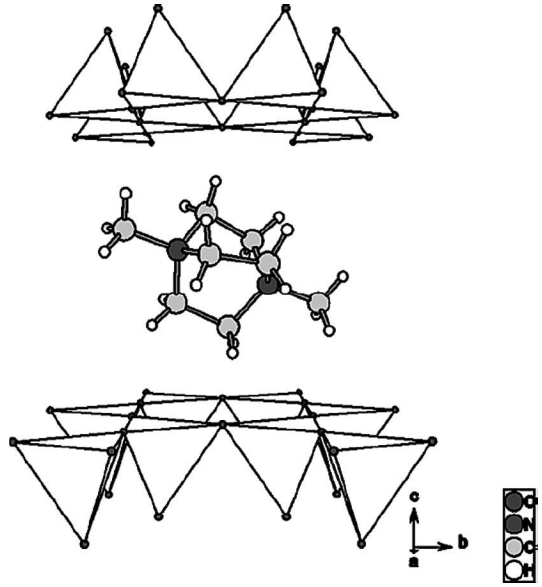

Figure 10. Orientation of the Me_2DABCO^{2+}- pillar in the interlayer space as determined by refinement of X-ray single-crystal data. Reprinted with permission from [19] Reprinted with permission from *Angewandte Chemie Int. Ed.*, A Route to Microporous Materials through Oxidative Pillaring of Micas, *47*, 1640–1644 (**2008**). Copyright Wiley-VCH Verlag GmbH & Co. KGaA.

Based on the crystal structure and the composition, the pore diameter of the microporous interlayer space could be estimated. Considering the site occupation factor of 0.22 for the pillars, the average intermolecular distance between the pillars is expected to be 11.7 Å. The pillar molecules are cylindrical with a van der Waals (vdW) diameter of 5.6 Å and a length of 8.8 Å. Taking the tilting angle into account, the projection of the latter into the *ab*-plane is approximately 8 Å. Thus a lower limit for d_{pore} of 3.7 Å and an upper limit of 6.1 Å may be deduced, respectively, while from the basal spacing observed, h_{int} = 4.7 Å.

The Ar-physisorption isotherm is of type I, as expected for such a coarse grained material, no interparticle mesopores are observed (Figure 11). Applying a non-local-DFT model a narrow pore size distribution with a pore diameter in the range of

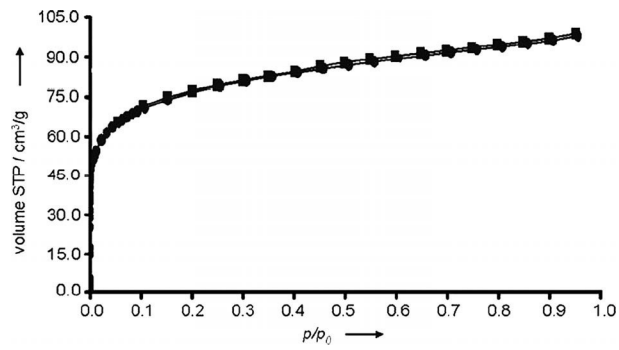

Figure 11. Physisorption Isotherm (Ar/Ar(l) at 87 K) of Me_2DABCO^{2+}- tainiolite.[19] Reprinted with permission from *Angewandte Chemie Int. Ed.*, A Route to Microporous Materials through Oxidative Pillaring of Micas, *47*, 1640–1644 (**2008**). Copyright Wiley-VCH Verlag GmbH & Co. KGaA.

5 to 7 Å could be calculated, which is in very good agreement with the estimates made from the structural model and a composition which is not tampered with surface impacts.

The good agreement between estimated and experimentally determined pore sizes underlines that whenever the analytics are not corrupted by non-negligible external surface effects, redundant data become consistent.

Contrary to PILCs derived from charge heterogeneous, nanoscopic clay minerals, in this case the pillar/host ratio together with pillar shape may be used to calculate micropore volume (Figure 12) and to estimate the maximum layer charge that might still provide interlayer microporosity with any given pillar.

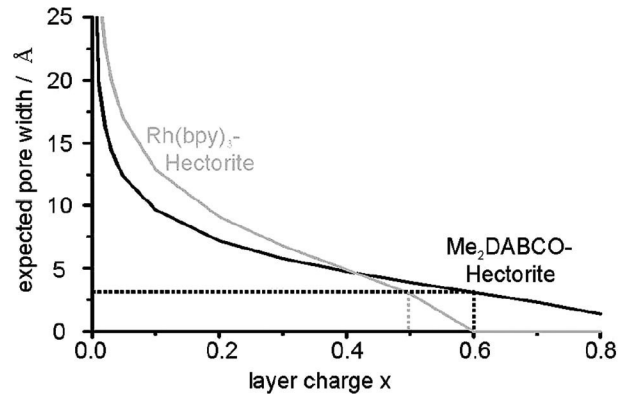

Figure 12. Expected pore size as a function of the layer charge for two types of pillars, Me_2DABCO^{2+} and $[Rh(bpy)_3]^{3+}$, differing in shape and equivalent area.[21;22] Reprinted from *Microporous Mesoporous Mater.*, *123*, A. Baumgartner, F. E. Wagner, M. Herling, J. Breu, "Towards a tunable pore size utilizing oxidative pillaring of the mica ferrous tainiolite", 253–259, **2009**, with permission from Elsevier.

5.1.2 Two-dimensionally Long-range Order of the Interlayer

As pointed out earlier, for clay minerals made at temperatures < 1000 K a two-dimensional long-range order of interlayer cations will be hampered by the heterogeneity of charge density. Even for synthetic hectorites obtained from the melt, so far only very few examples are know where such a two-dimensional superlattice of interlayer species could be proven unequivocally by the observation of '*interlayer' hk*-bands.

Tsvetkov and *White* intercalated complex ions like $Ir(diamsar)^{3+}$ (diamsar: 1,8-diamino-3,6,10,13,16,19-hexa-azabicyclo-[6.6.6]eicosan), $Hg(diamsarH_2)^{4+}$, and $Hg(diamsar)^{2+}$ into Na-montmorillonite and a high-charge synthetic fluorohectorite.[77] For the latter, a two dimensional long-rage order could be observed: "Six orders of the *c*-axis X-ray diffraction were resolved as well as peaks corresponding to the lateral free distance between cations".

When intercalating $[Ru(bpy)_3]^{2+}$ into a Na-fluorohectorite, λ-shaped peaks appear with low intensities, both factors are expected for *hk*-bands resulting from two-dimensional diffraction. Moreover, the peaks are different for enantiopure and the racemic intercalation compounds indicating, as expected, distinct in-plane structures of the enantiopure and the racemic interlayers, respectively.[78]

Zeitschrift für anorganische und allgemeine Chemie ZAAC Journal of Inorganic and General Chemistry

While for Me_2DABCO^{2+} pillared Cs-hectorite no '*interlayer' hk*-bands could be observed, with the slightly smaller 2H-$DABCO^{2+}$ superstructure reflections occurred.[18] They could be indexed with a 3 $a \times b$ supercell (Figure 1, bottom) of the parent synthetic silicate indicating a two-dimensional ordering of the pillars together with the three dimensionally ordered silicate layers (Figure 13).

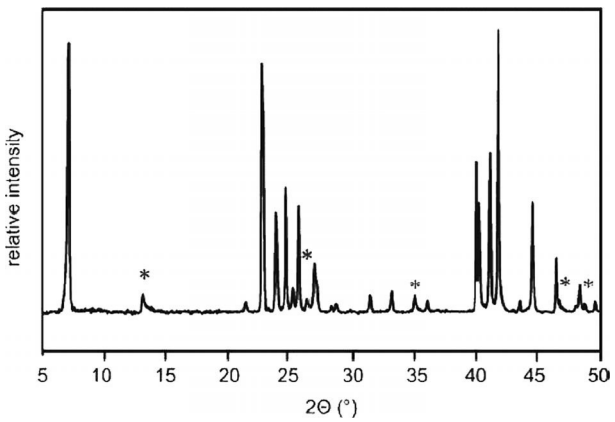

Figure 13. Powder X-ray diffraction pattern of 2H-$DABCO^{2+}$-hectorite. Asterisks (*) mark reflections due to the two dimensional diffraction from a 3 $a \times b$ super-cell.[18] M. Stöcker, W. Seidl, L. Seyfarth, J. Senker and J. Breu, *Chem. Commun.*, **2008**, 629 – Reproduced by the permission of The Royal Society of Chemistry.

The fact that the superlattice of the pillars is commensurate with the host lattice also corroborates the view that the structure of the interlayer space is determined by strong host-pillar interactions founded in the partial penetration of pillars into the hexagonal cavities.

Similar to $(Me_2DABCO^{2+})_{0.22}Fe^{2+/3+}{}_{1.85}Li_{0.90}Si_4O_{10}F_2$, Ar/Ar(l) physisorption measurements showed the 2H-$DABCO^{2+}$ pillared material to have a narrow pore size distribution with micropores of 4–7 Å in diameter.[20]

5.1.3 Fine Tuning the Micropores

All examples discussed so far combined pillars of largely differing equivalent areas with layered silicates of a charge density fixed during synthesis. The full potential of the pillaring approach can, however, only be taken advantage of if the charge density could be fine-tuned *post-synthesis*. Only such deliberate and fine-graded alteration of the pillar density will allow adjusting the pore size to a given adsorbate and thus will pave the way to maximize adsorption enthalpies and to improve selectivity (Figure 12).

As already mentioned, the layer charge usually is fixed during synthesis by the degree of isomorphous substitution in the tetrahedral and/or octahedral layer. There are two routes that allow for tailoring the layer charge *post- synthesis*:

a) Oxidation of octahedral transition metals

b) Utilizing the Hofmann-Klemen effect.

As already mentioned before, *Baumgartner* et al. used a Cs-tainiolite as a host material for pillaring with Me_2DABCO^{2+}.[19] This oxidative intercalation reduces the layer charge from $x = 0.98$ to $x = 0.46$ into the range of smectites. Tuning the pore size of the PILCs by oxidatively decreasing the layer charge and consequently the pillar density in the interlayer space beyond that limit, however, fails.[22] When applying increasingly severe oxidative environments by adding Br_2, 97 % of structural Fe^{2+} can be oxidized but the pillar density cannot be reduced further. Initially with low degrees of oxidation, charge neutrality is maintained by reducing the cation exchange capacity. However, at a certain mean octahedral bond length a change of the charge compensation mechanism is observed. Instead of de-intercalating interlayer cations, octahedral cations are expelled to the interlayer space. Due to this vacancy formation the cation exchange capacity stays constant despite further oxidation.

The second approach to tune the pore width utilizes a modified Hofmann-Klemen effect, described by *Jaynes* et al.[79,80] This method turned out to be generally applicable and does not suffer of charge reduction limits as demonstrated for a low charged potassium hectorite synthesized from melt ($[K_{0.48(2)}]^{inter}[Mg_{2.54(8)}Li_{0.43}]^{oct}$ $[Si_4]^{tet}O_{10}F_2$). The interlayer cation K^+ was first exchanged with Mg^{2+}. Subsequently, the material was annealed at 250 °C. At this temperature the mobility of interlayer Mg^{2+} and octahedral Li^+ is high enough to switch sites. As monitored by Li-AAS analytics and layer charge determinations according to the so-called alkylammonium method, concomitantly the layer charge is reduced.[81] The procedure may be repeated multiple times and the charge density is reduced stepwise. In Figure 14 and Figure 15, p re-

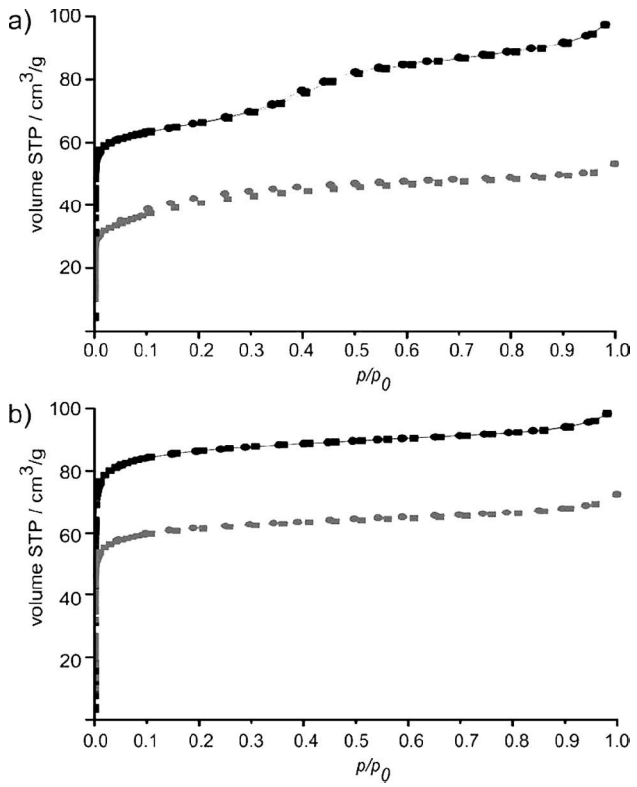

Figure 14. Physisorption isotherm (Ar/Ar(l)) of (a) Me_2DABCO–r_6–hectorite (black), Me_2DABCO-p-hectorite (gray), and (b) $Rh(bpy)_3$-r_6-hectorite (black), and $Rh(bpy)_3$-p-hectorite (gray).[21] Reprinted with permission from M. M. Herling, H. Kalo, S. Seibt, R. Schobert, J. Breu, *Langmuir* **2012,** *28,* 14713–14719. Copyright 2013 American Chemical Society.

Special Issue

fers to the pristine hectorite while r_6 refers to a material that has been charge-reduced by 6 consecutive Hofmann-Klemen cycles. This gradual fine tuning of a homogeneous layer charge in turn allows for tailoring the micropore size starting from one and the same layered host. On top of controlling the pillar density, the equivalent area of the pillar is yet another parameter to influence the micropore size (Figure 12, Figure 14, and Figure 15).

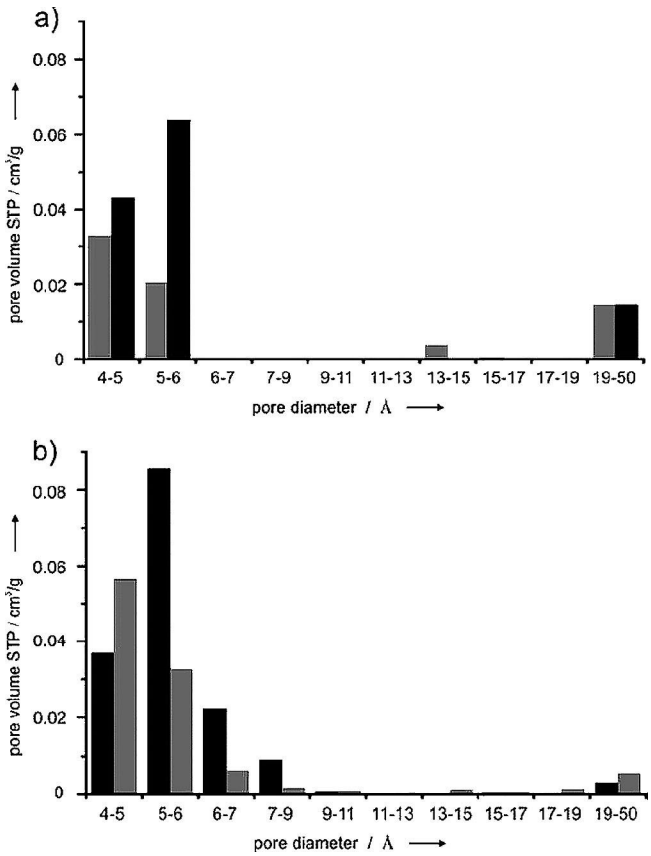

Figure 15. Pore size distributions of (a) Me_2DABCO–r_6–hectorite (black), Me_2DABCO-p-hectorite (gray), and (b) $Rh(bpy)_3$-r_6-hectorite (black), and $Rh(bpy)_3$-p-hectorite (gray).[21] Reprinted with permission from M. M. Herling, H. Kalo, S. Seibt, R. Schobert, J. Breu, *Langmuir* 2012, *28,* 14713–14719. Copyright 2013 American Chemical Society.

Figure 15 compares pore size distributions obtained by applying a non-local-DFT model for Me_2DABCO^{2+}- and $Rh(bpy)_3^{3+}$-pillared *p*-hectorite and r_6-hectorite. For both pillar agents, the maximum of the pore size distribution was shifted to larger pore widths with layer charge reduction.[21]

When comparing consecutive Hofmann-Klemen cycles it turns out that this *post-synthesis* adjustment of the pore widths can be done in steps as small as ≈ 0.1 Å. This quasi- continuously adjustable microporosity gives the option to model the interlayer cavities on the shape of particular guest molecules. This feature is unique to PILCs and is not available to MOFs whose porosity can be adjusted only in steps no smaller than the order of chemical bond lengths.

The micropore structure of the different charge-reduced Me_2DABCO^{2+}-hectorites was further characterized by sophisticated solid state NMR techniques.[23] The charge reduction process was monitored by ^{19}F MAS NMR that showed an increase in the octahedral Mg^{2+}:Li^+ ratio occurring concomitantly with the decrease in the layer charge as followed by atomic absorption spectroscopy. This corroborates a one-for-one replacement of octahedrally coordinated Li^+ with Mg^{2+}. Two-dimensional [^1H ^{19}F] HETCOR NMR was performed on Me_2DABCO–r_6–hectorite in order to identify possible alternative arrangements of the pillar inside the interlayer space but rather confirmed a uniform environment for all Me_2DABCO^{2+} pillars sandwiched between the rigid silicate layers.

Finally, hyperpolarized ^{129}Xe was applied to collect CF-HP ^{129}Xe MAS spectra. The ^{129}Xe-shifts observed for the different materials were then converted in pore widths applying the Demarquay and Fraissard model[63] and were in good agreement with the values obtained with physisorption data (5–7 Å).

6. Conclusion

Recent progress allows fine-tuning the charge density of the host lattice *post-synthesis* and now gives access to the full potential of the pillaring concept. By the fine-graded alteration of the pillar density and hence the pore size in steps as small as 0.1 Å a rational design of microporous hybrid materials with full control over size, shape, and chemical nature of micropores is at hand (Figure 12). Moreover, for the first time large functional (chirality, catalysis) pillaring agents may be used while still creating interlayer microporosity. Next, the potential of this pillaring approach should be explored in its full depth by applying the plethora of functional pillar molecules available. Systematic variation of charge density of the host, equivalent area of the cationic pillaring agents, and their chemical functionality are the building blocks for a highly modular access to microporous hybrid materials that have the potential to become par with MOFs in the fields of separation, gas storage, and catalysis. Pillaring itself is straight forward. Unfortunately, melt synthesis might represent a certain barrier to the research field but the authors will be happy to provide synthetic hectorites on request.

Moreover, much similar to third generation MOFs, the basal spacing of PILCs may expand further upon inclusion of appropriate sorbate molecules into the micropores. While MOFs exhibiting such gate opening or breathing effects have attracted much interest, for PILCs the field is terra incognita. Most likely breathing of micropores will be accompanied by a reorientation of the pillars and therefore a more rational design via the choice of the pillar shape should be easy.

Acknowledgments

This work was financially supported by the Deutsche Forschungsgemeinschaft (SFB 840, Project A6).

Zeitschrift für anorganische und allgemeine Chemie ZAAC Journal of Inorganic and General Chemistry

References

[1] W. Schmidt, *ChemCatChem* **2009**, *1*, 53–67.
[2] F. Schüth, *Annu. Rev. Mater. Res.* **2005**, *35*, 209–238.
[3] J. Weitkamp, *Solid State Ionics* **2000**, *131*, 175–188.
[4] S. I. Zones, *Microporous Mesoporous Mater.* **2011**, *144*, 1–8.
[5] A. Corma, *J. Catal.* **2003**, *216*, 298–312.
[6] S. Kitagawa, R. Kitaura, S. Noro, *Angew. Chem. Int. Ed.* **2004**, *43*, 2334–2375.
[7] O. M. Yaghi, M. O'Keeffe, N. W. Ockwig, H. K. Chae, M. Eddaoudi, J. Kim, *Nature* **2003**, *423*, 705–714.
[8] A. U. Czaja, N. Trukhan, U. Muller, *Chem. Soc. Rev.* **2009**, *38*, 1284–1293.
[9] J. R. Li, R. J. Kuppler, H. C. Zhou, *Chem. Soc. Rev.* **2009**, *38*, 1477–1504.
[10] L. Ma, C. Abney, W. Lin, *Chem. Soc. Rev.* **2009**, *38*, 1248–1256.
[11] Y. Liu, W. M. Xuan, Y. Cui, *Adv. Mater.* **2010**, *22*, 4112–4135.
[12] S. Kitagawa, M. Kondo, *Bull. Chem. Soc. Jpn.* **1998**, *71*, 1739–1753.
[13] G. Ferey, C. Serre, *Chem. Soc. Rev.* **2009**, *38*, 1380–1399.
[14] H. Kalo, M. W. Möller, M. Ziadeh, D. Dolejs, J. Breu, *Appl. Clay Sci.* **2010**, *48*, 39–45.
[15] J. Breu, W. Seidl, A. J. Stoll, K. G. Lange, T. U. Probst, *Chem. Mater.* **2001**, *13*, 4213–4220.
[16] M. Stöter, D. A. Kunz, M. Schmidt, D. Hirsemann, H. Kalo, B. Putz, J. Senker, J. Breu, *Langmuir* **2013**, *29*, 1280–1285.
[17] H. Kalo, M. W. Möller, D. A. Kunz, J. Breu, *Nanoscale* **2012**, *4*, 5633–5639.
[18] M. Stöcker, W. Seidl, L. Seyfarth, J. Senker, J. Breu, *Chem. Commun.* **2008**, 629–631.
[19] A. Baumgartner, K. Sattler, J. Thun, J. Breu, *Angew. Chem. Int. Ed.* **2008**, *47*, 1640–1644.
[20] M. Stöcker, L. Seyfarth, D. Hirsemann, J. Senker, J. Breu, *Appl. Clay Sci.* **2010**, *48*, 146–153.
[21] M. M. Herling, H. Kalo, S. Seibt, R. Schobert, J. Breu, *Langmuir* **2012**, *28*, 14713–14719.
[22] A. Baumgartner, F. E. Wagner, M. Herling, J. Breu, *Microporous Mesoporous Mater.* **2009**, *123*, 253–259.
[23] C. D. Keenan, M. M. Herling, R. Siegel, N. Petzold, C. R. Bowers, E. A. Rössler, J. Breu, J. Senker, *Langmuir* **2013**, *29*, 643–652.
[24] R. A. Schoonheydt, T. Pinnavaia, G. Lagaly, N. Gangas, *Pure Appl. Chem.* **1999**, *71*, 2367–2371.
[25] D. H. Brouwer, R. J. Darton, R. E. Morris, M. H. Levitt, *J. Am. Chem. Soc.* **2005**, *127*, 10365–10370.
[26] F. Bergaya, *Concerted European Action – Pillared Layered Structures* **1995**, Newsletter 7, 11–12.
[27] J. Breu, C. R. A. Catlow, *Inorg. Chem.* **1995**, *34*, 4504–4510.
[28] G. Lagaly, *Clay Miner.* **1981**, *16*, 1–21.
[29] E. J. Palin, M. T. Dove, A. Hernandez-Laguna, C. I. Sainz-Diaz, *Am. Mineral.* **2004**, *89*, 164–175.
[30] R. T. Martin, S. W. Bailey, D. D. Eberl, D. S. Fanning, S. Guggenheim, H. Kodama, D. R. Pevear, J. Srodon, F. J. Wicks, *Clays Clay Miner.* **1991**, *39*, 333–335.
[31] A. R. Mermut, G. Lagaly, *Clays Clay Miner.* **2001**, *49*, 393–397.
[32] J. Breu, N. Raj, C. R. A. Catlow, *J. Chem. Soc., Dalton Trans.* **1999**, 835–846.
[33] R. M. Barrer, *Pure Appl. Chem.* **1989**, *61*, 1903–1912.
[34] M. W. Möller, D. Hirsemann, F. Haarmann, J. Senker, J. Breu, *Chem. Mater.* **2010**, *22*, 186–196.
[35] M. W. Möller, U. A. Handge, D. A. Kunz, T. Lunkenbein, V. Altstadt, J. Breu, *ACS Nano* **2010**, *4*, 717–724.
[36] E. Ferrage, B. Lanson, N. Malikova, A. Plancon, B. A. Sakharov, V. A. Drits, *Chem. Mater.* **2005**, *17*, 3499–3512.
[37] N. Malikova, A. Cadene, E. Dubois, V. Marry, S. Durand-Vidal, P. Turq, J. Breu, S. Longeville, J. M. Zanotti, *J. Phys. Chem. C* **2007**, *111*, 17603–17611.
[38] V. Marry, N. Malikova, A. Cadene, E. Dubois, S. Durand-Vidal, P. Turq, J. Breu, S. Longeville, J. M. Zanotti, *J. Phys.: Condens. Matter* **2008**, *20*, 104205–104215.
[39] V. Marry, E. Dubois, N. Malikova, S. Durand-Vidal, S. Longeville, J. Breu, *Environ. Sci. Technol.* **2011**, *45*, 2850–2855.
[40] V. Marry, E. Dubois, N. Malikova, J. Breu, W. Haussler, *J. Phys. Chem. C* **2013**, *117*, 15106–15115.
[41] E. Ferrage, B. A. Sakharov, L. J. Michot, A. Delville, A. Bauer, B. Lanson, S. Grangeon, G. Frapper, M. Jimenez-Ruiz, G. J. Cuello, *J. Phys. Chem. C* **2011**, *115*, 1867–1881.
[42] E. Ferrage, B. Lanson, B. A. Sakharov, N. Geoffroy, E. Jacquot, V. A. Drits, *Am. Mineral.* **2007**, *92*, 1731–1743.
[43] D. M. Moore, R. C. Reynolds, in *X-ray Diffraction and the Identification and Analysis of Clay Minerals*, Oxford University Press, Oxford **1997,** pp. 263.
[44] Variation of coefficient (CV): standard abbreviation/mean value $\times$ 100.
[45] J. Breu, W. Seidl, A. Stoll, *Z. Anorg. Allg. Chem.* **2003**, *629*, 503–515.
[46] D. M. Moore, R. C. Reynolds, in *X-ray Diffraction and the Identification and Analysis of Clay Minerals*, Oxford University Press, Oxford **1997**, pp. 330.
[47] T. J. Pinnavaia, *Science* **1983**, *220*, 365–371.
[48] J. Thomas, B. F. Bohor, *Clays Clay Miner.* **1968**, *16*, 83–91.
[49] M. Kaneyoshi, A. Yamagishi, M. Tanaguchi, A. Aramata, *Clays Clay Miner.* **1993**, *41*, 1–6.
[50] A. Yamagishi, M. Taniguchi, Y. Imamura, H. Sato, *Appl. Clay Sci.* **1996**, *11*, 1–10.
[51] N. Kakegawa, A. Yamagishi, *Chem. Mater.* **2005**, *17*, 2997–3003.
[52] T. Kawasaki, T. Omine, K. Suzuki, S. Hisako, A. Yamagishi, K. Soai, *Org. Biomol. Chem.* **2009**, *7*, 1073–1075.
[53] R. M. Barrer, D. M. Macleod, *Trans. Faraday Soc.* **1955**, *51*, 1290–1300.
[54] G. W. Brindley, R. E. Sempels, *Clay Miner.* **1977**, *12*, 229–237.
[55] A. Gil, L. M. Gandia, M. A. Vicente, *Catal. Rev. Sci. Eng.* **2000**, *42*, 145–212.
[56] A. Gil, S. A. Korili, M. A. Vicente, *Catal. Rev. Sci. Eng.* **2008**, *50*, 153–221.
[57] A. Gil, S. A. Korili, R. Trujillano, M. A. Vicente, *Pillared Clays and Related Catalysts*, Springer, New York **2010**.
[58] M. A. Vicente, A. Gil, F. Bergaya, in *Developments in Clay Science Handbook of Clay Science Fundamentals* (Eds.: F. Bergaya, G. Lagaly), Elsevier, Amsterdam, **2013**, vol. 2, pp. 523–557.
[59] J. T. Kloprogge, *J. Porous Mater.* **1998**, *5*, 5–41.
[60] Z. Ding, J. T. Kloprogge, R. L. Frost, G. Q. Lu, H. Y. Zhu, *J. Porous Mater.* **2001**, *8*, 273–293.
[61] H. B. Lao, C. Detellier, *Clays Clay Miner.* **1994**, *42*, 477–481.
[62] P. Sozzani, S. Bracco, A. Comotti, M. Mauri, R. Simonutti, P. Valsesia, *Chem. Commun.* **2006**, 1921–1923.
[63] J. Demarquay, J. Fraissard, *Chem. Phys. Lett.* **1987**, *136*, 314–318.
[64] R. M. Barrer, D. L. Jones, *J. Chem. Soc. A* **1971**, 2594–2603.
[65] R. M. Barrer, *Clays Clay Miner.* **1989**, *37*, 385–395.
[66] R. M. Barrer, A. D. Millington, *J. Colloid Interface Sci.* **1967**, *25*, 359–372.
[67] S. M. Thomas, J. A. Bertrand, M. L. Occelli, J. M. Stencel, S. A. C. Gould, *Chem. Mater.* **1999**, *11*, 1153–1164.
[68] M. M. Mortland, V. Berkheiser, *Clays Clay Miner.* **1976**, *24*, 60–63.
[69] B. Y. Chen, H. Kim, S. D. Mahanti, T. J. Pinnavaia, Z. X. Cai, *J. Chem. Phys.* **1994**, *100*, 3872–3880.
[70] L. P. Meier, R. Nüesch, F. T. Madsen, *J. Colloid Interface Sci.* **2001**, *238*, 24–32.
[71] J. Beyer, H. G. von Reichenbach, *Clay Miner.* **2002**, *37*, 157–168.
[72] H. Kalo, W. Milius, J. Breu, *RSC Adv.* **2012**, *2*, 8452–8459.
[73] W. Seidl, J. Breu, *Z. Kristallogr.* **2005**, *220*, 169–176.
[74] J. Shabtai, N. Frydmann, R. Lazar, in *Proceedings of the Sixth International Congress on Catalysis* (Eds.:G. G. C. Bond, P. B. Wells, F. C. Tompkins), Chemical Society, London, **1977**, vol. B5, pp. 660–667.
[75] J. Breu, W. Seidl, J. Senker, *Z. Anorg. Allg. Chem.* **2004**, *630*, 80–90.

[76] R. Mariychuk, A. Baumgartner, F. E. Wagner, A. Lerf, A. Dubbe, R. Moos, J. Breu, *Chem. Mater.* **2007**, *19*, 5377–5387.
[77] F. Tsvetkov, J. White, *J. Am. Chem. Soc.* **1988**, *110*, 3183–3187.
[78] J. Breu, A. Stoll, K. G. Lange, T. Probst, *Phys. Chem. Chem. Phys.* **2001**, *3*, 1232–1235.
[79] U. Hofmann, R. Klemen, *Z. Anorg. Allg. Chem.* **1950**, *262*, 95–99.
[80] W. F. Jaynes, S. J. Traina, J. M. Bigham, C. T. Johnston, *Clays Clay Miner.* **1992**, *40*, 397–404.
[81] G. Lagaly, A. Weiss, *Kolloid - Z. Z. Polymere* **1971**, *243*, 48–55.

Received: October 25, 2013
Published Online: January 9, 2014

Appendix 2

Tailoring the Pore Sizes of Microprous Pillared Interlayered Clays through Layer Charge Reduction

Markus M. Herling[1], Hussein Kalo[1], Sebastian Seibt[2], Rainer Schobert[2] and Josef Breu[1,*]

[1]Lehrstuhl für Anorganische Chemie I, Universität Bayreuth, Universitätsstr. 30, 95440 Bayreuth, Germany

[2]Lehrstuhl für Organische Chemie I, Universität Bayreuth, Universitätsstr. 30, 95440 Bayreuth, Germany

*e-mail: josef.breu@uni-bayreuth.de

Langmuir **2012**, *28*, 14713-14719.

Langmuir

Article

pubs.acs.org/Langmuir

Tailoring the Pore Sizes of Microporous Pillared Interlayered Clays through Layer Charge Reduction

Markus M. Herling,[†] Hussein Kalo,[†] Sebastian Seibt,[‡] Rainer Schobert,[‡] and Josef Breu*,[†]

[†]Lehrstuhl für Anorganische Chemie I, and [‡]Lehrstuhl für Organische Chemie I, Universität Bayreuth, 95440, Germany

Supporting Information

ABSTRACT: A F-rich potassium hectorite, $[K_{0.48(2)}]^{inter}[Mg_{2.54(8)}Li_{0.43}]^{oct}[Si_4]^{tet}O_{10}F_2$, with a layer charge of $x = 0.48$ per formula unit (pfu) was synthesized by high temperature melt synthesis. After Mg-exchange, the layer charge could be reduced significantly post synthesis by annealing (250 °C) as confirmed by alkylammonium exchange and cation exchange capacity. By pillaring this new low charge material with Me_2DABCO^{2+} (*N*,*N*-dimethyl-1,1-diazabicyclo [2.2.2]octane dication) and $Rh(bpy)_3^{3+}$ (rhodium-tris-2,2′-bipyridin trication), we observed a remarkable increase in micropore volume and pore diameter by Ar/Ar(l) physisorption measurements. This method allows the tailoring of pore sizes of pillared clays by reducing the layer charge and consequently the pillar density.

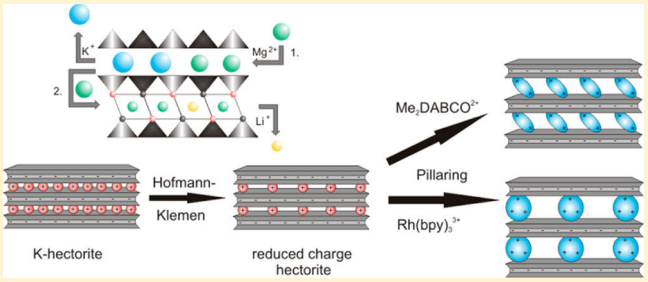

1. INTRODUCTION

Inorganic microporous materials have drawn a lot of attention in the past decade due to their wide applicability in material science, that is, as heterogeneous catalysts, molecular sieves, sensors, gas storage, or adsorbents.[1−5] Although zeolites have historically dominated these applications, more recently metal organic frameworks (MOFs) have supplemented the field of microporous materials. Pillared interlayered clays (PILCs) emerged in parallel, forming an alternative class of porous substrates. According to the IUPAC definition, pillaring describes the transformation of a layered compound into a thermally stable micro- and/or mesoporous material with retention of the layer structure. Furthermore, three criteria have to be fulfilled: (1) a chemical and thermal stability, (2) a determinable d_{001}-value, and (3) an accessible interlayer space.[6] The main advantage of this class of materials over zeolites and MOFs is the modular character, which allows post-synthesis modifications. The resulting porosity is dependent on both the layer charge of the silicate, and on the charge, size, and shape of the molecular pillar used. These pillars become part of the inner pore surface, where interesting features like chiral recognition or catalytic activity can easily be introduced with the right choice of pillar. However, organic or metal−organic PILCs are less robust, and the thermal stability is thus inferior to zeolites.

We have recently demonstrated that the intercalation of organic pillars into a layered silicate obtained by melt synthesis, which show homogeneous charge density, is a flexible and attractive route to generate microporosity.[7] This resulted in an advanced hybrid material with a narrow pore size distribution that could be used as a sorbent.[8−11] However, so far only moderate pore sizes could be realized even with the smallest organic divalent cations available such as Me_2DABCO^{2+}. The challenge to be tackled to make larger pore sizes accessible is to further reduce the charge density of the host clay (for nomenclature of clay minerals, for example, hectorite or tainiolite, see Martin et al.).[12] By direct melt synthesis of fluorohectorites, the minimum layer charge accessible is restricted by the range of possible minimum isomorphous substitution of Li^+ for Mg^{2+} in the octahedral sheet. This lower limit of the solid solution field is somewhat dependent on the type of interlayer cation and ranges from $x = 0.56$ to $x = 0.48$ pfu. Alternatively, PILCs can be accessed by oxidative pillaring of transition metal rich micas.[13] For instance, a microporous PILC was obtained by intercalating the molecular cylindrical shaped pillar Me_2DABCO^{2+} into a synthetic ferrous tainiolite $[Cs]^{inter}[Fe_2^{2+}Li]^{oct}[Si_4]^{tet}O_{10}F_2$. It was shown that oxidative conditions during the pillaring reaction promoted a significant reduction of the layer charge into the regime of smectites.[8,13] Unfortunately, even with strongly oxidizing conditions, the oxidative reduction of the layer charge was limited to 0.42 pfu.[9] As was already mentioned, besides the layer charge of the clay, the shape of the pillar restricts the pore width. In PILCs, the basal spacing will always be minimized due to the strong Coulomb attraction of polyanionic clay layer and cationic pillars in the interlayer. Consequently, nonspherical pillars will tend to orient their long axis parallel to the interlayer. The height of the interlayer space will thus be determined by the smallest extension of the pillar and might be even further reduced by partial penetration of the molecular pillar into the hexagonal hollows of the silicate layer surface. Access of probe molecules

Received: September 5, 2012
Revised: September 25, 2012
Published: September 25, 2012

into the cylindrical shaped micropores may therefore be hampered by an interlayer height, which is smaller than 3.4 Å even if larger pores exist between pillars. With the height of the silicate layer being 9.6 Å, the smallest basal spacing that will still ensure access of Ar to the cylindrically shaped micropores is approximately 13 Å; larger molecules might, however, need basal spacings larger than 15 Å.

Here, we now explore a third approach to overcome the lower limit of the layer charge of 0.42 pfu utilizing the so-called Hofmann–Klemen effect.[14] Jaynes et al. reported that the layer charge of hectorites can be reduced by isomorphic substitution of octahedral Li^+ by interlayer-Mg^{2+} by annealing the material at 250 °C.[15] In a first step, the interlayer cation (e.g., K^+) is exchanged by Mg^{2+}. During heat treatment in the second step, interlayer-Mg^{2+} then replaced octahedral Li^+ that in turn migrates into the interlayer. By each divalent Mg^{2+} replacing monovalent Li^+ in the octahedral layer, the layer charge is reduced correspondingly. The process is depicted in Figure 1.

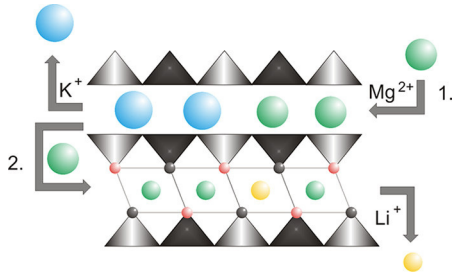

Figure 1. Scheme of the layer charge reduction by annealing utilizing the Hofmann–Klemen effect.

In this work, we present the synthesis of a low charged K-hectorite $[K_{0.48(2)}]^{inter}[Mg_{2.54(8)}Li_{0.43}]^{oct}[Si_4]^{tet}O_{10}F_2$. The layer charge was reduced post synthesis by the described routine. Finally, by intercalation of two pillars of different charge and shape, cylindrical shaped Me_2DABCO^{2+} and spherical shaped $Rh(bpy)_3^{3+}$, microporous materials of tailorable pore sizes were obtained.

2. MATERIALS AND METHODS

Sample Preparation. Stoichiometric amounts of high-purity reagents of $K_2Si_4O_9$ (Alfa Aesar, unhydrous), MgF_2 (Chempur, 99.9%), MgO (Alfa Aesar, 99.95%), Li_2SiO_3 (Alfa Aesar, 99.5%), and SiO_2 (Merck, fine granular, calcined) were weighed to a total of 50 g in Ar atmosphere in a molybdenum crucible. The crucible was sealed under high vacuum and then heated in a graphite furnace (Graphit HT-1900, Linn High Term) for the synthesis. The crucible was positioned horizontally in the furnace and rotated at 60 rpm to avoid segregation in the melt and consequent inhomogeneity of the material.[16] It was then heated from room temperature to 1750 °C (15 °C min^{-1}), left at 1750 °C for 70 min, and finally quenched to room temperature by switching off the power. Rotation was stopped at 1450 °C.

WDX Measurements. The chemical composition of the synthetic K-hectorite was determined by wavelength dispersive X-ray spectroscopy (WDX) using an electron microprobe (Jeol JXA-8200).

Charge Reduction Process. The pristine potassium hectorite (p-hectorite) was ground in a mortar, and the 125 μm fraction was sieved, dispersed in water, and treated three times with a 0.5 M $MgCl_2$ solution at 120 °C for ion exchange. The charge reduced hectorite (r-hectorite) was washed free of salts until a chloride test with a $AgNO_3$ solution was negative. The samples were then put in a quartz crucible and heated to 250 °C for 8–12 h according to literature.[15] After each heat treatment, the hectorite was again exchanged with Mg^{2+}, and the Li^+ release from the interlayer to the supernatant solution was determined by atomic absorption spectroscopy (AAS). This cycle of cation exchange followed by annealing was repeated several times (r_1–r_6-hectorite). $Me_2DABCOCl_2$ and $Rh(bpy)_3Cl_3$ were obtained according to literature procedures.[8,17] For pillaring, the p- and r-hectorites (100 mg) were treated hydrothermally four times for 12 h at 120 °C using 30 mg of $Me_2DABCOCl_2$ in 15 mL of H_2O or 20 mg of $Rh(bpy)_3Cl_3$ in 15 mL of H_2O.

The samples were also washed thoroughly with water until a chloride test with a $AgNO_3$ solution was negative.

CEC Determination. The CEC was determined according to DIN ISO 11260.[18] The layer charge density was determined according to the literature procedure by alkylammonium exchange with different chain lengths *n*.[19]

Powder X-ray Diffraction. The powder X-ray diffraction patterns (PXRD) were recorded with a STOE Stadi P powder diffractometer (transmission geometry, Cu Kα1 radiation (λ = 1.54056 Å), Ge monochromator, MYTHEN 1K detector).

Ar-Adsorption Measurements. Physisorption measurements were performed using a Quantachrome Autosorb 1 at Ar(l) temperature (87.35 K) with Ar. Prior to measurement, the samples were dried 24 h at 150 °C in high vacuum. The thermal stability of the pillars was verified by thermogravimetric analysis using a Mettler Toledo TGA/SDTA 851e from 25 to 800 °C at N_2-atmosphere with a heating rate of 10 °C/min. The pore sizes and volumes were calculated using a nonlocal DFT model (software Quantachrome Autosorb 1, version 2.11), Ar on zeolite (silica, cylindrical pores, equilibrium model).[20] The BET equation calculates the surface area of a monolayer adsorption and is applied to a linear part of the isotherm. This p/p_0 range is normally taken to be between 0.1 and 0.3 but has to be adjusted to lower p/p_0 values for microporous materials. Recommendations suggested by Rouquerol were followed for choosing the appropriate range of the isotherm.[21]

3. RESULTS AND DISCUSSION

In order to synthesize a fluorohectorite with the lowest possible layer charge that is directly accessible by melt synthesis, we chose a nominal composition of $[K_{0.3}]^{inter}[Mg_{2.7}Li_{0.3}]^{oct}[Si_4]^{tet}O_{10}F_2$, which is already in the miscibility gap. Consequently, a K-rich fluorohectorite was obtained in mixture with a K-poor (norbergite, $Mg_3SiO_4F_2$) impurity phase. The composition of the p-hectorite (pristine-hectorite) was determined by microprobe analysis (WDX) of three selected crystals (with 18, 10, and 8 points averaged) to be $[K_{0.48(2)}]^{inter}[Mg_{2.54(8)}Li_{0.43}]^{oct}[Si_4]^{tet}O_{10}F_2$, which should represent the lower layer charge limit for hectorite accessible by melt synthesis. At the same time, the side phase, norbergite, does not interfere with the different cation exchange and intercalation experiments used to manipulate and characterize the hectorite phase. It is inert under these conditions. The p-hectorite was obtained as a microcrystalline product (Figure S1) and was white in color. Considering the lower hydration enthalpy of K^+ as compared to Na^+, this K-hectorite does not spontaneously swell in humid air. The basal spacing was 10.0 Å.

Moreover, the diffractogram suggests that K-hectorite was not turbostratically disordered but rather showed only few planar defects. Turbostratic disorder refers to random, noncommensurable translations or rotations of adjacent silicate layers in the stack. As a consequence, all cross-peaks diminish, and in the diffractogramm only very few unsymmetric, λ-shaped *hk*-bands are observed aside from the still symmetrical 00*l* basal reflections. Clearly, we observe *hkl*-reflections allowing indexing of the diffractogram, suggesting a much improved stacking order, which in turn is in line with a highly ordered or at least semiordered crystalline material. Reference 22 gives a detailed discussion of different planar stacking faults observed in 2:1-

dx.doi.org/10.1021/la303573e | Langmuir 2012, 28, 14713–14719

layered silicates including typical PXRD patterns. The diffractogram featuring symmetrical reflections (Figure 2) can readily be indexed, and the following unit cell parameters were obtained: a = 5.23(1) Å, b = 9.06(2) Å, c = 10.09(2) Å, β = 99.33(3)°.

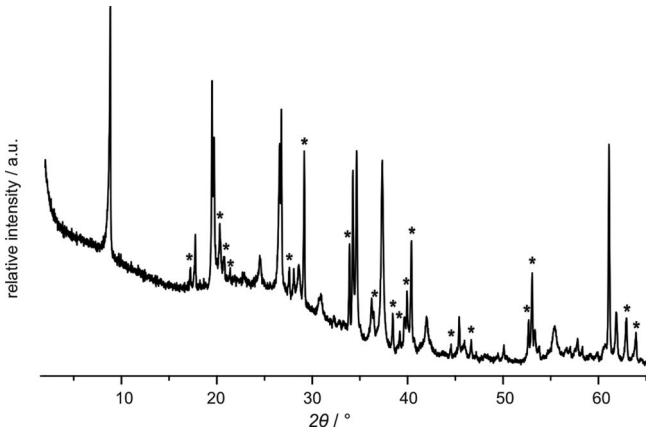

Figure 2. Powder X-ray diffraction pattern of a K-hectorite $[K_{0.48(2)}]^{inter}[Mg_{2.54(8)}Li_{0.43}]^{oct}[Si_4]^{tet}O_{10}F_2$ as synthesized. Reflections of the crystalline side-product, norbergite, are marked by asterisks.

The absolute layer charge could not be determined via the CEC because the edges of the layer contribute to the total CEC and because the weight fraction of hectorite in the mixture with norbergite cannot be determined with sufficient precision. Therefore, the charge density and its homogeneity were investigated according to Lagaly and Weiss.[23] With this method, the equivalent area of interlayer cations varies by increasing the chain length, n, of alkylammonium cations ($C_nH_{2n+1}NH_3^+$, n = 6–15).

With a certain chain length, a densely packed monolayer of intercalated alkylammonium will no longer be able to satisfy the charge density of the silicate layer, and some bilayers must be realized to ensure charge neutrality.[16] Taking the equivalent areas published by Lagaly, alkylammonium ions with a chain length of up to n = 6 are expected to still be able to counterbalance a layer charge of x = 0.48 pfu of a clay with $a \times b$ = 47.4 Å^2 in a monolayer arrangement.[19] Indeed, we observed a sharp basal reflection with d = 13.4 Å, indicating a monolayer with n = 6 (Figure 3).

Starting with n = 7, the basal reflection was broadened and gradually shifted to higher d-spacings due to random interstratifications of some bilayers. With n = 9, a superstructure reflection was observed at approximately 32 Å, indicating an ordered interstratification of mono- and bilayers. Such ordered interstratifications are only observed as a consequence of a homogeneous charge density.[16,24] Only bilayers (d = 17.5 Å) are present when n = 13. For the scope of this work, in particular, the beginning of the transition to some bilayers is of interest because it directly corresponds to the layer charge. If this transition occurs with n = 6, the equivalent areas suggested by Lagaly indicate that x < 0.48 pfu, while a beginning transition with n = 7 and n = 8 indicates x < 0.43 pfu and x < 0.39 pfu, respectively. Because of the stepwise increase of the equivalent area by the integer increase of n, the resolution of the Lagaly method is limited; only differences in x greater than 0.04 pfu can be observed. The determined lower layer charge limit of x < 0.48 pfu was therefore in perfect agreement with the formula of p-hectorite as determined by WDX measurements.

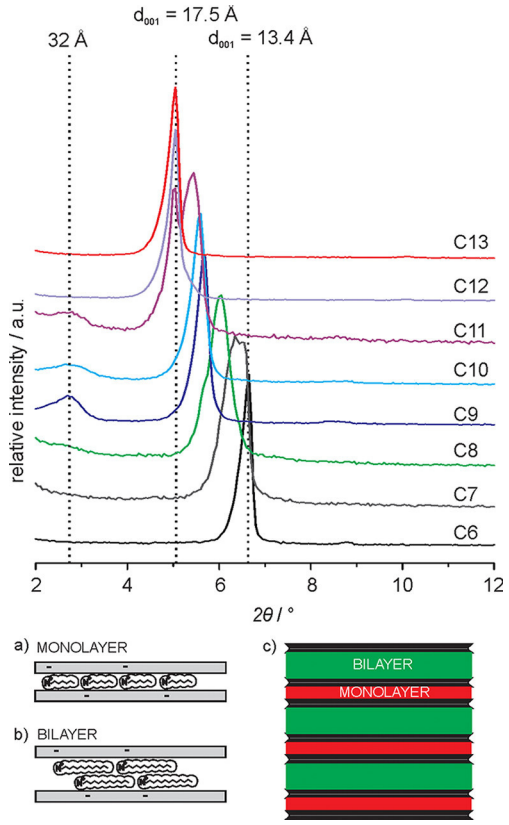

Figure 3. Evolution of PXRD profiles (p-hectorite) with increasing chain length (n = 6 to n = 14) upon alkylammonium exchange. The basal spacings expected for mono- (a), bilayer (b), and ordered interstratifications (c) of these two arrangements at 13.4, 17.5, and 32 Å, respectively, are marked by dotted lines.

Ignoring the contribution of the edges, for $[K_{0.48(2)}]^{inter}[Mg_{2.54(8)}Li_{0.43}]^{oct}[Si_4]^{tet}O_{10}F_2$ a CEC of 119 meq/100 g would be expected. Since neither the norbergite side-phase could be separated nor could its weight fraction be determined with sufficient precision, only the CEC of the mixture could be determined. Please note that while norbergite does not show any appreciable CEC itself, it contributes to the mass, and thus the specific CEC of the mixture is expected to be significantly lower than 119 meq/100 g. However, although the absolute CEC related to hectorite cannot be determined, the changes observed when reducing the layer charge contain valuable information. The norbergite weight fraction in the mixture does not change during heat treatments at 250 °C (please see Supporting Information Figures S3, S4).

The CEC as measured by intercalation of Ba^{2+}-cations into the interlayer was 84 meq/100 g for p-hectorite. Repeated Mg-exchange of p-hectorite followed by annealing at 250 °C leads to a gradual decrease of the layer charge by a modification of the so-called Hofmann–Klemen effect, a mechanism that is described in the Introduction (Figure 1).

Usually the Hofmann–Klemen effect has been used to reduce the charge of natural dioctahedral Li-exchanged montmorillonites where upon heat treatment the small interlayer cations migrate into empty octahedral sites. Consequently, because this method relies on octahedral vacancies, it will not work on trioctahedral smectites such as hectorite.

Moreover, while it was possible to mediate pore sizes of dioctahedral montmorillonites this way, the poorly defined and

dx.doi.org/10.1021/la303573e | Langmuir 2012, 28, 14713–14719

heterogeneous layer charge density distributions of these natural clays resulted in very broad pore size distributions of pillared derivatives. Here, we apply synthetic hectorite of high crystallinity, as evidenced by the diffraction pattern in Figure 2. Also, it is much easier to synthesize highly ordered trioctahedral clays through melt processing methods than it is to prepare dioctahedral derivatives under high pressure hydrothermal conditions. High processing temperatures (>800 °C) in turn ensure a nearly perfect solid solution of octahedral cations, and consequently the charge density distribution of such melt-synthesized trioctahedral representatives is superior. Thus, the pore size distribution observed for pillared derivatives of these hectorites is also greatly improved in comparison to earlier work on reduced charged natural montmorillonites. However, for trioctahedral hectorites as applied here, the method of charge reduction has to be modified. Instead of interlayer Li-cations migrating into empty octahedral sites, in this modified Hofmann–Klemen effect, divalent interlayer Mg-cations interchange position with monovalent octahedral Li-cations.

According to literature reports, the amount of octahedral Li^+ decreased with each heat treatment, while the interlayer Li^+ produced by the heat treatment is released to the supernatant by the subsequent Mg^{2+}-exchange.[15]

Figure 4 shows that the amount of Li^+ released in each Hofmann–Klemen cycle was approximately constant. With

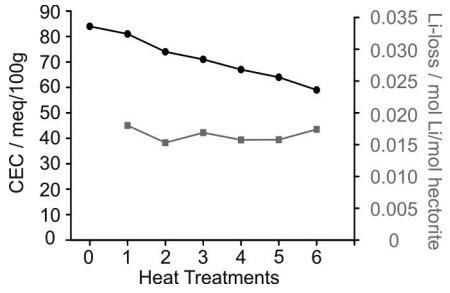

Figure 4. Lithium release (gray) and evolvement of CEC (black) as a function of repeated Hofmann–Klemen cycles.

each heat treatment about 0.016 of initially 0.43 octahedral Li^+ was lost. The small variations in the Li-loss of different cycles can be attributed to slightly different heat treatment durations (1–2 h).

As suggested by the mechanism sketched in Figure 1, the Li-loss coincides with a steady decrease of the CEC from initially 84 meq/100 g to 59 meq/100 g after six cycles.

The CEC reduction in turn was in line with the layer charge reduction seen with the Lagaly method. The limiting chain length, where the transition to some bilayers was observed, increased from n = 6 for p-hectorite to n = 8 for r_6-hectorite (Figure 5), indicating a final layer charge x < 0.39 pfu.

Thus, a reduction of layer charge of approximately 0.1 pfu could be achieved by six Hofmann–Klemen cycles. Contrary to what has been observed for p-hectorite, no superstructure reflection at 32 Å was observed with intermediate chain lengths for r_6-hectorite, suggesting that the charge homogeneity might be somewhat diminished by the layer charge reduction procedure. Nevertheless, it is still significantly narrower as compared to pillared derivatives of naturally occurring minerals with a poorly defined, heterogeneous layer charge resulting in a broad pore size distributions.

Reduction of the layer charge will concomitantly cut the number of pillars needed for charge neutrality, which will

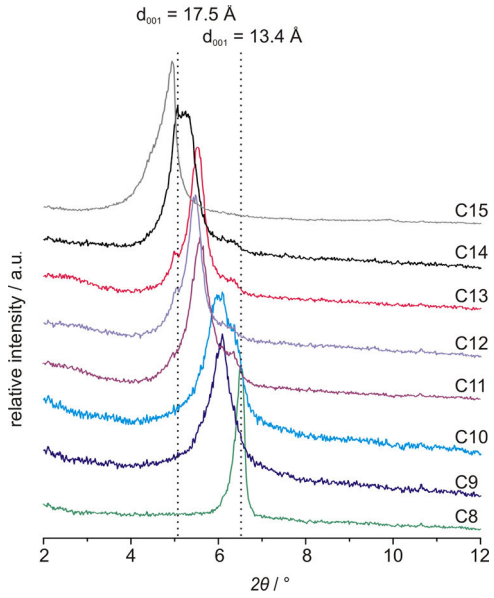

Figure 5. Evolution of PXRD profiles (r_6-hectorite) with increasing chain length (n = 8 to n = 15) upon alkyl-ammonium exchange. The basal spacings expected for mono- and bilayer arrangements at 13.4 and 17.5 Å, respectively, are marked by dotted lines.

further separate pillars from each other, and consequently the lateral pore size is expected to significantly increase. We therefore pillared both p- and r_6-hectorite with Me_2DABCO^{2+} and $Rh(bpy)_3^{3+}$. These two pillars differ in shape and charge and thus represent a broad range of possible micropore structures accessible with these clay hosts. While the first represents an ellipsoidal pillar, the latter may be regarded spherical in a first approximation.

With fixed layer charge, applying the spherical trivalent cation $Rh(bpy)_3^{3+}$ as pillar is expected to increase both the height and the width of the cylindrical micropores as compared to the more cigar-like divalent Me_2DABCO^{2+} (Figure 6).

Assuming a hexagonal arrangement of pillars in the interlayer space and charge neutrality, the distance between the pillars can be calculated from the charge density of the clay:[8,9,11]

$$y/(d^2_{\text{pillar}} \sin 60°) = x/a^2 \sin 60° \quad (1)$$

where y is the charge of the pillar; d_{pillar} is the intermolecular distance between the pillars in the ab plane; x is the layer charge; and a is the unit cell axis a of the host lattice.

Combining the van der Waals diameter of the pillar and the distance between the pillars, the mean pore width can then be estimated as a function of the layer charge x. As illustrated in Figure 7, a reduction of the layer charge by 0.1 pfu would result in an increase of the pore width of up to 2 Å.

The hydrothermal intercalation of both the p- and the r_6-hectorite with Me_2DABCO^{2+} and $Rh(bpy)_3^{3+}$ led to a microporous material. Upon pillaring, the 001 reflection of the silicate is shifted to 14.4 Å for Me_2DABCO^{2+} and 17.5 Å for $Rh(bpy)_3^{3+}$, respectively (please see Supporting Information Figures S3, S4). Both PILCs obtained were thermally stable to temperatures >300 °C (Figure S2).

The 00*l*-series of all PILCs were highly rational, indicating that all interlayer spaces have been pillared.[25] The variation coefficients of the 00*L*-series were determined to be 0.30, 0.10, 0.33, and 0.07 for Me_2DABCO-p-hectorite, Me_2DABCO-r_6-

dx.doi.org/10.1021/la303573e | Langmuir 2012, 28, 14713–14719

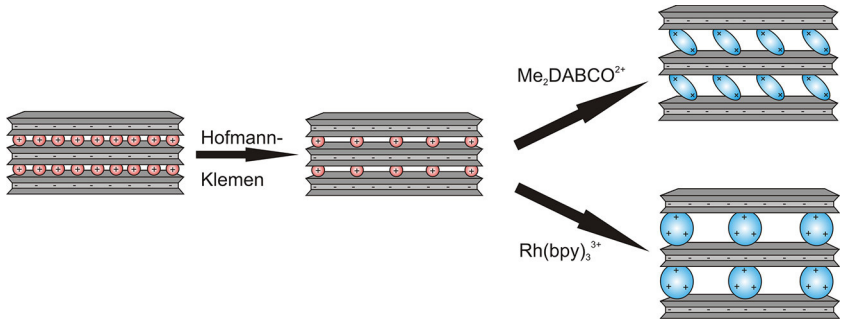

Figure 6. Illustration of the pillaring process starting with the as-synthesized p-hectorite, followed by layer charge reduction, which allows one to modify the distance between the pillars. The height of the interlayer spaces is crucially dependent on both the size and shape of the pillars.

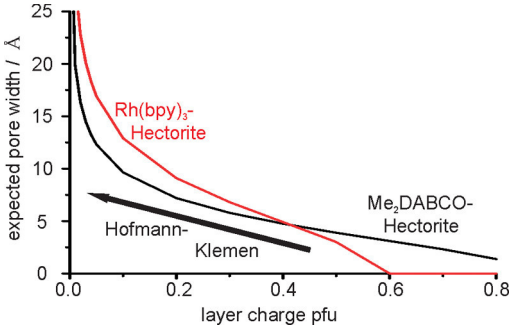

Figure 7. Estimated pore size as a function of layer charge x pfu for $Rh(bpy)_3$- and Me_2DABCO-hectorite.

hectorite, $Rh(bpy)_3$-p-hectorite, and $Rh(bpy)_3$-r_6-hectorite, respectively.

Adsorption of pillars in excess of the CEC via intersalation of ion pairs clearly could be ruled out by EDX analysis, which showed no Cl^- anions. Apparently, due to the good solubility of both pillar molecules in water, repeated and careful washing with water following pillaring assured a complete removal of pillars in excess of the CEC.

Physisorption measurements with Ar/Ar(l) indicated a Type I isotherm for all four materials without significant signs of hysteresis (Figure 8), representing a typical microporous material.

The increase of the pore volume of Me_2DABCO-r_6-hectorite between 0.35 and 0.5 p/p_0 may be attributed to increased surface roughness and interparticle porosity induced by the repeated heat treatment at 250 °C.

The narrow pore size distribution of the PILC's indicated a regular arrangement of the pillar molecules in the interlayer space.[9,10] The pore sizes and volumes of the micropores <10 Å are listed in Table 1, and pore size distributions are shown in Figure 9.

For both pillars, reduction of layer charge yielded significantly higher micropore volumes for PILC-r-hectorites as compared to PILC-p-hectorites. The pillar density decreased and the distance between adjacent pillars in the plane of the interlayer increased by reduction of the layer charge. The height of the interlayer is however not affected, basal spacings of p- and r-samples did not differ, and interlayer heights of 4.8 and 7.9 Å for Me_2DABCO^{2+}- and $Rh(bpy)_3^{3+}$-PILCs, respectively, can be deduced from the basal spacings observed. The shape of the cylindrical pores is determined by both interpillar distance and height of the interlayer. The maxima of the pore width distribution were shifted by 1−2 Å toward larger pores for

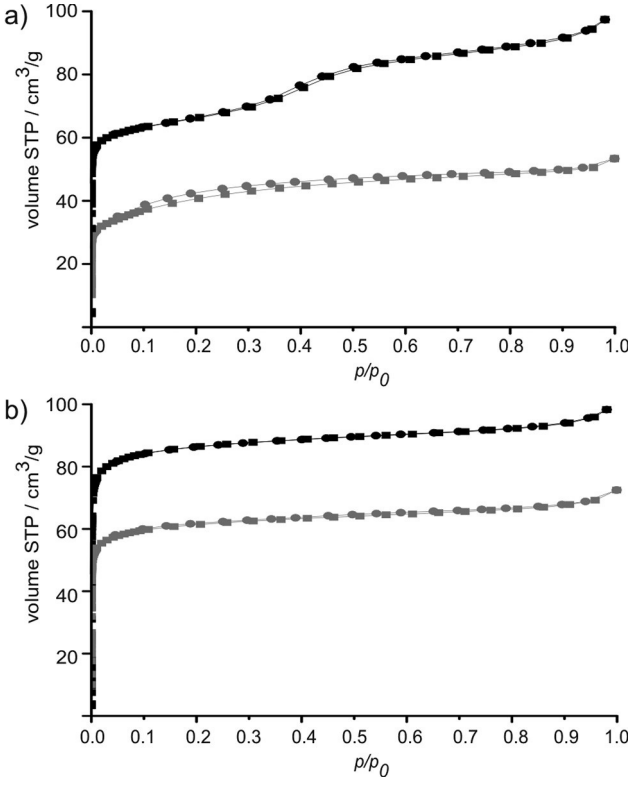

Figure 8. Physisorption isotherm (Ar/Ar(l)) of (a) Me_2DABCO-r_6-hectorite (black), Me_2DABCO-p-hectorite (gray), and (b) $Rh(bpy)_3$-r_6-hectorite (black), and $Rh(bpy)_3$-p-hectorite (gray).

Table 1. Ar/Ar(l) Physisorption Measurements at 87.35 K

host	pillar	basal spacing [Å]	pore volume (<10 Å) [cm^3/g]	BET surface [m^2/g]
p-hectorite	Me_2DABCO^{2+}	14.4	0.053	149
	$Rh(bpy)_3^{3+}$	17.5	0.112	211
r_6-hectorite	Me_2DABCO^{2+}	14.4	0.150	223
	$Rh(bpy)_3^{3+}$	17.5	0.164	341

samples with reduced layer charge. The magnitude of the shift is in agreement with expectations expressed in Figure 7.

The effect of layer charge reduction becomes even more obvious when comparing the pore volumes of micropores. The pore volume (<10 Å) of Me_2DABCO-hectorites could be increased by 95% from 0.077 to 0.150 cm^3/g, while the pore volume of $Rh(bpy)_3$-hectorite could be increased by 46% from 0.112 to 0.164 cm^3/g.

dx.doi.org/10.1021/la303573e | Langmuir 2012, 28, 14713−14719

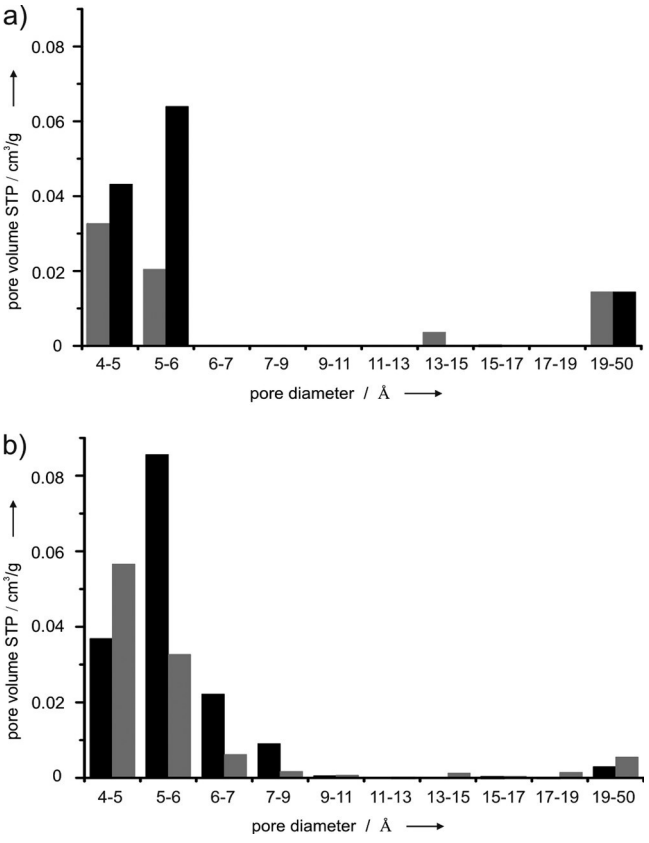

Figure 9. Pore size distributions of (a) Me_2DABCO-r_6-hectorite (black), Me_2DABCO-p-hectorite (gray), and (b) Rh(bpy)$_3$-r_6-hectorite (black), and Rh(bpy)$_3$-p-hectorite (gray).

In line with expectations, the spherical $Rh(bpy)_3^{3+}$ creates larger pores and higher pore volumes as compared to Me_2DABCO^{2+} because the spherical shape assured a greater interlayer height and the higher charge of the pillar allowed for fewer, further separated pillars.

4. CONCLUSION

The layer charge of K-hectorite $[K_{0.48(2)}]^{inter}[Mg_{2.54(8)}Li_{0.43}]^{oct}[Si_4]^{tet}O_{10}F_2$ can be reduced post synthesis in small and finite steps utilizing the Hofmann–Klemen effect. Pillaring these layered materials with molecular pillars yields a significant increase in both micropore volume and pore width upon charge reduction. The shape and size of the micropores of PILCs are however not only determined by the layer charge of the hectorite, but crucially depend on the charge, size, and shape of the pillar applied. Being able to fine-tune the layer charge and to choose from an infinite number of cationic pillars allows for tailoring the microporous structure of PILCs in a highly modular way, while at the same time introducing desired functionalities via the pillar.

■ ASSOCIATED CONTENT

Supporting Information

SEM-image of the p-hectorite, thermogravimetric analysis of Me_2DABCO-r_6-hectorite and Rh(bpy)$_3$-r_6-hectorite, and X-ray powder diffraction patterns and log *P* plots of both intercalated p- and r_6-hectorites with Me_2DABCO^{2+} and $Rh(bpy)_3^{3+}$. This material is available free of charge via the Internet at http://pubs.acs.org

■ AUTHOR INFORMATION

Corresponding Author

*E-mail: josef.breu@uni-bayreuth.de.

Notes

The authors declare no competing financial interest.

■ ACKNOWLEDGMENTS

This work was financially supported by the Deutsche Forschungsgemeinschaft (SFB 840). We thank the Bayerisches Geoinstitut, Bayreuth, Germany for the WDX measurements.

■ REFERENCES

(1) Cheetham, A. K.; Ferey, G.; Loiseau, T. Open-framework inorganic materials. *Angew. Chem., Int. Ed.* **1999**, *38*, 3268–3292.
(2) Kaskel, S.; Schuth, F.; Stocker, M. Metal-organic open frameworks (MOFs). *Microporous Mesoporous Mater.* **2004**, *73*, 1.
(3) Ogawa, M.; Kuroda, K. Photofunctions of intercalation compounds. *Chem. Rev.* **1995**, *95*, 399–438.
(4) Ohtsuka, K. Preparation and properties of two-dimensional microporous pillared interlayered solids. *Chem. Mater.* **1997**, *9*, 2039–2050.
(5) Thomas, J. M. The Bakerian Lecture, 1990 - New microcrystalline catalysts. *Philos. Trans. R. Soc., A* **1990**, *333*, 173.
(6) Schoonheydt, R. A.; Pinnavaia, T.; Lagaly, G.; Gangas, N. Pillared clays and pillared layered solids. *Pure Appl. Chem.* **1999**, *71*, 2367–2371.
(7) Tsapatsis, M.; Maheshwari, S. Pores by pillaring: Not always a maze. *Angew. Chem., Int. Ed.* **2008**, *47*, 4262–4263.
(8) Baumgartner, A.; Sattler, K.; Thun, J.; Breu, J. A route to microporous materials through oxidative pillaring of micas. *Angew. Chem., Int. Ed.* **2008**, *47*, 1640–1644.
(9) Stöcker, M.; Seidl, W.; Seyfarth, L.; Senker, J.; Breu, J. Realisation of truly microporous pillared clays. *Chem. Commun.* **2008**, *5*, 629–631.
(10) Stöcker, M.; Seyfarth, L.; Hirsemann, D.; Senker, J.; Breu, J. Microporous PILCs - Synthesis, pillaring mechanism and selective cation exchange. *Appl. Clay Sci.* **2010**, *48*, 146–153.
(11) Baumgartner, A.; Wagner, F. E.; Herling, M.; Breu, J. Towards a tunable pore size utilizing oxidative pillaring of the mica ferrous tainiolite. *Microporous Mesoporous Mater.* **2009**, *123*, 253–259.
(12) Martin, R. T.; Bailey, S. W.; Eberl, D. D.; Fanning, D. S.; Guggenheim, H.; Kodama, H.; Pevear, D. R.; Srodon, J.; Wicks, J. J. Report of the Clay Minerals Society Nomenclature Committee; Revised classification of clay materials. *Clays Clay Miner.* **1991**, *39*, 333–335.
(13) Mariychuk, R.; Baumgartner, A.; Wagner, F. E.; Lerf, A.; Dubbe, A.; Moos, R.; Breu, J. Synthesis, structure, and electric conductivity of ferrous tainiolite and its oxidative conversion into coarse-grained swellable smectite. *Chem. Mater.* **2007**, *19*, 5377–5387.
(14) Hofmann, U.; Klemen, R. Verlust der Austauschfaehigkeit von Lithiumionen an Bentonit durch Erhitzung. *Z. Anorg. Allg. Chem.* **1950**, *262*, 95–99.
(15) Jaynes, W. F.; Traina, S. J.; Bigham, J. M.; Johnston, C. T. Preparation and characterization of reduced-charge hectorites. *Clays Clay Miner.* **1992**, *40*, 397–404.
(16) Breu, J.; Seidl, W.; Stoll, A. J.; Lange, K. G.; Probst, T. U. Charge homogeneity in synthetic fluorohectorite. *Chem. Mater.* **2001**, *13*, 4213–4220.
(17) Takagi, Y.; Komatsu, T.; Kitabata, Y. Crystallization of zeolite beta in the presence of chiral amine or rhodium complex. *Microporous Mesoporous Mater.* **2008**, *109*, 567–576.
(18) Soil quality - Determination of effective cation exchange capacity and base saturation level using barium chloride solution (DIN ISO 11260: 1997-05).
(19) Lagaly, G. Characterization of clays by organic-compounds. *Clay Miner.* **1981**, *16*, 1–21.
(20) Thommes, M. *Nanoporous Materials: Science and Engineering*; Imperial College Press: London, 2004.

(21) Rouquerol, J.; Llewellyn, P.; Rouquerol, F. *Studies in Surface Science and Catalysis Characterization of Porous Solids - VII*; Elsevier: Amsterdam, 2007; Vol. *160*, pp 49−56.
(22) Breu, J.; Seidl, W.; Stoll, A. Fehlordnung bei Smectiten in Abhängigkeit vom Zwischenschichtkation. *Z. Anorg. Allg. Chem.* **2003**, *629*, 503−515.
(23) Lagaly, G.; Weiss, A. Arrangement and orientation of cationic tensides on silicate surfaces. 4. Arrangement of alkyl-ammonium ions in low-charged silicates of films. *Kolloid Z. Z. Polym.* **1971**, *243*, 48.
(24) Möller, M. W.; Hirsemann, D.; Haarmann, F.; Senker, J.; Breu, J. Facile scalable synthesis of rectorites. *Chem. Mater.* **2010**, *22*, 186−196.
(25) Moore, D. M.; Reynolds, R. C. *X-Ray Diffraction and the Identification and Analysis of Clay Minerals*; Oxford University Press: Oxford, 1997.

Supporting Information

Tailoring the Pore Sizes of Microporous Pillared Interlayered Clays through layer charge reduction

Markus M. Herling[†], Hussein Kalo[†], Sebastian Seibt[‡], Rainer Schobert[‡], Josef Breu[†]*

Figures

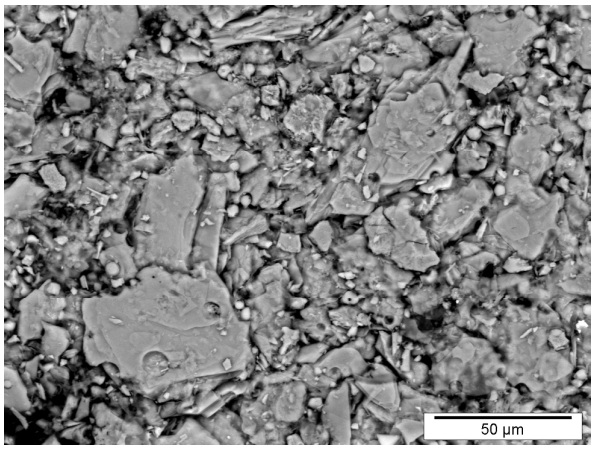

Figure S1. REM image of p-hectorite $[K_{0.48(2)}]^{inter}[Mg_{2.54(8)}Li_{0.43}]^{oct}[Si_4]^{tet}O_{10}F_2$

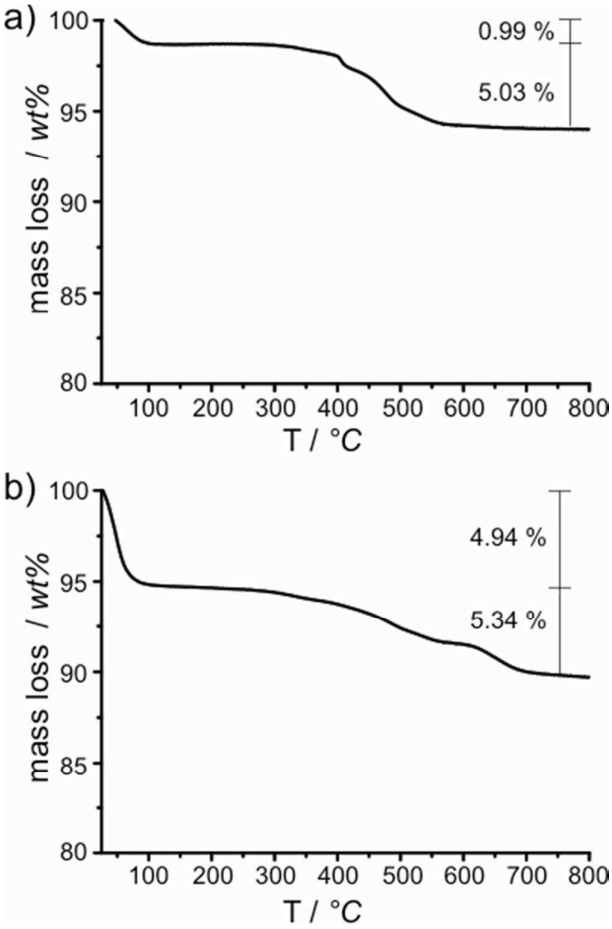

Figure S2. Thermogravimetric analysis of a) Me_2DABCO-r_6-hectorite and b) $Rh(bpy)_3$-r_6-hectorite from 25 °C to 800 °C in N_2 atmosphere (heating rate 10 °C min^{-1}). First mass loss is contributed to water loss; second mass loss is due to decomposition of the pillar.

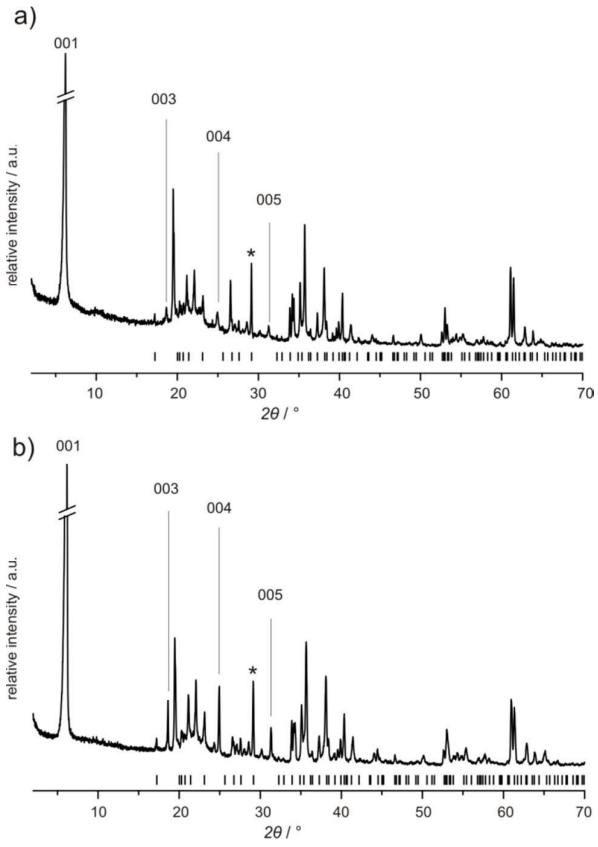

Figure S3. Powder X-ray diffraction patterns of a) Me_2DABCO-p-hectorite and b) Me_2DABCO-r_6-hectorite.

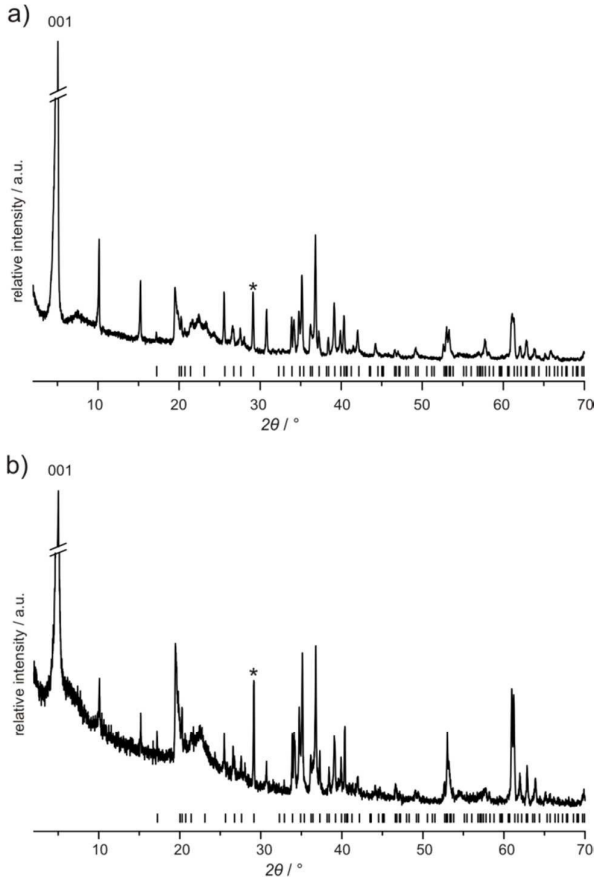

Figure S4. Powder X-ray diffraction patterns of a) $Rh(bpy)_3$-p-hectorite and b) $Rh(bpy)_3$-r_6-hectorite.

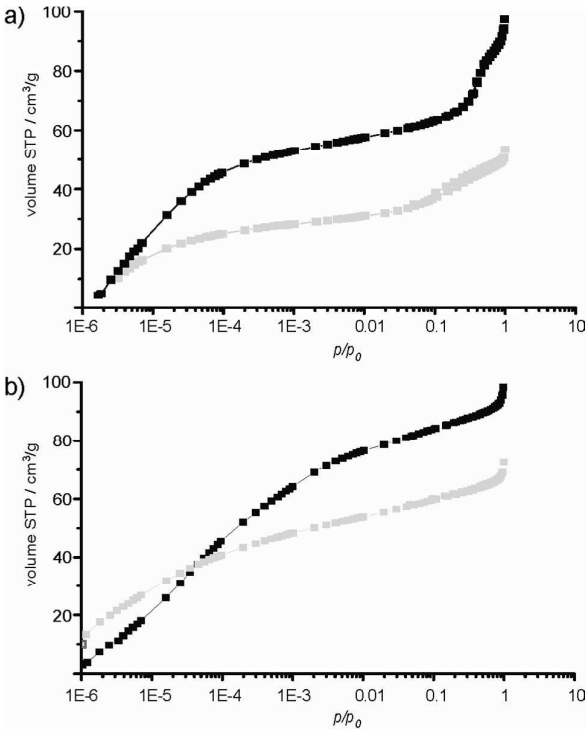

Figure S5. Physisorption isotherm (log (Ar/Ar(l))) of a) Me_2DABCO-r_6-hectorite (black), Me_2DABCO-p-hectorite (grey), b) $Rh(bpy)_3$-r_6-hectorite (black), and $Rh(bpy)_3$-p-hectorite.

Appendix 3

Porosity of Pillared Clays Studied by Hyperpolarized ^{129}Xe NMR Spectroscopy and Xe Adsorption Isotherms

Caroline D. Keenan[1], Markus M. Herling[2], Renée Siegel[1], Nikolaus Petzold[3], Clifford R. Bowers[4], Ernst A. Rössler[3], Josef Breu[2] and Jürgen Senker[1,*]

[1]Inorganic Chemistry III, Universität Bayreuth, 95447 Bayreuth, Germany

[2]Inorganic Chemistry I, Universität Bayreuth, 95447 Bayreuth, Germany

[3]Department of Chemistry, University of Florida, Gainesville, Florida 32611, United States

[4]Experimental Physics II, Universität Bayreuth, 95447 Bayreuth, Germany

*e-mail: juergen.senker@uni-bayreuth.de

Langmuir **2013**, *29*, 643-652.

Langmuir

Article

pubs.acs.org/Langmuir

Porosity of Pillared Clays Studied by Hyperpolarized ^{129}Xe NMR Spectroscopy and Xe Adsorption Isotherms

Caroline D. Keenan,[†] Markus M. Herling,[‡] Renée Siegel,[†] Nikolaus Petzold,[∥] Clifford R. Bowers,[§] Ernst A. Rössler,[∥] Josef Breu,[‡] and Jürgen Senker*,[†]

[†]Inorganic Chemistry III, Universität Bayreuth, 95447 Bayreuth, Germany

[‡]Inorganic Chemistry I, Universität Bayreuth, 95447 Bayreuth, Germany

[§]Department of Chemistry, University of Florida, Gainesville, Florida 32611, United States

[∥]Experimental Physics II, Universität Bayreuth, 95447 Bayreuth, Germany

Supporting Information

ABSTRACT: The influence of the layer charge on the microstructure was studied for a series of three hybrid pillared interlayered clays based on the organic dication Me_2DABCO^{2+} and charge reduced synthetic fluorohectorites. To get a detailed picture of the local arrangements within the interlayer space, multinuclear solid-state NMR spectroscopy was performed in conjunction with high-resolution ^{129}Xe MAS NMR, temperature-dependent wide-line 1D and 2D ^{129}Xe NMR, and Ar/Ar(l) and Xe/Xe(l) physisorption measurements. The resulting layer charge (x) for the three samples are 0.48, 0.44, and 0.39 per formula unit (pfu). The samples exhibit BET equivalent surfaces between 150 and 220 m^2/g and pore volumes which increase from 0.06 to 0.11 cm^3/g while the layer charge reduces. 1D and 2D ^{1}H, ^{13}C, ^{19}F, and ^{29}Si MAS data reveal that the postsynthetic charge reduction induces regions with higher defect concentrations within the silicate layers. Although the pillars tend to avoid these defect-rich regions, a homogeneous and regular spacing of the Me_2DABCO^{2+} pillars is established. Both the Ar/Ar(l) physisorption and ^{129}Xe NMR measurements reveal comparable pore dimensions. The trend of the temperature-dependent wide-line ^{129}Xe spectra as well as the exchange in the EXSY spectra is typical for a narrow 2D pore system. ^{129}Xe high-resolution experiments allow for a detailed description of the microstructure. For x = 0.48 a bimodal distribution with pore diameters between 5.9 and 6.4 Å is observed. Reducing the layer charge leads to a more homogeneous pore structure with a mean diameter of 6.6 Å (x = 0.39). The adsorption enthalpies ΔH_{ads} determined from the temperature-dependent ^{129}Xe chemical shift data fit well to the ones derived from the Xe/Xe(l) physisorption measurements in the high-pressure limit while the magnitude of ΔH_{ads} in the low-pressure limit is significantly larger. Thus, the ^{129}Xe data are influenced by adsorbate−adsorbent as well as adsorbate−adsorbate interactions.

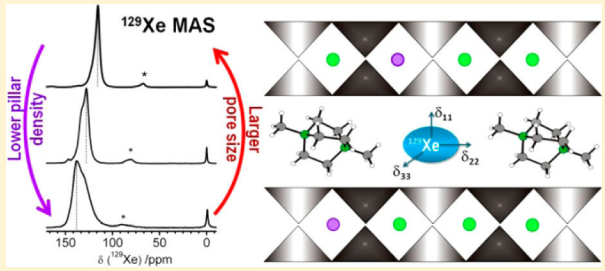

1. INTRODUCTION

Aside from zeolites and metal−organic frameworks (MOFs),[1] pillared interlayered clays (PILCs) have emerged as new microporous materials with a unique property profile.[2,3] PILCs are characterized by the intercalation of aptly dimensioned cationic complexes, oligometalates, or organocations in the interlayer of polyanionic lamellar materials.[4−7] Since the pillars are held in place by nondirectional electrostatic interactions, their charge, shape, and polarity may be varied in a wide range. Because of this modular character, PILCs allow for a meticulous adjustment of their microporosity. The interpillar distance depends on the charges of both the silicate and the pillars, while the pore morphology is governed by both size and shape of the pillars which become part of the pore surface. With the exception of the pillar charge these parameters can be adjusted in minute increments. In contrast, alterations in the porosity of MOFs are only possible by chemically expanding the linker molecule, resulting in a minimal step size on the order of a couple of angstroms. This offers the option to fine-tune the interlayer cavities of PILCs so as to closely fit the shape of substrate molecules which is a unique feature of PILCs available to neither zeolites nor MOFs.

Until recently, the exploitation of the potential of PILCs remained severely hampered by homogeneity deficiencies of the naturally occurring inorganic host materials like montmorillonite. These are, as a rule, nanocrystalline, structurally disordered substrates with an inhomogeneous layer charge density, leading to a lack of long-range order of the pillar arrays and a broad pore size distribution (from micro- to mesopores).[8] Despite these shortcomings, natural clays have been used for the synthesis of hybrid[9,10] layered silicates with "immobilized" organic molecules. For most of these applica-

Received: November 12, 2012
Revised: December 11, 2012
Published: December 16, 2012

tions the individual contributions of interlayer space reactivity versus surface reactivity and interparticle porosity to the overall substrate adsorption remained largely unclear.

Breu et al. have previously reported that layered silicates with exceedingly homogeneous charge density are accessible by melt synthesis.[11−16] The intercalation of appropriately dimensioned organic cations then leads to microporous PILCs characterized by a narrow pore size distribution and a high degree of long-range order of the pillar arrays as demonstrated by X-ray diffraction and solid-state NMR spectroscopy.[4−7] The last obstacle on the way to highly ordered PILCs with fully tunable pore sizes was the limited reducibility of the layer charge crucial for achieving maximum interpillar distance and the largest possible accessible pore sizes. It has only recently been found that the layer charge of synthetic potassium hectorite, $[K_{0.48(2)}]^{inter}[Mg_{2.54(8)}Li_{0.43}]^{oct}[Si_4]^{tet}O_{10}F_2$, can be reduced in a stepwise fashion below 0.40 pfu. This is realized by postsynthesis utilizing a modified Hofmann−Klemen effect.[17−19] This is done by first replacing the interlayer cations, e.g., K^+, of pristine hectorite with Mg^{2+} followed by annealing at 250 °C, which leads to isomorphic substitution of octahedral Li^+ by this interlayer Mg^{2+} and to a corresponding reduction of the layer charge. Pillaring these layered materials with simple molecules such as Me_2DABCO^{2+} (*N*,*N*-dimethyl-1,1-diazabicyclo[2.2.2]-octane dication) results in a significant increase in micropore volume and width.[19]

With this method for the fabrication of hectorites with finely graduated layer charges in place, a series of analogous PILCs derived from hectorites were prepared that were charge reduced up to six Mg^{2+}-exchange/annealing cycles and then pillared with Me_2DABCO^{2+}.[19] While previously the micropores of these materials were only characterized by measuring Ar-adsorption isotherms, here we perform an in-depth analysis applying solid-state 1D ^1H, ^{13}C, ^{19}F and ^{29}Si, and 2D $^{19}F\{^1H\}$ and $^1H\{^{13}C\}$ heteronuclear correlation (HETCOR) NMR spectroscopic experiments to study the arrangement of the intercalated Me_2DABCO^{2+} and investigate the degree of structural disorder within the clay support and pillar environments. This includes probing changes within the tetrahedral and octahedral sheets of the PILCs with reduced layer charge as well as investigating potential selective positioning of the organic pillar within the inorganic matrix. Additionally, the homogeneity of the micropore distribution with changing pillar density are studied by hyperpolarized (HP) ^{129}Xe NMR methods in conjunction with Ar/Ar(l) and Xe/Xe(l) physisorption measurements. In particular, we utilize CF-HP ^{129}Xe NMR under MAS to obtain high-resolution HP ^{129}Xe spectra in order to accurately probe the micropore size distribution. The potential influence of the pillar density within the interlayer space on Xe adsorption properties is examined as well.

The ^{129}Xe NMR chemical shift parameters are very sensitive to both pore size and geometry due to the large polarizabilty of its electronic cloud and have been proven useful in characterizing the adsorptive and structural properties of a broad variety of microporous, nanostructured materials.[20−26] The spectral enhancement afforded by ^{129}Xe HP methods is unique in its ability to report on even small modifications in porosity, pore size/structure, and connectivity with changing environmental parameters of a resident microstructure.[27−30] The introduction of continuous-flow hyperpolarization (CF-HP)[31−34] methods increases the signal-to-noise ratio even further and allows for faster measurements. For a distinct adsorption site, the observed chemical shift δ_{obs} is characterized by a sum of potential perturbations on the Xe nucleus, expressed as[35] $\delta_{obs} = \delta_{ref} + \delta_S + \delta_{Xe-Xe}\rho_{Xe} + \delta_{SAS} + \delta_{E,M}$. Here, δ_{ref} refers to the gas phase Xe shift extrapolated to zero pressure (0 ppm), δ_S reflects Xe−surface interactions, δ_{Xe-Xe} denotes contributions from Xe−Xe collisions (depending on the xenon density ρ_{Xe}), and δ_{SAS} accounts for interactions between Xe and strong adsorption sites, while $\delta_{E,M}$ arises from potential electric and/or magnetic fields induced by the absorbed environment. HP methods generally employ dilute ρ_{Xe} in order to effectively avoid the Xe−Xe contribution to the δ_{obs}.

2. MATERIALS AND METHODS

Sample Preparation. Details concerning the synthesis and pillaring process of the low charged potassium hectorite is described elsewhere.[19] The host clay is based on a synthetic K-hectorite ($[K_{0.48(2)}]^{inter}[Mg_{2.54(8)}Li_{0.43}]^{oct}[Si_4]^{tet}O_{10}F_2$). The pristine hectorite (p-hectorite) was first exchanged with Mg^{2+} and charge reduced by subsequent wash/heat treatments at 250 °C. Here, $r_{(n)}$ indicates the number of wash/heat cycles performed on the charged reduced samples. For pillaring, 100 mg of p-hectorite, 3 times (r_3-hectorite), and 6 times charge reduced (r_6-hectorite) were treated hydrothermally four times for 12 h at 120 °C using 30 mg of $Me_2DABCOCl_2$ in 15 mL of H_2O. The samples were also washed thoroughly with water until a chloride test with an $AgNO_3$ solution was negative. Dried samples were packed in the glovebox for all measurements, unless stated otherwise.

Ar Adsorption. Physisorption measurements were performed using a Quantachrome Autosorb 1 at Ar(l) temperature (87.35 K). Prior to measurement, the samples were dried at 150 °C for 24 h in high vacuum. The pore sizes and volumes were calculated using a nonlocal DFT model (software Quantachrome Autosorb 1, version 2.11, Ar on zeolite/silica, cylindrical pores, equilibrium model).[36]

Xe Adsorption. Xenon physisorption measurements were performed at different temperatures (180, 187, and 195 K) with Xe (purity 4.8). Prior to measurement, the samples were dried at 150 °C for 24 h in high vacuum. The isosteric heat of adsorption was calculated by using the Clausius−Clapeyron equation where R is the gas constant, θ the fraction of the adsorbed sites at a pressure p, and T the temperature.

$$-\Delta H^\circ_{ad} = R\{[\partial(\ln p)]/[\partial(1/T)]\}_\theta \quad (1)$$

Powder X-ray Diffraction. The powder X-ray diffraction patterns (PXRD) of the samples were recorded with a STOE Stadi P powder diffractometer (transmission geometry, Cu Kα_1 radiation (λ = 1.540 56 Å), Ge monochromator, MYTHEN 1K detector). The samples were dried for 24 h at 150 °C.

Solid-State NMR Spectroscopy. Spectra were recorded on Bruker Avance III 400 and Avance II 300 spectrometers operating at B_0 fields of 9.4 and 7.1 T, respectively. Chemical shifts of both ^1H and ^{13}C nuclei were referenced indirectly to TMS using adamantane, while ^{19}F and ^{29}Si were referenced using NaF (−221 ppm from $CFCl_3$) and $N(SiMe_3)_3$ (2.4 ppm from TMS). All cross-polarization (CP) experiments were performed using a ramped (from 50 to 100%) ^1H lock pulse during the contact time. SPINAL-64[37] decoupling was employed during the acquisition time for all CP-MAS and heteronuclear chemical shift correlation (HETCOR) spectra with a radio frequency (rf) field strength of 50 kHz.

The $^{13}C\{^1H\}$ CP-MAS NMR experiments were performed at 9.4 T on a double-resonance 4 mm Bruker MAS probe operating at a rotation frequency of 10 kHz. The ^1H and ^{13}C 90° pulse lengths were 3.2 and 3.0 μs, respectively. Measurements utilized a contact time (τ_{cp}) of 3.0 ms with a ^1H RF of 78 kHz and ^{13}C RF of 47 kHz. The $^{13}C\{^1H\}$ HETCOR experiments were obtained using the PRESTO-II[38] sequence employing the symmetry based $R18_1^7$ sequence for the magnetization transfer which lasted 88.9 μs (corresponding to an incomplete cycle of 16 180° pulses).

dx.doi.org/10.1021/la304502r | *Langmuir* 2013, 29, 643−652

The ^{1}H and ^{19}F NMR experiments were recorded at 7.1 T on a triple-resonance 4 mm Bruker MAS probe operating at a rotation frequency of 12.5 kHz. The ^{1}H and ^{19}F could be simultaneously tuned using an external splitter and filters. The ^{1}H and ^{19}F 90° pulse lengths were set to 3.3 and 2.7 μs, respectively. The 2D $^{1}H\{^{19}F\}$ HETCOR spectrum was acquired using a CP with a contact time of 500 μs and a ^{19}F and ^{1}H RF field of 69 kHz (with a ramp from 50 to 100%) and 50 kHz, respectively.

^{29}Si and ^{13}C experiments performed at 7.1 T were acquired on a triple-resonance 7 mm Bruker MAS probe operating at a rotation frequency of 4.0 kHz. The $^{13}C\{^{1}H\}/^{29}Si\{^{1}H\}$ CP Hartmann−Hahn match conditions were obtained with RF field strengths of 50 and 26 kHz for the ^{13}C and ^{29}Si, respectively, with corresponding ^{1}H RF fields of 44 (with ^{13}C) and 30 kHz (with ^{29}Si). The ^{13}C and ^{29}Si CP-MAS experiments utilized contact times of 3.0 and 8.0 ms, respectively. The ^{29}Si single-pulse experiments (SP) were acquired using a 45° pulse length of 4.4 μs and a recycle delay of 60 s.

Hyperpolarized ^{129}Xe NMR Spectroscopy. A home-built polarizer was used for all hyperpolarized ^{129}Xe NMR experiments. A gas mixture comprised of 1%:2%:97%, $Xe:N_2:He$ (by volume) was polarized using 30 W of diode laser power (Coherent Inc.) tuned to the Rb D_1 line ($\lambda \cong 794$ nm), providing a polarization of about 5%. The total overpressure was maintained at 6.2 bar; the low mole fraction of Xe within the gas mixture ensures limited Xe−Xe contributions to the observed ^{129}Xe chemical shift at room temperature (and higher). The flow rate remained relatively constant during the experiment time (~300 sccm). Specific details concerning the design principles and performance quality will be available in a subsequent article.

Variable temperature (VT) HP ^{129}Xe NMR spectra were obtained on an Avance II 300 Bruker spectrometer. The static double resonance Bruker probe was modified to incorporate CF-HP ^{129}Xe through a 3.0 mm inner diameter PEEK sample holder. Variable pressure experiments were performed using naturally abundant, thermally polarized Xe gas using the same probe and coil employed for the VT, CF-HP experiments. CF-HP ^{129}Xe 2D EXSY measurements were obtained with a recycle delay of 1 s; mixing times (τ_m) were varied between 2 and 500 ms. It should be noted that the recycle delay under CF is limited by the replacement of the HP ^{129}Xe gas rather than the relaxation time.[32] While this allows for fast acquisition of the 2D spectra, it can limit the amount of detectable HP ^{129}Xe gas during the exchange time. Here, the ^{129}Xe 90° pulse length was set to 3.7 μs. All ^{129}Xe spectra were referenced using the internal Xe gas peak under hyperpolarized conditions (0 ppm).

CF-HP ^{129}Xe MAS NMR measurements were performed on a 7 mm Bruker MASCAT probe at a rotation frequency of 4.0 kHz. The Xe-MASCAT probe utilizes a stream of HP ^{129}Xe gas mixture (1%:2%:97%, $Xe:N_2:He$) which is vented to atmosphere, where the gas flow is created by the pressure difference. A backpressure of 6.2 bar within the pumping cell is maintained in order to retain sufficient ^{129}Xe HP levels. Additional details of a similar probe are available in the literature.[39] Adequate flow was determined by an initial change in the MAS rotation frequency (about −5 Hz) due to the additional force introduced to the rotor along the magic angle by the gas stream. While we cannot specify a value for the applied flow rate under these conditions, we are sure that the partial pressure of ^{129}Xe is significantly lower than the 0.062 bar utilized within the CF-HP ^{129}Xe measurements as the applied partial pressure of ^{129}Xe within the MAS rotor was <0.020 bar. As such, the observed chemical shifts are deemed to be within the boundaries of the ^{129}Xe limiting shift. Contributions of δ_{Xe-Xe} can then be neglected.

3. RESULTS AND DISCUSSION

The XRD analysis indicates the successful formation of microporous material upon pillaring with Me_2DABCO^{2+} (see Figure S1). The d_{001} values of all three samples (p-, r_3-, and r_6-Me_2DABCO^{2+}-hectorite) are identical, resulting in a basal spacing of 14.0 Å. Physisorption measurements with Ar/Ar(1) are consistent with previous reports, exhibiting a Type-I isotherm, representing a microporous material (Figure S2). It should be noted that nonspherical pillars like Me_2DABCO^{2+} tend to orient their long axis parallel to the interlayer gallery, the height of which will thus be determined by the smallest extension of the pillar.[4,5] It is also worth mentioning that while the interpillar distance may be fine-tuned by reducing the charge density of the hectorite, the interlayer height remains constant as indicated by similar basal spacings (Table 1). Thus,

Table 1. Ar/Ar(l) Physisorption Measurements at 87.35 K

host	pillar	basal spacing [Å]	pore vol (<20 Å) [cm^3/g]	BET surface [m^2/g]
p-hectorite	Me_2DABCO^{2+}	14.0	0.059	149
r_3-hectorite	Me_2DABCO^{2+}	14.0	0.070	149
r_6-hectorite	Me_2DABCO^{2+}	14.0	0.107	223

the pore size is actually adjusted in an anisotropic fashion with one dimension being kept constant. The values for the pore volumes (pore width <20 Å) are shown in Table 1, while the pore size distribution is provided in Figure 1. Both parameters shift toward the formation of larger pores with increasing wash/annealing cycles.

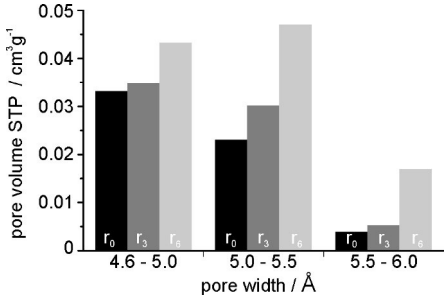

Figure 1. Pore size distribution for p-Me_2DABCO^{2+}-hectorite (black), r_3-Me_2DABCO^{2+}-hectorite (dark gray), and r_6-Me_2DABCO^{2+}-hectorite (light gray).

Changes in the trioctahedral occupation have a marked effect on the ^{19}F chemical shift. As such, modifications in the Mg^{2+}/Li^{+} connectivity, and thus octahedral layer composition, are directly observable through ^{19}F MAS NMR.[40−42] The more electronegative the trioctahedral environment, the more deshielded the ^{19}F nucleus becomes. As such, ^{19}F MAS NMR spectroscopy provides an alternate probe for the Mg^{2+}/Li^{+} ratio which correlates with the layer charge assuming that no other charge compensating mechanisms are in action and one Li^{+} is replaced by one Mg^{2+}. Two distinct, chemically nonequivalent fluorinated sites are observed under CP-MAS conditions for all samples with resonances centered around −174.0 and −180.5 ppm (Figure 2). In accordance with the literature,[40−42] we attribute the peaks with the smaller shift values to Li^{+} containing trioctahedral sites, indicated by the red cluster of resonances in Figure 2. The higher shift values are subsequently assigned to $[Mg^{2+}]_3$ trioctahedral environments (blue cluster of resonances in Figure 2). Norbergite ($Mg_3SiO_4F_2$), which forms during the synthesis of the hectorite educts as an impurity,[19] was identified by comparing $^{19}F\{^{1}H\}$ CP-MAS to quantitative ^{19}F SP spectra and found to be centered near −176.6 ppm for all samples (gray line, Figure 2).

dx.doi.org/10.1021/la304502r | Langmuir 2013, 29, 643−652

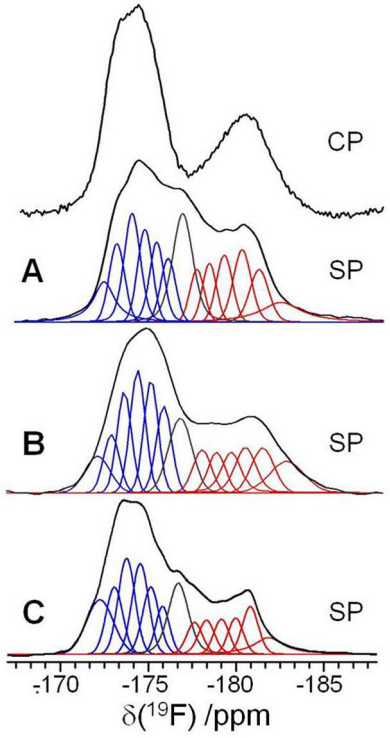

Figure 2. ^{19}F MAS single-pulse (SP) spectra of p-, r_3-, and r_6-Me_2DABCO^{2+}-hectorite (A, B, and C, respectively), measured at a rotation frequency of 12.5 kHz. The $^{19}F\{^1H\}$ CP-MAS NMR spectrum of p-Me_2DABCO^{2+}-hectorite is given for comparison (top spectra) as it clearly locates the spectral position of the impurity, norbergite.

The fine structure exhibited within the SP ^{19}F MAS line shape suggests a minor influence of differences within the second coordination sphere. As such, spectral deconvolution was performed on all spectra in order to obtain quantitative information on the relative $[Mg^{2+}]_3$ to $[Mg^{2+}]_2[Li^+]$ environmental ratio (see Table 2). Interestingly, a shift difference of roughly 6 ppm in the ^{19}F NMR resonance associated with the one-for-one substitution of Li^+ for Mg^{2+} is pretty well maintained over each cluster of resonances. As expected, the Mg^{2+} content increases with reduced layer charge. Ratios for all samples (p-, r_3-, and r_6-hectorite) are consistent with those obtained from atomic absorption spectroscopy (AAS), demonstrating that indeed a one-to-one replacement of Li^+ with Mg^{2+} takes place within the octahedral layer. Thus, no cation vacancies are formed and the Mg^{2+}/Li^+ ratio is representative for the layer charge. It should be noted that the minimum number of resonances were used in order to obtain an adequate refinement.

Table 2. Relative Mg^{2+}-to- Li^+ Ratios Obtained from AAS for p-, r_3-, and r_6-Hectorite Samples Are Compared to Values Extracted from the Deconvoluted ^{19}F MAS NMR Spectra

sample	layer charge	Mg^{2+}:Li^+ (AAS)	Mg^{2+}:Li^+ (^{19}F NMR)
p-hectorite	0.48	5.9(1):1	5.8:1
r_3-hectorite	0.44	6.9(1):1	6.8:1
r_6-hectorite	0.39	7.9(1):1	8.1:1

2D $^1H\{^{19}F\}$ HETCOR NMR was performed on r_6-hectorite in order to identify whether the intercalated pillars preferentially arrange themselves within the interlayer space. This is done by correlating the ^1H species from the organic pillar to the 1D ^{19}F environments located within the inorganic host clay. Consistent with the results of the ^{19}F NMR experiments (Figure 2), at least two distinct chemical environments can be extracted from the 2D $^1H\{^{19}F\}$ HETCOR spectrum for both the Li^+-containing and Mg^{2+}-rich trioctahedral domains (Figure 3A). A clear correlation is observed for the ^1H of both $-CH_2-$ and $-CH_3$ species of Me_2DABCO^{2+} and all trioctahedral fluorine atoms.

A similar splitting is observed within the $-CH_2-$ and $-CH_3$ associated ^1H resonances within the 2D $^{13}C\{^1H\}$ HETCOR spectrum between various ^{13}C and ^1H species of the intercalated Me_2DABCO^{2+} in r_6-hectorite (Figure 3B). Analogous experiments performed on p-hectorite confirm the existence of multiple types of ^1H environments (Figure S3, Supporting Information). In addition, the relative peak ratios within each ^1H species ($-CH_3$ and $-CH_2-$) appear to be reflective of the changing Mg^{2+} to Li^+ ratios with layer charge. 1D projections over the ^1H domain are provided for both p- and r_6-hectorite for comparison (Figure S4). As such, we assign the $-CH_2-$ and $-CH_3$ ^1H species possessing the higher relative intensity to the $[Mg^{2+}]_3$ trioctahedral domain. The upfield component of each ^1H species (now associated with the Li^+-containing triad) decreases with the reduced layer charge, consistent with the ^{19}F MAS spectra. It should be noted that the ^{13}C CP-MAS spectra of the p-, r_3- and r_6-Me_2DABCO^{2+}-hectorite are quite similar and consistent with previously published results (see Figure S5).[43]

Data obtained from both $^1H\{^{19}F\}$ and $^{13}C\{^1H\}$ 2D HETCOR measurements indicate that the Me_2DABCO^{2+} pillars correlate equally with both Mg^{2+}-rich and Li^+-containing trioctahedral environments within the clay support. This lack of selectivity suggests a quite uniform layer charge distribution over the surface of the host silicate material. In addition, the correlation between the $-OH$ environment (attributed to the edge of the silicate layer) and the electrostatically neutral $[Mg^{2+}]_3$ trioctahedral environment suggest that the Li^+ ions are well incorporated within the octahedral layer.

The SP ^{29}Si NMR spectrum of p-hectorite (Figure 4, top) exhibits two distinct signals at −93.8 and −61.0 ppm. The main resonance accounts for ^{29}Si within a Q^3 environment which is characterized by a SiO_4 tetrahedron bound to three neighboring SiO_4 tetrahedra through bridging oxygen atoms.[44] The symmetric nature of this resonance reflects a significant degree of order within the tetrahedral and octahedral layers. The smaller resonance at −61 ppm is attributed to the Q^0 environment of the impurity phase, norbergite ($Mg_3SiO_4F_2$)—the lack of nearby protons makes it indiscernible under CP-MAS conditions. The main resonance shifts to −94.0 and −94.4 ppm for r_3-hectorite and r_6-hectorite, respectively. This upfield shift with reduced layer charge is expected and likely due to modifications in the nearest-neighbor structural environment with cation occupancy, reflecting adjustments in the mean Si−O−Si bond angle.[45−47] The shoulder located upfield of the main peak within the ^{29}Si spectra of both r_3 and r_6-hecotrite becomes more distinct with increasing wash/annealing cycles.

According to the literature, a one-for-one replacement of Li^+ for Mg^{2+} will result in a slight upfield shift in the ^{29}Si resonance due to electronegativity effects.[48] Thus, the progressive separation in the ^{29}Si resonances indicates an increase in structural disorder within the tetrahedral layer. The lack of enhancement of the upfield component with CP suggests

dx.doi.org/10.1021/la304502r | Langmuir 2013, 29, 643−652

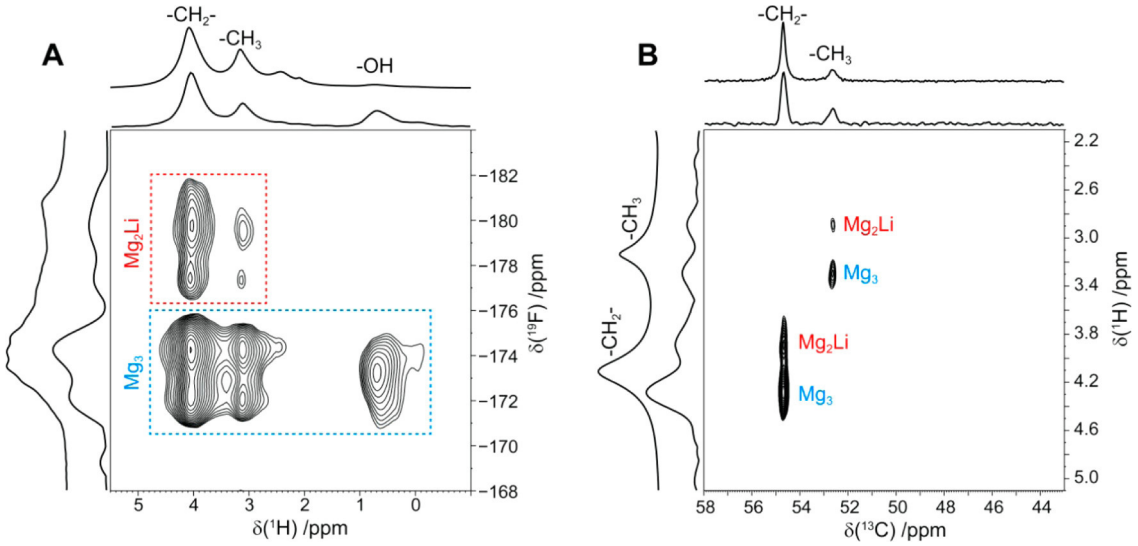

Figure 3. (A) $^{1}H\{^{19}F\}$ CP-HETCOR and (B) $^{13}C\{^{1}H\}$ PRESTO-HETCOR spectra of r_6-Me_2DABCO^{2+}-hectorite. 1D spectra of the corresponding nuclei are provided above the projections for comparison.

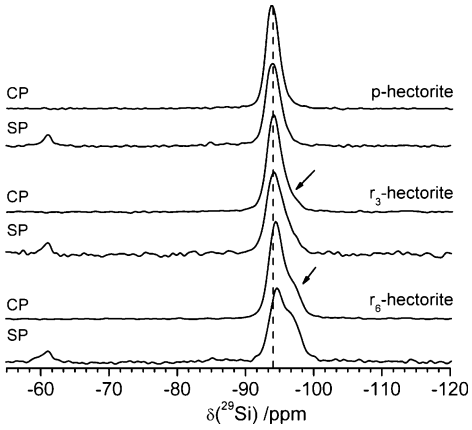

Figure 4. ^{29}Si HPDEC and corresponding ^{29}Si $\{^{1}H\}$CP-MAS NMR spectra of p-hectorite, r_3-hectorite, and r_6-Me_2DABCO^{2+}-hectorite (top to bottom).

weaker interactions with the intercalated pillared species, indicating that the pillars avoid distorted environments within the intercalation process. Similar line shapes were observed in fluoromica intercalated with octadecylammonium ions.[49] However, in contrast to our system, these trends were attributed to vacancies created within the octahedral layer during the ion exchange process.

So far, the results of the ^{1}H, ^{13}C, ^{19}F, and ^{29}Si solid-state NMR measurements indicate a regular spacing of the pillar Me_2DABCO^{2+} within the interlayer space as evidenced by the lack of preferential correlation between the ^{1}H species of the Me_2DABCO^{2+} pillar and the Mg^{2+}-rich and Li^{+}-containing trioctahedral environments. The decreased sensitivity of the secondary Q^3 site within the ^{29}Si spectra under CP-MAS conditions (upfield peak within r_3- and r_6-hectorite) suggests that the organic pillars avoid the distorted silicon environments introduced within the host clay with the charge reduction process. Since we observe a one-to-one replacement of Li^{+} with Mg^{2+}, we consider only structural distortions. We do not envisage a partial transition into a dioctahedral material.

The variable temperature (VT) CF–^{129}Xe NMR spectra are characterized by a broad shape typical for a chemical shift anisotropy (CSA) at high and low temperatures (Figure 5). This shape is either caused by a markedly heterogeneous pore

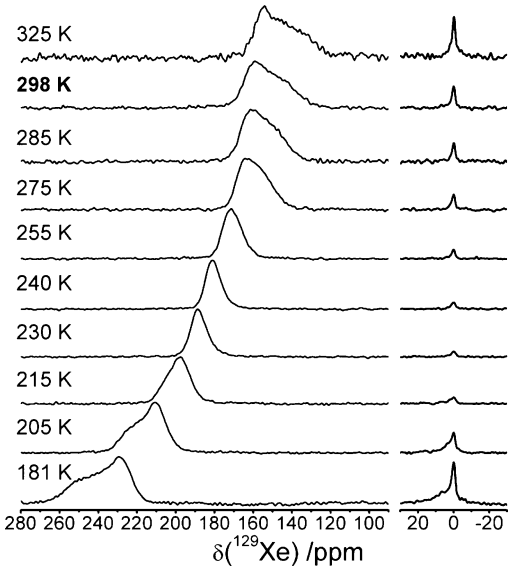

Figure 5. Variable temperature CF-HP ^{129}Xe NMR spectra of Xe adsorbed within p-Me_2DABCO^{2+}-hectorite.

microstructure with large and small cavities or arise from inhomogeneities in the electric field surrounding the Xe nucleus due to spatially confined environments. The latter case refers to the classic CSA line shape within microporous, channel-like systems (e.g., carbon nanotubes) where at low Xe loading conditions the CSA is characterized by a positive span ($\Omega = \delta_{zz} - \delta_{iso}$). The surface interactions δ_S with the walls perpendicular to the axis normal are dominant and δ_{Xe-Xe} contributions along the channel length are negligible.[50−52] An increase in ρ_{Xe} results in a competition between the two, eventually leading in the reversal in the sign of the CSA when $\delta_{Xe-Xe} > \delta_S$. Contrary to a channel-like system, Xe in PILC materials has limited mobility along the axis normal and free mobility within the $x-y$-plane, resulting in a higher degree of confinement between the silicate sheets (axis normal). A line

dx.doi.org/10.1021/la304502r | Langmuir 2013, 29, 643−652

shape resulting from a spatial constraint of the adsorbed ^{129}Xe atom would result in a negative span in the CSA at low loading, where $\delta_{zz} < \delta_{iso}$. Similar to channel-like systems, the sign is reversed when $\delta_{Xe-Xe} > \delta_S$. However, differences in the adsorption properties of the heterogeneous microstructure within the porous matrix may also manifest as changes in the ^{129}Xe line shape.

To distinguish between these two scenarios, 2D exchange (2D EXSY) spectra were measured at both high and low Xe loadings using CF-HP ^{129}Xe NMR spectroscopy.

CF-HP ^{129}Xe 2D EXSY spectra were performed at 298 and 195 K. As can be seen in their corresponding VT spectra (Figure 5), these temperatures possess opposite signs in their CSA. Diagonal elements indicate nonexchanging Xe species during the mixing time and off-diagonal elements signify exchange between regions with different chemical shifts. At ambient temperature (low Xe loading) the cross-peaks between the gaseous and adsorbed species of Xe are distributed over the whole chemical shift range of the CSA broadened line shape (Figure 6A). The exchange between the PILC lattice and the gas phase takes place on the order of 100 ms. The boxlike shape centered around the CSA pattern of the adsorbed Xe is attributed to interparticle diffusion, where the desorbed gas phase Xe is reabsorbed into a neighboring crystallite possessing a different orientation with respect to the magnetic field. This is supported by the nearly identical time scales of the exchange processes between Xe_{gas}–$Xe_{adsorped}$ and $Xe_{adsorped}$–$Xe_{adsorped}$ (Figure S6).

As seen in Figure 6B, a drastic change in the adsorbed phase dynamics is observed at high loading (low temperatures). Not only is the boxlike shape exchange pattern unobservable at a τ_m of 100 ms, the gas phase cross-peaks are lacking as well. These results indicate that all available HP ^{129}Xe gas is condensed within the PILC pore environment, suggesting a denser packing and a limited exchange capacity with the gas phase. Still within the interlayer space Xe diffusion will take place although without a visible effect on the cross-intensity. This strongly favors the second scenario of a homogeneous but confined microstructure. As seen in the VT CF-HP ^{129}Xe spectrum under static conditions, the anisotropic broadening due to competing internal interactions might obscure the presence of similar but multiple sites. As such, high-resolution CF-HP ^{129}Xe MAS NMR was further employed in order to identify subtle changes in the micropore size distribution with changing surface conditions.

The high-resolution CF-HP ^{129}Xe MAS spectra (Figure 7) show a nearly complete averaging of CSA broadening for all samples as evidenced by the very small spinning sidebands. Thus, we can associate the broadness of the spectral line shape with the pore size distribution and assign the main peak intensities (and their shoulders) to pores having distinct volumes. As a reminder, a reduction in layer charge leads to a decrease in the pillar density within the interlayer space. The subsequent increase in the average micropore width manifests as changes in the ^{129}Xe chemical shift parameters. This allows for an estimation of the effective pore diameter directly from the observed ^{129}Xe chemical shift values via the mean free path model,[53] assuming no charge induced shifts by divalent Me_2DABCO^{2+} intercalated pillars. The empirical relationship between the mean free path (λ) of Xe within a microporous void and the limiting ^{129}Xe chemical shift ($\delta_S > \delta_{Xe-Xe}$) is given by $\delta_0 = 243 \times [2.054/(2.054 + \lambda)]$ according to the Demarquay–Fraissard model.[53] The numeric value of λ can then be related to the effective pore diameter (D_{eff}) assuming either a cylindrical or spherical pore geometry. Considering the 2D pore network and small interlayer height of our PILC materials, we assumed a cylindrical model for our analysis,

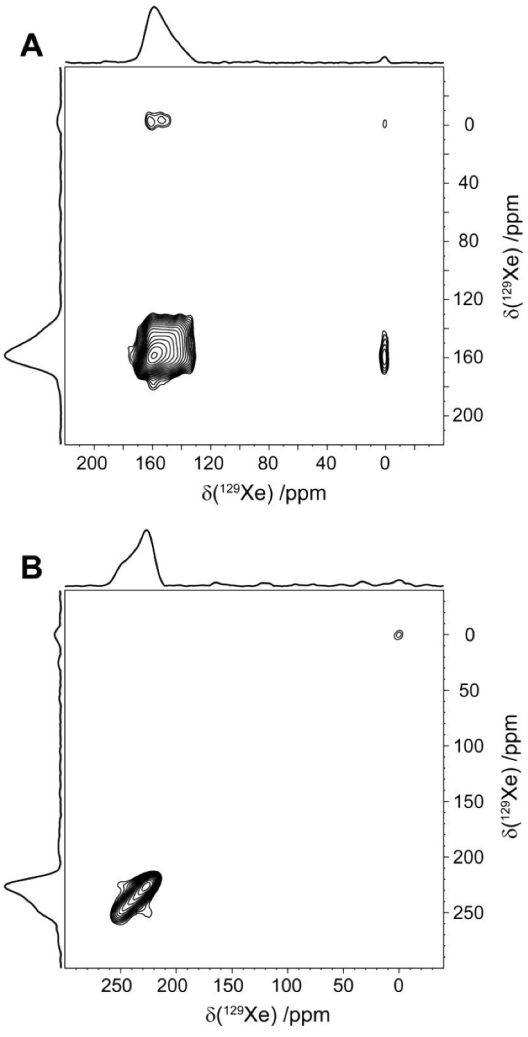

Figure 6. 2D EXSY spectra of CF-HP ^{129}Xe p-Me_2DABCO^{2+}-hectorite under static conditions, measured at (A) 298 K and (B) 195 K and a mixing time of 100 ms.

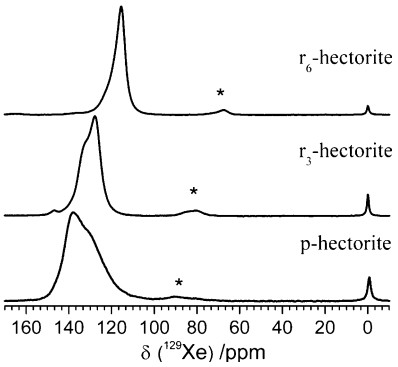

Figure 7. CF-HP ^{129}Xe MAS spectra of Xe adsorbed within p-, r_3-, and r_6-Me_2DABCO^{2+}-hectorite measured at 298 K (ν_{rot} = 4 kHz). Asterisks indicate spinning sidebands.

dx.doi.org/10.1021/la304502r | Langmuir 2013, 29, 643–652

where $D_{eff}^{cyl} = \lambda + D_{Xe}$. The van der Waals diameter (D_{Xe}) of a Xe atom is set to 4.4 Å.

A least two pore environments were considered for each sample: the main peak and its corresponding shoulder(s). The experimentally determined δ_S values (and thus δ_0) of each sample and their corresponding effective diameters are provided in Table 3. Not only does the average pore diameter

Table 3. Experimentally Determined Pore Size Distributions within PILCs Using CF-HP ^{129}Xe MAS NMR, Using a Numeric Model Described within the Text[a]

sample	δ_0 (ppm)	λ (Å)	D_{eff}^{cyl} (Å)	rel %
p-hectorite	139.1	1.53	5.9	0.52
	131.0	1.76	6.2	0.26
	124.4	1.95	6.4	0.22
r_3-hectorite	134.8	1.65	6.0	0.42
	129.0	1.82	6.2	0.58
r_6-hectorite	119.5	2.12	6.5	0.34
	115.5	2.27	6.7	0.66

[a]Here, δ_0 indicates the limiting ^{129}Xe chemical shift, λ the mean free path, D_{eff}^{cyl} the effective pore diameter (assuming a cylindrical pore geometry), and rel % the relative percent of each distinct environment obtained from deconvoluted spectra.

increase with Mg^{2+} content, but the micropore size distribution becomes more homogeneous as well. This is evident from the proportionality of the upfield shifts with respect to the pore size and specific narrowing of the adsorbed Xe resonance with reduced layer charge. The integrated intensities of the peaks (main versus shoulder) within each spectrum reflect the population ratios, provided that no preferential adsorption occurs. Accordingly, a comparison of the deconvoluted peaks associated with the adsorbed ^{129}Xe (see Table 3) within p-hectorite suggests a higher occurrence of "smaller" pores, wherein three distinct environments were considered due to the substantially broad resonance. The population of "larger" pores becomes more noticeable with reduced charge, as seen by the relative intensity and upfield position of the shoulder with respect to the main peak for both the r_3- and r_6-Me_2DABCO^{2+}-hectorite. Additionally, high-resolution ^{129}Xe MAS measurements were performed on hydrated r_3-Me_2DABCO^{2+}-hectorite. The presence of water increases the interlayer distance, accompanied by the reorientation of the Me_2DABCO^{2+} molecule with swelling (Figure S7). Contrary to intuition, ^{129}Xe MAS spectra show that the accessible pore volume is larger for the hydrated samples compared to the dry ones.

The adsorption properties of the PILCs can be determined by evaluating the temperature dependence of the ^{129}Xe chemical shift. Of particular interest is the effect of changing the interpillar distance on the physical parameters related to Xe adsorption. The p- and r_6-Me_2DABCO^{2+}-hectorite samples were chosen for analysis as they possess the highest and lowest pillar density, respectively. The VT CF–^{129}Xe NMR spectra shown in Figure 5 were deconvoluted at each temperature in order to extract the isotropic chemical shifts and CSA anisotropies (coupling constant ΔCS_{aniso} and asymmetry η) using the program DMFIT.[54] η had a negligible effect on the refinement and was set to zero over the whole temperature range. A plot of the ΔCS_{aniso} and δ_{iso} is given in Figure 8.

The isosteric adsorption energy (ΔH_{ads}) reflects alterations in the thermodynamic parameters with changing adsorbate–absorbent interactions. The adsorption energies (under high loading conditions) for Xe in p- and r_6-Me_2DABCO^{2+}-hectorite are determined using the relation[55]

$$\delta_{iso} = \delta_s + \Delta\delta(pk\ \exp(-\Delta H_{ads}/RT)) / (T^{1/2} + pk\ \exp(-\Delta H_{ads}/RT)) \quad (2)$$

Here, the isotropic chemical shifts (δ_{iso}) are taken from Figure 8A, which shows the refined temperature-dependent isotropic shift values of spectra displayed Figure 5. Here, p denotes the relative pressure, δ_s the Xe-surface induced shift, T the temperature, R the ideal gas constant, ΔH_{ads} the adsorption enthalpy, and k the temperature-independent portion of the Langmuir constant. The variation in the isotropic chemical shift with temperature shows a steady linear increase above 300 K; the lack of change above 300 K reflects the infinite dilute limit of the Xe–surface interactions (Figure 8A). The resulting limiting shift is found to be 142.9 ppm for the p-hectorite and 121.0 ppm for r_6-hectorite. The corresponding D_{eff} values of 5.8 and 6.5 Å are similar to those obtained from the high-resolution CF-HP ^{129}Xe MAS spectra (Table 3). As shown in Figure 8B, the observed Xe CSA trend is the same for in both p- and r_6-Me_2DABCO^{2+}-hectorite over the whole temperature range.

Fitting the experimental results to the aforementioned model (see Figure 8A) yields adsorption enthalpies of −14(1) and −17(1) kJ/mol for the p- and r_6-Me_2DABCO^{2+}-hectorite, respectively, which are typical values for physisorption processes. The more favorable adsorption enthalpy observed within the r_6-hectorite can be attributed to stronger lateral

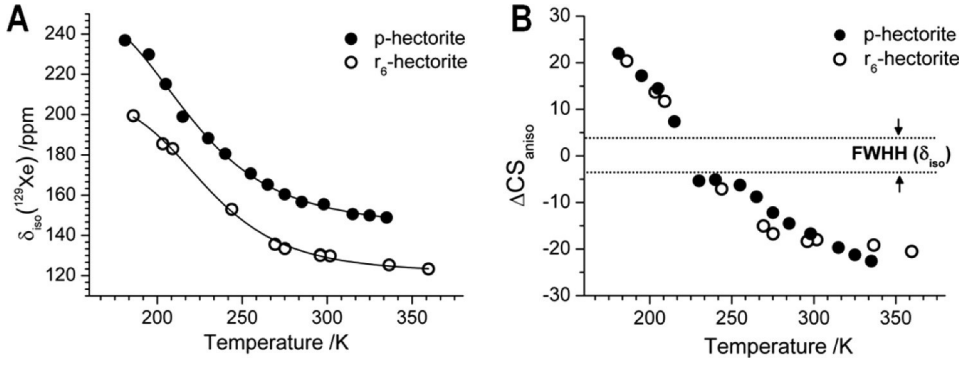

Figure 8. Plots of the refinement parameters δ_{iso} (A) and ΔCS_{aniso} (B) for p- (closed symbols) and r_6-Me_2DABCO^{2+}-hectorite (open symbols). The solid lines in (A) denote the fit of refined parameters extracted from VT, CF-HP ^{129}Xe NMR data shown in Figure 5, to eq 2.

dx.doi.org/10.1021/la304502r | Langmuir 2013, 29, 643–652

interactions between adsorbed Xe within the interlayer space. Similar effects have been shown in TiO_2 nanotubes, where isosteric heats of adsorption were found to increase with channel length.[56] In comparison, Xe physisorption measurements (Figure 9) show a decrease in the isosteric heat of

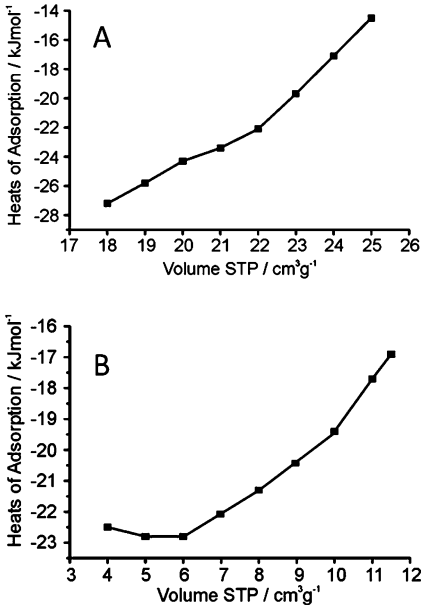

Figure 9. Isosteric heat of adsorption from physisorption measurements of p-hectorite with Xe at 180, 187, and 195 K (A) and at 273 and 298 K (B).

adsorption with loading. Here, we attribute the higher isosteric heats of adsorption at low loadings (between −27 and −22 kJ/mol) to energies dominated by adsorbate−adsorbent interactions. The progressive increase in the isosteric enthalpy at elevated pressures (−14 to −17 kJ/mol) result from competing adsorbate−adsorbate interactions in the lateral plane, which effectively lower the binding energy. Because of the confined interlamellar spacing (4.4 Å), it is unlikely that more than a monolayer forms on the internal surface. As such, the values determined from variable temperature CF-HP ^{129}Xe measurements reflect high loading conditions. Much lower partial pressures will be utilized in order to avoid the effects of Xe−Xe interactions in the future.

4. CONCLUSIONS

Here, we utilized solid-state NMR spectroscopic techniques to investigate structural changes in PILCs with reduced layer charge, while CF-HP ^{129}Xe NMR methods and Xe physisorption measurements were used to probe changes on the interface with changing surface conditions. Consistent with XRD and physisorption experiments, results obtained from solid-state NMR spectroscopy show regular spacing of the intercalated Me_2DABCO^{2+} pillars between the rigid clay supports. ^{19}F single-pulse NMR allowed for quick identification of Mg^{2+} rich and Li^+ containing trioctahedral domains, enabling quantitative determination of the Mg^{2+}/Li^+ ratio. By comparing the data to values from chemical analysis, we could prove a one-to-one exchange of one Li^+ with one Mg^{2+} retaining the trioctahedral character of PILCs. This then allows for an alternative method to determine the layer charge. ^{29}Si single-pulse NMR spectra indicate increased disorder within the tetrahedral sheet with reduced layer charge, likely due to structural distortions created in octahedral layer (Li^+ sites filled with Mg^{2+} in particular) with increasing wash/annealing cycles. Interestingly, the ordering of the Me_2DABCO^{2+} pillars are unaffected by these distortions—in fact, the ^{29}Si CP-MAS spectra show that they avoid them altogether.

Surface and adsorption studies using CF-HP ^{129}Xe NMR techniques highlight specific properties. Measurements under static conditions (VT and 2D EXSY experiments) (i) show easy accessibility to and from the gas phase, (ii) indicate that spatial constrictions along the axis normal manifest as CSA broadening, and (iii) prove that intercrystalline diffusion takes place on the order of a few 100 ms. The isotropic chemical shifts determined from deconvoluted VT ^{129}Xe NMR spectra allowed for the extraction of the isosteric heat of adsorption for both pristine and reduced charge (r_6)-hectorite samples. A comparison to Xe physisorption measurements suggest CF-HP ^{129}Xe determined ΔH_{ads} reflect values obtained in the high loading limit. To reduce the adsorbate−adsorbate interactions which mask the adsorbate−adsorbent interactions, significantly lower partial pressures are required for adequate extraction of the pure Xe−surface isosteric heats of adsorption. This will be possible only if the ^{129}Xe polarization can be increased beyond 30%.

CF-HP ^{129}Xe MAS NMR demonstrates the utility of the technique for reducing CSA broadened line shapes for the accurate determination of the pore size distribution. As such, we can conclude that lower layer charge results in narrower pore size distributions and larger interpillar distances. This study proves the utility of CF-HP ^{129}Xe and solid-state NMR methods in elucidating the structural and surface changes of synthetic 2-dimensional layered silicates on the microscopic scale.

■ ASSOCIATED CONTENT

Ⓢ Supporting Information

Powder X-ray diffraction patterns and physisorption isotherms Ar/Ar(l) for p-, r_3-, and r_6-Me_2DABCO^{2+}-hectorite; ^{13}C{^{1}H} PRESTO-HETCOR spectra of p-Me_2DABCO^{2+}-hectorite and the 1D projections for both p-hectorite and r_6-hectorite samples; ^{13}C CP-MAS NMR spectrum of p-, r_3-, and r_6-Me_2DABCO^{2+}-hectorite; cross-peak analysis of HP ^{129}Xe in p-hectorite, resulting from 2D EXSY spectra; swelling effect of hydrated r_3-Me_2DABCO^{2+}-hectorite probed with high-resolution ^{129}Xe MAS NMR. This material is available free of charge via the Internet at http://pubs.acs.org.

■ AUTHOR INFORMATION

Corresponding Author

*E-mail juergen.senker@uni-bayreuth.de.

Notes

The authors declare no competing financial interest.

■ ACKNOWLEDGMENTS

This work was financially supported by the Deutsche Forschungsgemeinschaft (SFB 840). Special thanks to Dr. M. Dvoyashkin for his assistance at the University of Florida.

■ ABBREVIATIONS

PILCs, pillared interlayered clays; MOFs, metal−organic frameworks; Me_2DABCO^{2+}, *N*,*N*-dimethyl-1,1-diazabicyclo-[2.2.2]octane dication; rf, radio frequency; CF-HP, continuous-flow hyperpolarized; NMR, nuclear magnetic resonance;

MAS, magic angle spinning; CP, cross-polarization; HETCOR, heteronuclear correlation; EXSY, exchange spectroscopy; VT, variable temperature; CSA, chemical shift anisotropy.

REFERENCES

(1) Cheetham, A. K.; Ferey, G.; Loiseau, T. Open-framework inorganic materials. *Angew. Chem., Int. Ed.* **1999**, *38*, 3268−3292.

(2) Schoonheydt, R. A.; Pinnavaia, T.; Lagaly, G.; Gangas, N. Pillared clays and pillared layered solids. *Pure Appl. Chem.* **1999**, *71* (2), 2367−2371.

(3) Tsapatsis, M.; Maheshwari, S. Pores by pillaring: Not always a maze. *Angew. Chem., Int. Ed.* **2008**, *47*, 4262−4263.

(4) Baumgartner, A.; Sattler, K.; Thun, J.; Breu, J. A route to microporous materials through oxidative pillaring of micas. *Angew. Chem., Int. Ed.* **2008**, *47*, 1640−1644.

(5) Stöcker, M.; Seidl, W.; Seyfarth, L.; Senker, J.; Breu, J. Realisation of truly microporous pillared clays. *Chem. Commun. (Cambridge, U. K.)* **2008**, *5*, 629−631.

(6) Stöcker, M.; Seyfarth, L.; Hirsemann, D.; Senker, J.; Breu, J. Microporous PILCs - Synthesis, pillaring mechanism and selective cation exchange. *Appl. Clay Sci.* **2010**, *48*, 146−153.

(7) Baumgartner, A.; Wagner, F. E.; Herling, M.; Breu, J. Towards a tunable pore size utilizing oxidative pillaring of the mica ferrous tainiolite. *Microporous Mesoporous Mater.* **2009**, *123*, 253−259.

(8) Nijs, H.; De Bock, M.; Maes, N.; Vansant, E. F. Theoretical evaluation of the microporosity of pillared layered double hydroxides. *J. Porous Mater.* **1999**, *6* (4), 307−321.

(9) Gomez-Romero, P.; Sanchez, C. In *Functional Hybrid Materials*; Gomez-Romero, P. S. C., Ed.; Wiley-VCH: Weinheim, 2004.

(10) Yamagishi, A. In *Dynamic Processes on Solid Surfaces*; Tamaru, K., Ed.; Plenum Press: New York, 1993; p 307.

(11) Breu, J.; Seidl, W.; Stoll, A. J.; Lange, K. G.; Probst, T. U. Charge homogeneity in synthetic fluorohectorite. *Chem. Mater.* **2001**, *13*, 4213−4220.

(12) Breu, J.; Seidl, W.; Stoll, A. Fehlordnung bei smectiten in abhängigkeit vom zwischenschichtkation. *Z. Anorg. Allg. Chem.* **2003**, *629*, 503−515.

(13) Möller, M. W.; Hirsemann, D.; Haarmann, F.; Senker, J.; Breu, J. Facile scalable synthesis of rectorites. *Chem. Mater.* **2010**, *22*, 186−196.

(14) Mariychuk, R.; Baumgartner, A.; Wagner, F. E.; Lerf, A.; Dubbe, A.; Moos, R.; Breu, J. Synthesis, structure, and electric conductivity of ferrous tainiolite and its oxidative conversion into coarse-grained swellable smectite. *Chem. Mater.* **2007**, *19*, 5377−5387.

(15) Kalo, H.; Möller, M. W.; Ziadeh, M.; Dolejs, D.; Breu, J. Large scale melt synthesis in an open crucible of Na-fluorohectorite with superb charge homogeneity and particle size. *Appl. Clay Sci.* **2010**, *48* (1−2), 39−45.

(16) Kalo, H.; Möller, M. W.; Kunz, D. A.; Breu, J. How to maximize the aspect ratio of clay nanoplatelets. *Nanoscale.* **2012**, *4* (18), 5633−5639.

(17) Hofmann, U.; Klemen, R. Verlust der austauschfaehigkeit von Lithiumionen an bentonit durch erhitzung. *Z. Anorg. Allg. Chem.* **1950**, *262*, 95−99.

(18) Jaynes, W. F.; Traina, S. J.; Bigham, J. M.; Johnston, C. T. Preparation and characterization of reduced-charge hectorites. *Clays Clay Miner.* **1992**, *40*, 397−404.

(19) Herling, M. M.; Kalo, H.; Seibt, S.; Schobert, R.; Breu, J. Tailoring the pore sizes of microporous pillared interlayered clays through layer charge reduction. *Langmuir* **2012**, *28* (41), 14713−14719.

(20) Springuel-Huet, M. A.; Bonardet, J. L.; Fraissard, J. ^{129}Xe-NMR of physisorbed xenon used as a probe for the study of microporous solids. *Appl. Magn. Reson.* **1995**, *8* (3−4), 427−456.

(21) Springuel-Huet, M. A.; Bonardet, J. L.; Gédéon, A.; Fraissard, J. ^{129}Xe NMR for studying surface heterogeneity: well-known facts and new findings. *Langmuir* **1997**, *13* (5), 1229−1236.

(22) Simonov, P. A.; Filimonova, S. V.; Kryukova, G. N.; Moroz, E. M.; Likholobov, V. A.; Kuretzky, T.; Boehm, H. P. ^{129}Xe NMR study of carbonaceous materials: effects of surface chemistry and nanotexture. *Carbon* **1999**, *37* (4), 591−600.

(23) Cheng, C.-Y.; Stamatatos, T. C.; Christou, G.; Bowers, C. R. Molecular wheels as nanoporous materials: differing modes of gas diffusion through Ga_{10} and Ga_{18} wheels probed by hyperpolarized ^{129}Xe NMR spectroscopy. *J. Am. Chem. Soc.* **2010**, *132* (15), 5387−5393.

(24) Hoffmann, H. C.; Assfour, B.; Epperlein, F.; Klein, N.; Paasch, S.; Senkovska, I.; Kaskel, S.; Seifert, G.; Brunner, E. High-pressure in-situ ^{129}Xe NMR spectroscopy and computer simulations of breathing transitions in the metal−organic framework $Ni_2(2,6\text{-ndc})_2(dabco)$ (DUT-8(Ni). *J. Am. Chem. Soc.* **2011**, *133* (22), 8681−8690.

(25) Wang, L.-Q.; Wang, D.; Liu, J.; Exarhos, G. J. Probing porosity and pore interconnectivity in self-assembled TiO_2−graphene hybrid nanostructures using hyperpolarized ^{129}Xe NMR. *J. Phys. Chem. C* **2011**, *116* (1), 22−29.

(26) Comotti, A.; Bracco, S.; Sozzani, P.; Horike, S.; Matsuda, R.; Chen, J.; Takata, M.; Kubota, Y.; Kitagawa, S. Nanochannels of two distinct cross-sections in a porous Al-based coordination polymer. *J. Am. Chem. Soc.* **2008**, *130* (41), 13664−13672.

(27) Shiratori, N.; Lee, K. J.; Miyawaki, J.; Hong, S.-H.; Mochida, I.; An, B.; Yokogawa, K.; Jang, J.; Yoon, S.-H. Pore structure analysis of activated carbon fiber by microdomain-based model. *Langmuir* **2009**, *25* (13), 7631−7637.

(28) Pawsey, S.; Kalebaila, K. K.; Moudrakovski, I.; Ripmeester, J. A.; Brock, S. L. Pore structure and interconnectivity of CdS aerogels and xerogels by hyperpolarized Xenon NMR. *J. Phys. Chem. C* **2010**, *114* (31), 13187−13195.

(29) Zaheer, M.; Keenan, C. D.; Hermannsdörfer, J.; Roessler, E.; Motz, G.; Senker, J.; Kempe, R. Robust microporous monoliths with integrated catalytically active metal sites investigated by hyperpolarized ^{129}Xe NMR. *Chem. Mater.* **2012**, *24* (20), 3952−3963.

(30) Huang, S.-J.; Huh, S.; Lo, P.-S.; Liu, S.-H.; Lin, V. S. Y.; Liu, S.-B. Hyperpolarized ^{129}Xe NMR investigation of multifunctional organic/inorganic hybrid mesoporous silica materials. *Phys. Chem. Chem. Phys.* **2005**, *7* (16), 3080−3087.

(31) Walker, T. G.; Happer, W. Spin-exchange optical pumping of noble-gas nuclei. *Rev. Mod. Phys.* **1997**, *69* (2), 629−642.

(32) Goodson, B. M. Nuclear magnetic resonance of laser-polarized noble gases in molecules, materials, and organisms. *J. Magn. Reson.* **2002**, *155* (2), 157−216.

(33) Zook, A. L.; Adhyaru, B. B.; Bowers, C. R. High capacity production of > 65% spin polarized xenon-129 for NMR spectroscopy and imaging. *J. Magn. Reson.* **2002**, *159* (2), 175−182.

(34) Moudrakovski, I. L.; Lang, S.; Ratcliffe, C. I.; Simard, B.; Santyr, G.; Ripmeester, J. A. Chemical shift imaging with continuously flowing hyperpolarized xenon for the characterization of materials. *J. Magn. Reson.* **2000**, *144* (2), 372−377.

(35) Springuel-Huet, M.; Demarquay, J.; Ito, T.; Fraissard, J. ^{129}Xe-NMR of xenon adsorbed on zeolites: determination of the dimensions of the void space from the chemical shift δdL(^{129}Xe). In *Studies in Surface Science and Catalysis*; Grobet, P. J., Mortier, W. J., Vansant, E. F., Schulz-Ekloff, G., Eds.; Elsevier: Amsterdam, 1988; Vol. *37*, pp 183−189.

(36) Thommes, M. *Nanoporous Materials: Science and Engineering*; Imperial College Press: London, 2004.

(37) Fung, B. M.; Khitrin, A. K.; Ermolaev, K. An improved broadband decoupling sequence for liquid crystals and solids. *J. Magn. Reson.* **2000**, *142* (1), 97−101.

(38) Zhao, X.; Hoffbauer, W.; Schmedt auf der Günne, J.; Levitt, M. H. Heteronuclear polarization transfer by symmetry-based recoupling sequences in solid-state NMR. *Solid State Nucl. Magn. Reson.* **2004**, *26* (2), 57−64.

(39) Nossov, A.; Guenneau, F.; Springuel-Huet, M.-A.; Haddad, E.; Montouillout, V.; Knott, B.; Engelke, F.; Fernandez, C.; Gedeon, A. Continuous flow hyperpolarized ^{129}Xe-MAS NMR studies of microporous materials. *Phys. Chem. Chem. Phys.* **2003**, *5* (20), 4479−4483.

(40) Huve, L.; Delmotte, L.; Martin, P.; Le Dred, R.; Baron, J.; Saehr, D. ^{19}F MAS-NMR study of structural fluorine in some natural and synthetic 2:1 layer silicates. *Clays Clay Miner.* **1992**, *40* (2), 186−191.
(41) Labouriau, A.; Kim, Y.-W.; Chipera, S.; Bish, D. L.; Earl, W. L. A ^{19}F nuclear magnetic resonance study of natural clays. *Clays Clay Miner.* **1995**, *43* (6), 697−704.
(42) Kaviratna, H.; Pinnavala, T. J. Acid hydrolysis of octahedral Mg^{2+} sites in 2:1 layered silicates: an assessment of edge attack and gallery access mechanisms. *Clays Clay Miner.* **1994**, *42* (6), 717−723.
(43) Breu, J.; Seidl, W.; Senker, J. Synthese von dreidimensional geordneten einlagerungsverbindungen des hectorits. *Z. Anorg. Allg. Chem.* **2004**, *630* (1), 80−90.
(44) Kirkpatrick, R. J.; Smith, K. A.; Schramm, S.; Turner, G.; Yang, W.-H. Solid-state nuclear magnetic resonance spectroscopy of minerals. *Annu. Rev. Earth Planet. Sci* **1985**, *13*, 29−47.
(45) Weiss, C. A.; Altaner, S. P.; Kirkpatrick, R. J. High-resolution ^{29}Si NMR spectroscopy of 2:1 layer silicates; correlations among chemical shift, structural distortions, and chemical variations. *Carbon* **1987**, *72* (9−10), 935−942.
(46) Kinsey, R. A. K.; James, R.; Hower, J.; Smith, K.; Oldfield, E. High resolution aluminum-27 and silicon-29 nuclear magnetic resonance spectroscopic study of layer silicates, including clay minerals. *Am. Mineral.* **1985**, *70*, 537−548.
(47) Gertsmans, A.; Urbanczyk, L.; Jérôme, R.; Robert, J.-L.; Grandjean, J. XRD and NMR characterization of synthetic hectorites and the corresponding surfactant-exchanged clays. *Clay Miner.* **2008**, *43* (2), 205−212.
(48) d'Espinose de la Caillerie, J.-B.; Fripiat, J. J. A reassessment of the ^{29}Si MAS-NMR spectra of sepiolite and aliminated sepiolite. *Clay Miner.* **1994**, *29*, 313−318.
(49) Cattaneo, A. S.; Bracco, S.; Comotti, A.; Galimberti, M.; Sozzani, P.; Eckert, H. Structural characterization of pristine and modified fluoromica using multinuclear solid-state NMR. *J. Phys. Chem. C* **2011**, *115* (25), 12517−12529.
(50) Jameson, C. J.; de Dios, A. C. Xe nuclear magnetic resonance line shapes in nanochannels. *J. Chem. Phys.* **2002**, *116* (9), 3805−3821.
(51) Meersmann, T.; Logan, J. W.; Simonutti, R.; Caldarelli, S.; Comotti, A.; Sozzani, P.; Kaiser, L. G.; Pines, A. Exploring single-file diffusion in one-dimensional nanochannels by laser-polarized ^{129}Xe NMR spectroscopy. *J. Phys. Chem. A* **2000**, *104* (50), 11665−11670.
(52) Comotti, A.; Bracco, S.; Ferretti, L.; Mauri, M.; Simonutti, R.; Sozzani, P. A single-crystal imprints macroscopic orientation on xenon atoms. *Chem. Commun.* **2007**, *4*, 350−352.
(53) Demarquay, J.; Fraissard, J. ^{129}Xe NMR of xenon adsorbed on zeolites. Relationship between the chemical shift and the void space. *Chem. Phys. Lett.* **1987**, *136*, 314−318.
(54) Massiot, D.; Fayon, F.; Capron, M.; King, I.; Le Calvé, S.; Alonso, B.; Durand, J. O.; Bujoli, B.; Gan, Z.; Hoatson, G. Modelling one and two-dimensional solid-state NMR spectra. *Magn. Reson. Chem.* **2002**, *40* (1), 70−76.
(55) Anedda, R.; Soldatov, D. V.; Moudrakovski, I. L.; Casu, M.; Ripmeester, J. A. A new approach to characterizing sorption in materials with flexible micropores. *Chem. Mater.* **2008**, *20* (9), 2908−2920.
(56) Lee, S. M.; Lee, S. C.; Mehrotra, V.; Kim, H. J.; Lee, H. C. Hyperpolarized ^{129}Xe NMR study of TiO_2 nanotubes. *Bull. Korean Chem. Soc.* **2012**, *33* (2), 512−514.

Supporting Information

The Porosity of Pillared Clays Studied by Hyperpolarized ^{129}Xe NMR Spectroscopy and Xe Adsorption Isotherms

Caroline D. Keenan, Markus M. Herling, Renée Siegel, Nikolaus Petzold, Clifford R. Bowers, Ernst A. Rössler, Josef Breu, Jürgen Senker*

Figures

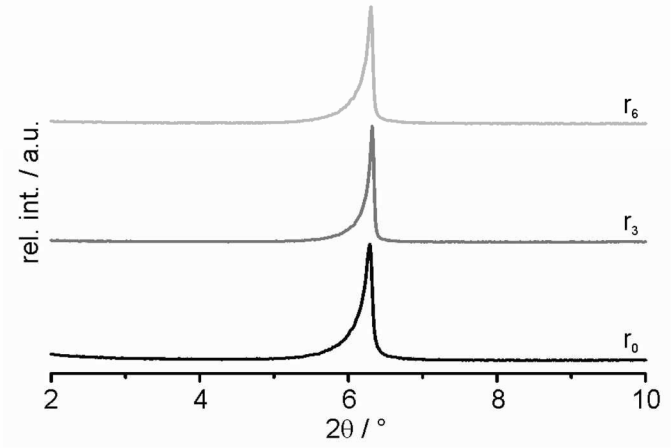

Figure S1. Powder X-ray diffraction pattern for p- (black), r_3- (dark grey), and r_6- Me_2DABCO^{2+}-hectorite (light grey).

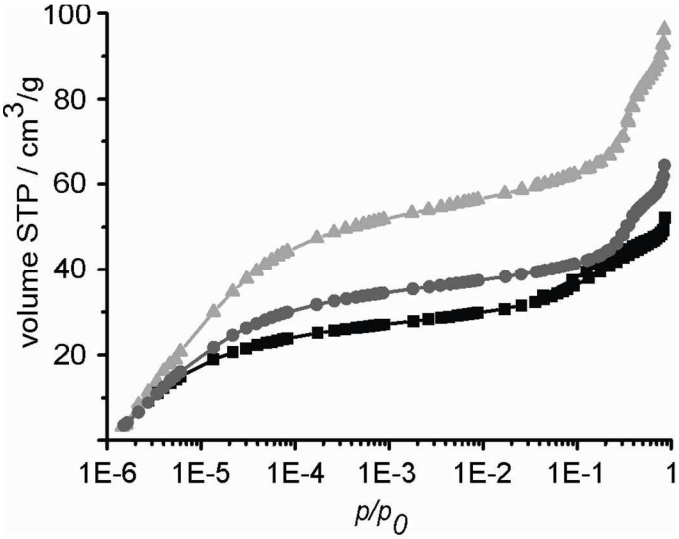

Figure S2. Physisorption isotherm Ar/Ar(l) for p- (■), r_3- (●), and r_6- Me_2DABCO^{2+}-hectorite (▲).

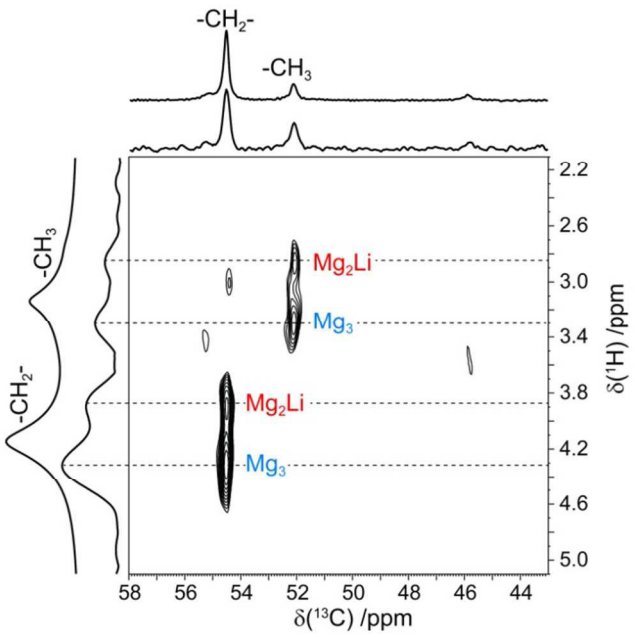

Figure S3. $^{13}C\{^{1}H\}$ PRESTO-HETCOR of p-Me_2DABCO^{2+}-hectorite.

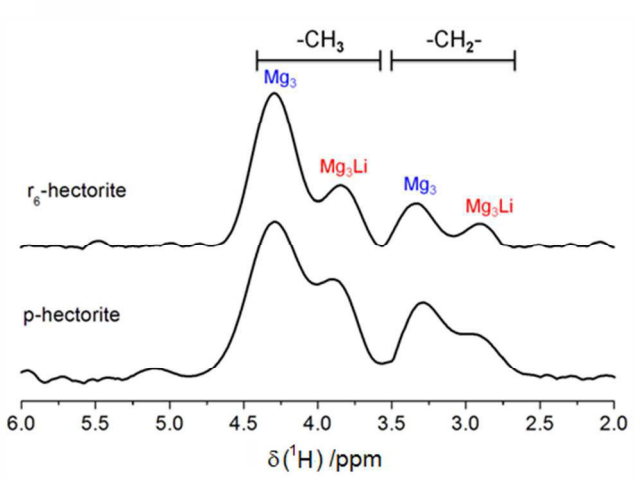

Figure S4. The 1D projections extracted from 2D ^{13}C-^{1}H PRESTO-HETCOR spectra of p- and r_6- Me_2DABCO^{2+}-hectorite.

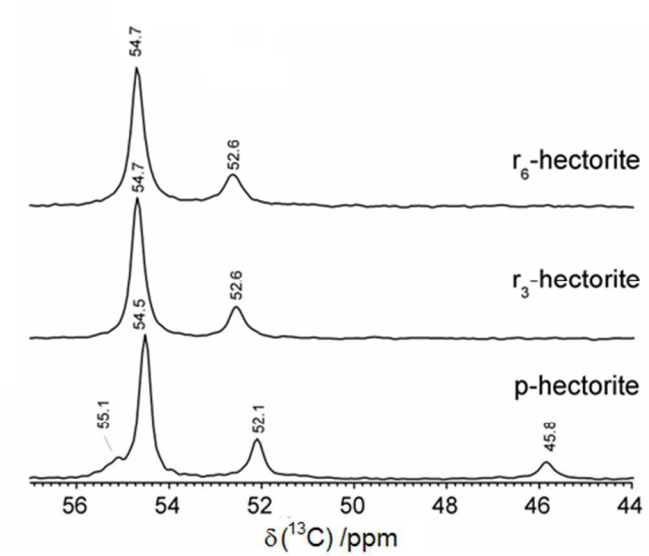

Figure S5. ^{13}C CP/MAS NMR spectra of p-, r_3- and r_6-Me_2DABCO^{2+}-hectorite.

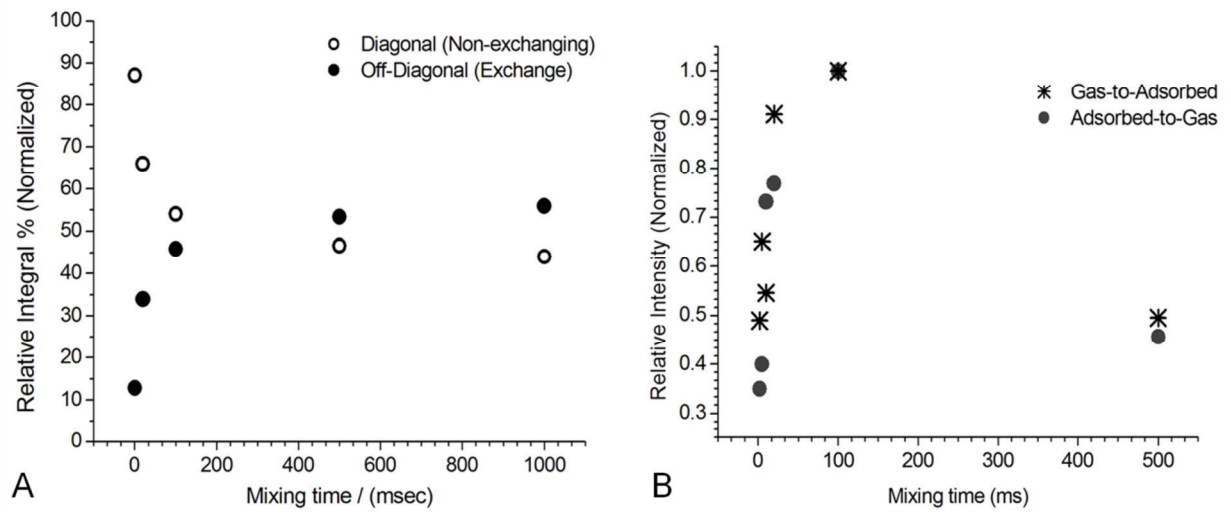

Figure S6. Summary plots showing the integrated cross-peak areas between A) adsorbed↔adsorbed Xe species (box-like shape in 2D EXSY spectrum, **Figure 6A**) and B) gaseous ↔adsorbed Xe (off-diagonal elements in 2D EXSY spectrum) for p-Me_2DABCO^{2+}-hectorite.

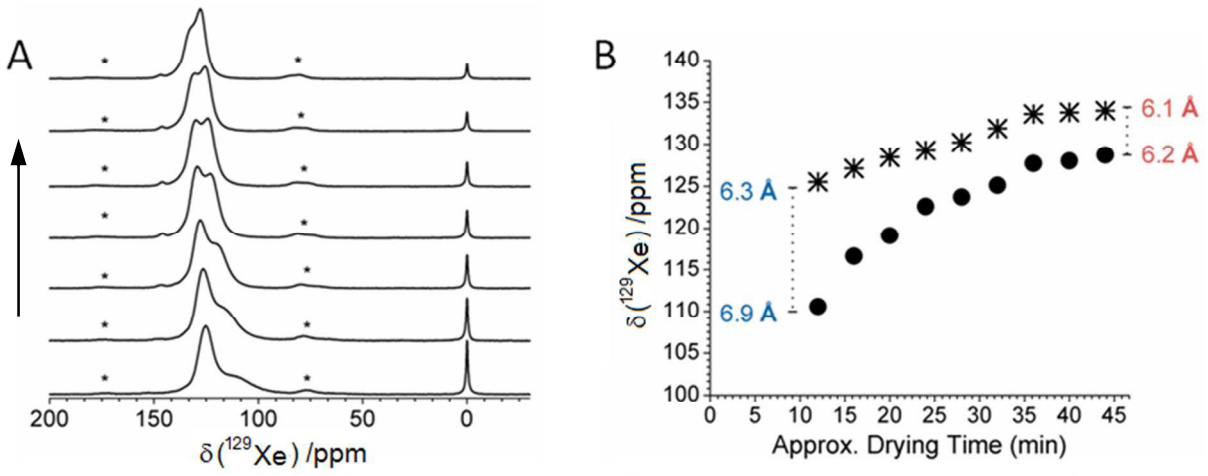

Figure S7. A) CF-HP ^{129}Xe MAS spectra of Xe adsorbed within hydrated r_3- Me_2DABCO^{2+}-hectorite as a function of dehydration time (increasing in the direction of the arrow), measured at 298 K and a rotation frequency of 4 kHz. B) A plot tracing the changing of the adsorbed Xe resonances with drying time.

The basal spacing (d_{001}) is largely dependent on the size and chemical nature of the molecules trapped with the silicate layers. As such, the adsorption of water within PILCs can modify the physical/chemical properties of the interlayer space, having consequence on potential reaction processes. The dependence of the effective pore diameter with water content was studied by exposing hydrated r_3-Me_2DABCO^{2+}-hectorite to a stream of CF-HP ^{129}Xe and monitoring the ^{129}Xe chemical shift behavior over time. Previous results suggest that the presence of water swells the interlayer space.[54] High resolution CF-HP ^{129}Xe MAS NMR spectra exhibit two distinct domains upon initial exposure, namely a symmetric narrow lineshape accompanied by a broader side peak (**S7A**, above). Spectra were recorded approximately 3 minutes apart, under a constant flow of HP ^{129}Xe gas. As discussed previously, lower chemical shift values correlate with larger effective pore sizes. The upfield component (larger pore size) is noticeably more sensitive to prolonged exposure to the HP ^{129}Xe gas mixture. This is seen more clearly in the

summary plot in **S7B**. After approximately 35 minutes, no change in the chemical shift or lineshape is observed. Applying the Demarquay-Fraissard model to both extremes (high versus low water content) indicates a 0.7Å decrease in effective pore size with dehydration. Interestingly, the progressive decrease in the gas peak amplitude with drying suggests more favorable gas adsorption due to increased hydrophobicity of the material. Such properties may have consequence on potential interlayer reactions.

Appendix 4

MOPS – A New Class of Stereo and Size Selective Class of Microporous Hybrid Materials

Markus M. Herling[1], Mathias Schwedes[2], Sebastian Seibt[2], Hussein Kalo[1], Ulrike Lacher[2], Rainer Schobert[2] and Josef Breu[1,*]

[1]Lehrstuhl für Anorganische Chemie I, Universität Bayreuth, Universitätsstr. 30, 95440 Bayreuth, Germany

[2]Lehrstuhl für Organische Chemie I, Universität Bayreuth, Universitätsstr. 30, 95440 Bayreuth, Germany

*e-mail: josef.breu@uni-bayreuth.de

To be submitted.

MOPS – A new class of stereo and size discriminative microporous hybrid materials

Authors: Markus M. Herling[1], Mathias Schwedes[2], Sebastian Seibt[2], Hussein Kalo[1], Ulrike Lacher[2], Rainer Schobert[2,*] and Josef Breu[1,*]

Affiliations:

[1]Lehrstuhl für Anorganische Chemie I, Universität Bayreuth, Universitätsstr. 30, 95447 Bayreuth, Germany.

[2] Lehrstuhl für Organische Chemie I, Universität Bayreuth, Universitätsstr. 30, 95447 Bayreuth, Germany

*Corresponding author: E-Mail: rainer.schobert@uni-bayreuth.de, josef.breu@uni-bayreuth.de

Abstract:

Eight new Microporous Organically Pillared Layered Silicates (MOPS), termed UBT-1 to UBT-8, were obtained by pillaring synthetic hectorites of four distinct layer charge densities with (–)- or (+)-Co(sep)Cl_3 (sep = $C_{12}H_{30}N_8$ = 1,3,6,8,10,13,16,19-octaazabicyclo[6.6.6]-eicosane). These new hybrid materials feature chiral micropores of defined widths and narrow pore width distributions which can discriminate guest molecules by size and chiral configuration. This was demonstrated by the preferential absorption of but-3-yn-2-ol from its gaseous mixture with the slightly larger 2-methyl-but-3-yn-2-ol and of one of its enantiomers from its gaseous racemate. UBT-1 pillared with (+)-Co(sep)$^{3+}$ favored the adsorption of *R*-but-3-yn-2-ol while UBT-5 pillared with (–)-Co(sep)$^{3+}$ adsorbed preferentially *S*-but-3-yn-2-ol. The efficiency of these separations depended on the pore width which in turn was adjustable via the layer charge of the silicate. MOPS represent a novel class of continuously tunable chiral adsorbents with many conceivable fields of application such as resolution of racemates, desymmetrisation, or catalytic transformations, that all depend on a defined spatial contact with their immediate environment.

Introduction

Chiral recognition has been identified as one of the biggest challenges for the design of future inorganic microporous materials *(1,2)*. Metal–organic frameworks (MOFs) have lately been engineered for the storage of gases *(3)*, for the adsorption and separation of small molecules *(4-6)*, and for heterogeneous catalysis. In particular, MOFs comprising enantiopure organic linkers or metal ligands were employed for the resolution of racemates *(7-9)* and for the asymmetric conversion of prochiral substrates *(10-15)*. For these reactions to proceed with high optical yields a particular MOF has to be devised for any individual substrate. Changing the latter more than marginally requires the synthesis of a different MOF from scratch. While sharing with MOFs the basic concepts of "functional porosity" and "component modularity", only Microporous Organically Pillared Layered silicates (MOPSs) allow a continuous porosity tuning *(16)*. MOPSs are prepared by intercalation of cationic molecules - such as metal complexes or organocations - in the interlayer space of ionic lamellar materials. These molecular "pillars" may be varied in charge, size, and shape, and may be decorated with chemical functional groups or be deployed in an enantiopure form (Fig. 1). Insofar, the pillars in MOPSs are reminiscent of the "linkers" in MOFs. However, there are also substantial differences. In MOFs the linkers are coordinated to individual three-dimensionally distributed node metals whereas in MOPSs there is no rigid linkage between the two-dimensional interlayer surfaces of the clay host and the pillars which are held in place only by non-directional electrostatic interactions. As a consequence, the porosity of MOPSs depends, apart from the nature of the pillars, solely on the homogeneity and magnitude of the negative layer charge of the silicate. Breu *et al.* have recently developed methods to fully control these two properties. Layered silicates with homogeneous charge densities were made accessible on a large scale by an expeditious melt synthesis *(17,18)*. When intercalated with appropriate cations MOPSs result that are characterized by narrow pore size distributions and a high degree of long-range order of the pillar arrays *(19-22)*.

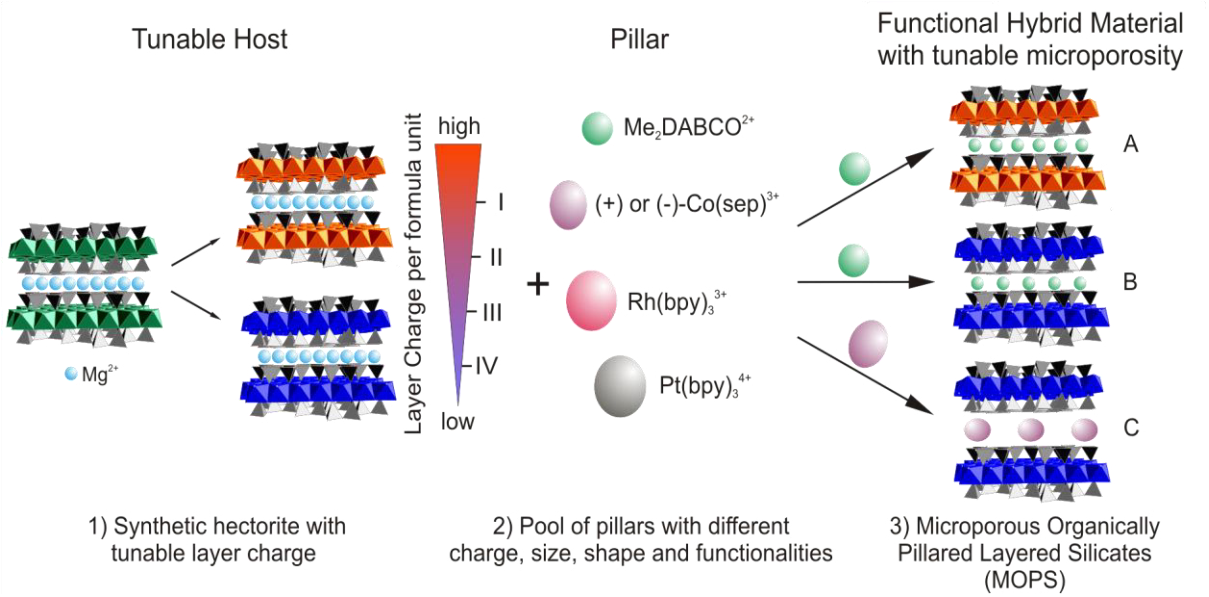

Fig. 1. Assembly of Microporous Organically Pillared Layered Silicates (MOPSs) with tunable microporosity by intercalation of functional cationic pillars of varying size, shape and charge into synthetic hectorite of homogeneous and continuously adjustable layer charge.

The Breu group also recently found a way *(25)* to reduce the layer charge of these synthetic silicates based on the Hofmann-Klemen effect *(23)* and the charge reduction procedure by Jaynes et al.*(24)*The layer charge in turn defines the packing density of the molecular pillar arrays in the interlayer space (*cf* A↔B) in Fig. 1)). The height of the interlayer space can be customised independently via the size of the pillars (*cf* B↔C) in Fig. 1. Thus functional MOPS with continuously adjustable microporosity *(26)* are now available for the first time and in large quantities. The option to model their interlayer cavities on the shape of particular guest molecules is a unique feature not available to MOFs whose porosity can be adjusted only in steps no smaller than the order of chemical bond lengths, nor to crystalline organic hosts such as bile acids or ureas *(27)* traditionally used for the inclusion resolution of small guest compounds.

Results & Discussion:

The intercalation of chiral pillars affords chiral MOPSs that for the first time allow the discrimination of adsorbed guest molecules by size and chirality in a finely tunable and modular way. This is demonstrated in the following for eight MOPSs, UBT-1 to UBT-8, with different pore size distributions. These chiral MOPS were obtained by pillaring synthetic hectorites of varying charge density with enantiopure cobalt sepulchrate trichloride, (–) or (+)-Co(sep)Cl_3 (sep = $C_{12}H_{30}N_8$ = 1,3,6,8,10,13,16,19-octaazabicyclo[6.6.6]-eicosane). Upon pillaring the interlayer distance of the hectorites increased from 9.6 Å to 16.1(1) Å as to powder X-ray diffraction analyses (Fig. S1, Supporting Information). The *00l*-series of all four MOPSs were highly rational, indicating that all interlayer spaces have exactly the same gallery height *(28)*.

Physisorption measurements with Ar/Ar(l) indicated a type I isotherm for all four materials without significant signs of hysteresis, (Fig. S2, Supporting Information) typical of microporous materials. Figure S3 (Supporting Information) illustrates the continuous increase of micropore size distributions when going from UBT-1 to UBT-4. The observed shift in the volume-weighted mean pore diameters originates from larger interpillar distances as a direct consequence of charge reduction. The total increase of the median pore diameter in the series was only ca. 0.5 Å (Fig. 2). However, it is exactly this tuneability of the porosity in minute gradations that enables a trade-off between accessibility of the inter-pillar void by organic substrates and their discrimination by size, shape or chirality via intimate contact with the pillars. It should be noted that non-spherical pillars tend to orient their long axis parallel to the interlayer gallery whose height will thus be determined by the smallest extension of the pillar. The height of the interlayers might even be further reduced by partial penetration of the pillars into the hexagonal hollows of the silicate layer surfaces. Given the 9.6 Å height of the hectorite silicate layer, the minimum basal spacing that will allow access of Ar to the approximately cylindrically shaped micropores is 13 Å, whereas larger molecules might need basal spacings distinctly greater than 15 Å. It is also worthy of note that while the interpillar distance may be fine-tuned by reducing the charge density of the hectorite, the interlayer height remains constant as indicated by the equal basal spacing of 16.1(1) Å for all MOPSs UBT-1 to UBT-8. Thus the pore size is actually adjusted in an anisotropic fashion with one dimension being kept constant.

To probe the relevance of the narrow and gradually adjustable pore size distributions of this novel class of microporous hybrid materials for their sorption properties they were first tested for size and shape selectivity towards small organic molecules of slightly different size. Two alcohols of similar polarity, shape and vapor pressure, namely but-3-yn-2-ol and 2-methyl-but-3-yn-2-ol, were adsorbed from their equilibrium gas phase mixture at 4 °C by dry UBT-1 to UBT-4 (Fig. 3). It proved crucial to set the experiments under inert atmosphere to preclude the adsorption of water molecules which show a high affinity for the MOPSs.

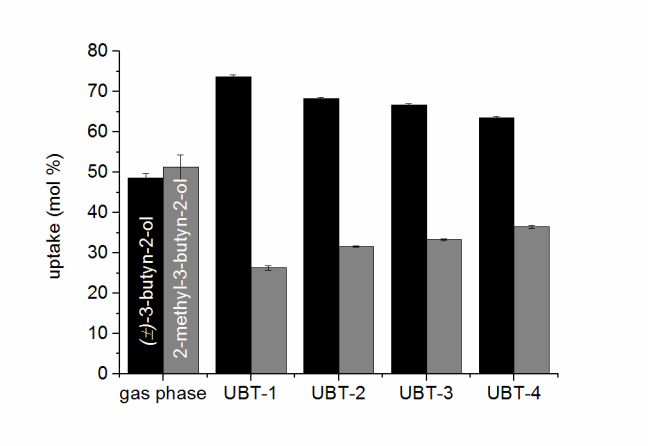

Fig. 3. Size selective adsorption of a mixture of but-3-yn-2-ol and 2-methyl-but-3-yn-2-ol in MOPS UBT-1 to UBT-4 from equilibrium gas phase at 4 °C.

While the smaller but-3-yn-2-ol was adsorbed by UBT-1 to UBT-4 in amounts ranging from 1.58 to 1.98 mmol / g, its larger methyl derivative was adsorbed in significantly lower amounts (0.57 – 1.01 mmol / g) (Fig. 3), table S1 in Supporting Information). This suggests that probe molecules of a size and shape that allows them to better dovetail into the micropores are more susceptible and responsive to even minute changes of the pore geometry than the argon atoms used for the physisorption measurements. Furthermore, the course of the absolute amounts of alcohols adsorbed by each of the four MOPSs is different for the two substrates. The one for the larger tertiary alcohol rises continuously with a maximum for UBT-4 whereas that for the smaller secondary alcohol peaks with UBT-2 and declines notably for UBT-4 possibly because its wider pores begin to lose their grip on the adsorbate.

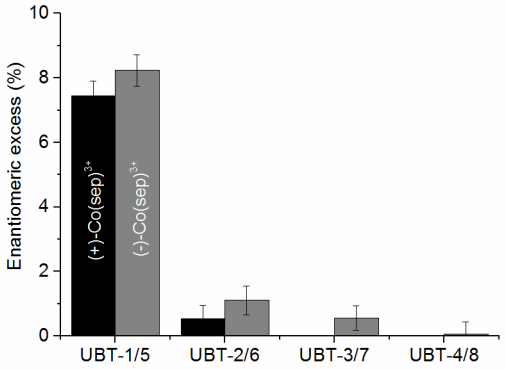

Fig. 4. Diastereoselective discrimination upon adsorption of (±)-but-3-yn-2-ol in MOPSpillared with (+)-Co(sep)$^{3+}$(UBT-1 to UBT-4) and (-)-Co(sep)$^{3+}$ (UBT-5 to UBT-8): excess (%) of major enantiomer adsorbed by UBT-1 through UBT-8.

Interestingly, UBT-1 and UBT-5 not only showed the maximum adsorption capacity for but-3-yn-2-ol but also represent the optimum adsorbent for the discrimination of the enantiomers in a racemic mixture of *R*- and *S*-but-3-yn-2-ol (Fig. 4). UBT-1 preferentially adsorbed *R*-but-3-yn-2-ol whereas UBT-5 favored the adsorption of *S*-but-3-yn-2-ol. A plausible assumption is that if the pillars are packed very tightly into micropores, as for UBT-1/5, stereodiscrimination is most efficient while for UBT-2/6 and UBT-3/7 with slightly larger micropores, the chiral adsorbate may not get into sufficiently intimate contact with the chiral micropore of the adsorbent. Obviously, the fine-tuning of the pore shapes and widths is of paramount importance for the efficiency of the chiral discrimination by MOPSs. It is a hallmark of this novel class of microporous materials that their modular character allows an adjustment of these parameters to any given substrate with an unprecedented fineness and accuracy and with a flexibility which is difficult to achieve with MOFs. The best enantiomeric excess (8.2 % and 7.5 %) observed in our study matches comparable values reported for the stereoselective sorption of MOFs *(7, 29,30)*. This degree of adsorptive selectivity should be fully sufficient to allow for a complete chiral resolution of suitable guest substrates when the material is applied as a stationary phase in chromatography beds with greater effective plate numbers.

A correlation of the available external surface area of the new MOPS with the observed adsorption capacities clearly shows that the size and stereo discrimination is indeed a bulk phenomenon and that the differential retention of the guest compounds is related to the interlayer

space. The synthetic clays applied here represent a coarse grained material with lateral dimensions in the µm range. The basal reflections (Fig. S1, Supporting Information) are narrow and the full widths of half maximium indicate a typical thickness of the clay platelets of 72 nm when applying the Scherrer equation. This suggests that less than 5% of the total specific surface is attributed to external basal surface area. Moreover, the adsorption capacities correspond well with the micropore volumes as determined by argon adsorption. From the known density of but-3-yn-2-ol a molecular volume of 73.77 cm^3/mol can be derived. Assuming the same molecular volume for but-3-yn-2-ol when adsorbed in the MOPSs, the observed adsorption capacities for the UBT-1 to UBT-4 indicate that more than 100% of the micropore volume as determined by argon adsorption measurements is occupied. The finding that intercalated but-3-yn-2-ol is more densely packed than its liquid state is perfectly in line with literature precedence of similar adsorbates behaving more like crystals rather than liquids *(31)*.

Conclusion:

In conclusion, evidence was provided for the first time for the size and stereo discriminative adsorption of small organic substrates in the interlayer micropores of MOPSs. The option of sorting molecules by size arises from the fact that we can gradually adjust the pore width while retaining a very narrow pore width distribution (Fig. S3).

This tuneability of pores became possible by a process of stepwise reduction of the layer charge of the synthetic host hectorite. For the stereo discrimination to be efficient, appropriately dimensioned arrays of enantiopure interlayer pillars are required that closely fit the shape of the chiral substrate molecules. MOPSs offer a unique way to gradually adjust the distance between pillars and hence the size and shape of the micropores. They represent a novel class of tunable chiral adsorbents with many conceivable fields of application such as resolution of racemates, desymmetrisation, or catalytic transformations, that all depend on a defined spatial contact with their immediate environment.

References and Notes:

1. M. E. Davis, *Nature* **417**, 813–821 (2002).

2. R. E. Morris, X. Bu, *Nat. Chem.* **2**, 353–361 (2010).

3. L. J. Murray, M. Dinca, J. R. Long, *Chem. Soc. Rev.* **38**, 1294–1314 (2009).

4. M. C. Das *et al.*, *J. Am. Chem. Soc.* **134**, 8703–8710 (2012).

5. Z.-Y. Gu, X.-P. Yan, *Angew. Chem. Int. Ed.* **49**, 1477–1480 (2010).

6. M. Padmanaban *et al.*, *Chem. Commun.* **47**, 12089–12091 (2011).

7. W. Wang *et al.*, *Chem. Commun* **48**, 7022–7024 (2012).

8. C. Zhu, G. Yuan, X. Chen, Z. Yang, Y. Cui, *J. Am. Chem. Soc.* **134**, 8058–8061 (2012).

9. S.-M. Xie, Z.-J. Zhang, Z.-Y. Wang, L.-M. Yuan, *J. Am. Chem. Soc.* **133**, 11892–11895 (2011).

10. Y. Liu, W. Xuan, Y. Cui, *Adv. Mater.* **22**, 4112–4135 (2010).

11. D. Dang, P. Wu, C. He, Z. Xie, C. Duan, *J. Am. Chem. Soc.* **132**, 14321–14323 (2010).

12. W. Lin, *Top. Catal.* **53**, 869–875 (2010).

13. M. Yoon, R. Srirambalaji, K. Kim, *Chem. Rev.* **112**, 1196–1231 (2012).

14. J. M. Falkowski, S. Liu, C. Wang, W. Lin, *Chem. Commun.* **48**, 6508–6510 (2012).

15. L. Ma, J. M. Falkowski, C. Abney, W. Lin, *Nature Chem.* **2**, 838–846 (2010).

16. M. Tsapatsis, S. Maheshwari, *Angew. Chem. Int. Ed.* **47**, 4262–4263 (2008).

17. H. Kalo, M. W. Möller, D. A. Kunz, J. Breu, *Nanoscale* **4**, 5633–5639 (2012).

18. M. W. Möller, D. Hiersemann, F. Haarmann, J. Senker, J. Breu, *Chem. Mater.* **22**, 186–196 (2010).

19. A. Baumgartner, K. Sattler, J. Thun, J. Breu, *Angew. Chem. Int. Ed.* **47**, 1640–1644 (2008).

20. M. Stöcker, W. Seidl, L. Seyfarth, J. Senker, J. Breu, *Chem. Commun.* **5**, 629–631 (2008).

21. M. Stöcker, L. Seyfarth, D. Hirsemann, J. Senker, J. Breu, *Appl. Clay Sci.* **48**, 146–153 (2008).

22. A. Baumgartner, F. E. Wagner, M. Herling, J. Breu, *Microporous Mesoporous Mater.* **123** 253–259 (2009).

23. U. Hofmann, R. Klemen, *Anorg. Allg. Chem.* **262**, 95–99 (1950).

24. W. F. Jaynes, S. J. Traina, J. M. Bigham, C. T. Johnston, *Clays Clay Miner.* **40**, 397–404 (1992).

25. M. M. Herling, H. Kalo, S. Seibt, R. Schobert, J. Breu, *Langmuir* **28**, 14713–14719 (2012).

26. C. D. Keenan *et al.*, *Langmuir* **29**, 643-652 (2013).

27. J. L. Atwood, J. E. D. Davies, D. D. MacNicol, *Inclusion Compounds (*Academic Press, New York, 1984) vol. 1, 2.

28. D. M. Moore, R. C. Reynolds, *X-Ray Diffraction and the Identification and Analysis of Clay Minerals* (Oxford Univ. Press, Oxford, 1997).

29. K. Suh, M. P. Yutkin, D. N. Dybtsev, V. P. Fedin, K. Kim, *Chem. Commun.* ***48***, 513–515 (2012).

30. D. N. Dybtsev *et al.*, *Angew. Chem. Int. Ed.* **45**, 916–920 (2006).

31. S. J. You *et al.*, *Angew. Chem. Int. Ed.* **52**, 3891-3895 (2013).

32. K. Kitajima, F. Koyama and N. Takusagawa, *Bull. Chem. Soc. Jpn.* **58**, 1325–1326 (1985).

33. J. Breu, W. Seidl, A. J. Stoll, K. G. Lange and T. U. Probst, *Chem. Mater.* **13**, 4213–4220 (2001).

34. I. I. Creaser *et al.*, *J. Am. Chem. Soc.* **104**, 6016–6025 (1982).

35. I. I. Creaser, J. MacB. Harrowfield, A. J. Herlt, A. M. Sargeson, J. Springborg, *J. Am. Chem. Soc.* **99**, 3181–3182 (1977).

36. L. R. Gahan, P. C. Healy, G. J. Patch, *J. Chem. Educ.* **66**, 445–446 (1989).

37. M. Thommes, *Nanoporous Materials: Science and Engineering (*Imperial College Press, London, 2004).

38. J. Rouquerol, P. Llewellyn, F. Rouquerol, *Studies in Surface Science and Catalysis Characterization of Porous Solids - VII* (Elsevier, Amsterdam, 2007) vol. 160, pp. 49–56.

Supplementary Materials:

Materials and Methods

Figures S1-S3

Tables S1-S3

References (*32-38*)

Supplementary Materials:

Synthesis of the MOPS:

The fluorohectorite $[Na_{0.47(3)}]^{inter}[Mg_{2.59(5)}Li_{0.17(3)}]^{oct}[Si_4]^{tet}O_{10}F_2$ used was synthesized via melt synthesis (*17, 21, 32*)). The high purity reagents (in total ~45 g) of SiO_2 (Merck, fine granular, calcined), MgF_2 (Chempur, 99.99%), MgO (Alfa Aesar 99.95%), Li_2SiO_3 (Alfa Aesar 99.95%), and Na_2O–$2SiO_2$-glass were weighed into a molybdenum crucible in an Ar atmosphere in accordance with a stoichiometric composition of $[Na_{0.6}]^{inter}[Mg_{2.6}Li_{0.2}\square]^{oct}[Si_4]^{tet}O_{10}F_2$ (target composition). Na_2O–$2SiO_2$-glass was produced by melting Na_2CO_3 (Aldrich, 99.9%) and SiO_2 (Merck, fine granular, calcined) in a 1:2 molar ratio at 1050 °C for 10 h to ensure complete release of carbon dioxide. The molybdenum crucible was sealed so as to be gas-tight using the procedure described elsewhere *(33)*. The crucible was heated in a graphite furnace (Graphit HT-1900, Linn High Therm) for the synthesis. To prevent inhomogeneity of the product owing to gravity segregation in the melt, the crucible was positioned horizontally in the furnace and rotated at 50 rpm. The crucible was heated from room temperature (RT) to 1750 °C (20 °C min^{-1}), left at 1750 °C for 1 h, then cooled to 1300 °C with a cooling rate of 50 °C min^{-1}, followed by a cooling rate of 10 °C min^{-1} from 1300 °C to 1050 °C, and finally it was quenched by switching off the power. The crucible was opened under an Ar atmosphere and the synthetic Sodium fluorohectorite was stored in a Glovebox.

For pillaring, the hectorites (100 mg) were treated hydrothermally four times for 12 h at 60 °C with 18 mg of cobalt sepulchrate trichloride, (–)-$Co(sep)Cl_3$ or (+)-$Co(sep)Cl_3$ (sep = $C_{12}H_{30}N_8$ = 1,3,6,8,10,13,16,19-octaazabicyclo[6.6.6]-eicosane) *(34, 35, 36)* in 5 mL H_2O.

The *powder X-ray diffraction patterns (PXRD)* of the dry samples were recorded with a STOE Stadi P powder diffractometer (transmission geometry, $CuK_{\alpha 1}$ radiation (λ = 1.54056 Å), Ge monochromator, MYTHEN 1K detector).

Argon Adsorption Measurements were performed using a Quantachrome Autosorb 1 at Ar(l) temperature (87.35 K) with Ar employing samples pre-dried for 24 h at 100 °C in high vacuum. The pore sizes and volumes were calculated using a non-local DFT model (software version 2.11, Ar on zeolite/silica, cylindrical pores, equilibrium model) *(37)*. The volume-weighted mean micropore width corresponds to the point where the total pore volume in the micropore regime (< 2 nm) was half filled. The BET equation calculates the surface area of a monolayer adsorption and is applied to a linear part of the isotherm. This p/p_0 range is normally taken to lie between 0.1 and 0.3 but has to be adjusted to lower p/p_0 values for microporous materials. Recommendations suggested by Rouquerol were followed for choosing the appropriate range of the isotherm *(38)*.

TEM (transmission electron microscopy) micrographs were taken on a Zeiss EM922 Omega operating at 200 kV. For investigation of the silica platelets the sample was embedded in a resin (EpoTek 301) and 50 nm thin cuts were prepared with a Leica EM UC7 equipped with a diamond knife and deposited onto TEM grids (lacey carbon films, copper, 200 mesh).

The supernatant of the adsorption experiments was analysed by GC-FID on a Shimadzu GC-2010 equipped with a chiral Lipodex E column (25 m) under the following conditions: 0.5 µL injection volume, split 1:100, T_{inj} 250 °C, constant flow of hydrogen carrier gas (1.2 mL/min = 40 cm/s), T_{det} 250 °C; column temperature initially 40 °C (3 min) then raised to 120 °C (10 °C/min). Quantities of but-3-yn-2-ol in the individual samples were determined by external calibration. Enantiomers were identified and assigned by chromatographic comparison with authentic pure (+)- and (–)-but-3-yn-2-ol.

Adsorption experiments:

Adsorption of a mixture of 2-methyl-but-3-yn-2-ol and (±)*-but-3-yn-2-ol*. The MOPSs UBT-1 to UBT-4 pillared with (+)-$Co(sep)^{3+}$ were heated at 100 °C under high vacuum (10^{-6} bar) for 24 h, cooled and transferred to an argon glove box. There, three 10 mg samples of each MOPS were weighed into open Eppendorf plastic vials (1.5 mL) which were placed in a horizontally adjusted 50 mL Schlenk tube together with an open glass weighing tube containing 300 µL of a mixture

of 153 µL 2-methyl-but-3-yn-2-ol and 147 µL (±)-but-3-yn-2-ol to secure a saturated atmosphere with a molar ratio of 51.3:48.7. The Schlenk tube was stoppered and kept at 4 °C for 48 h. Then it was connected to an argon line and after removal of the 2-methyl-but-3-yn-2-ol / but-3-yn-2-ol source the sample vials were each treated with 500 µL of dry acetone p.a.. The vials were sealed, vortexed for 1 min, treated with a cooled ultrasonic bath for 30 min to desorb the alcohols from the inorganic material, and centrifuged.

Adsorption of (±)-*but-3-yn-2-ol*. The MOPSs UBT-1 to UBT-4 pillared with (+)-$Co(sep)^{3+}$ and UBT-5 to UBT-8 pillared with (-)-$Co(sep)^{3+}$ were heated at 100 °C under high vacuum (10^{-6} bar) for 24 h, cooled and transferred to an argon glove box. Three 10 mg samples of each MOPS were weighed into open Eppendorf plastic vials (1.5 mL) which were placed in a horizontally adjusted 50 mL Schlenk tube together with an open glass weighing tube containing 300 µL of (±)-but-3-yn-2-ol to secure a saturated atmosphere. The Schlenk tube was stoppered and kept at 4 °C for 48 h. Then it was connected to an argon line and after removal of the but-3-yn-2-ol source the sample vials were each treated with 500 µL of dry acetone p.a.. The vials were sealed, vortexed for 1 min, treated with a cooled ultrasonic bath for 30 min to desorb the but-3-yn-2-ol from the inorganic material, and centrifuged.

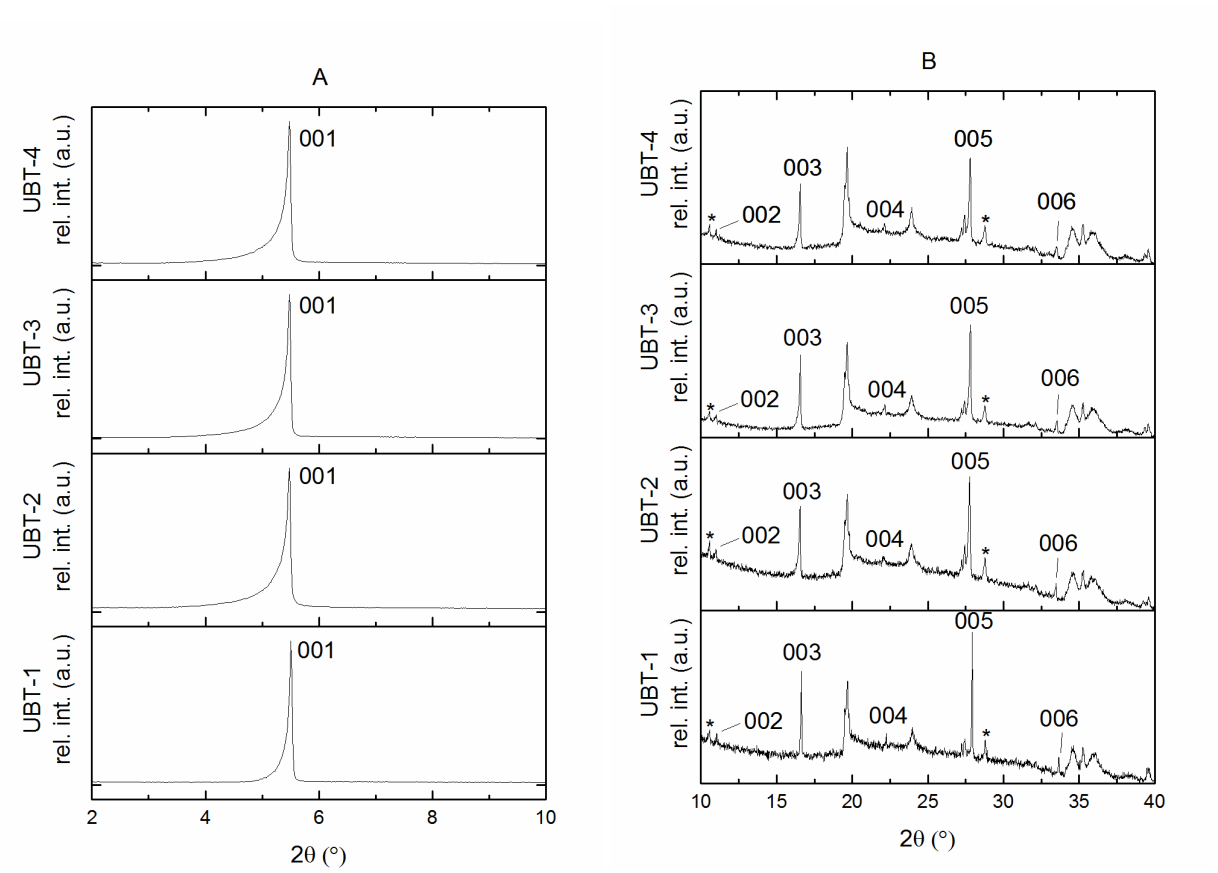

Fig. S1. Powder X-ray diffraction pattern of UBT-1 to UBT-4 from (A) 2-10° 2θ and (B) 10-40° 2θ; asterisks mark the protoamphibole sidephase.

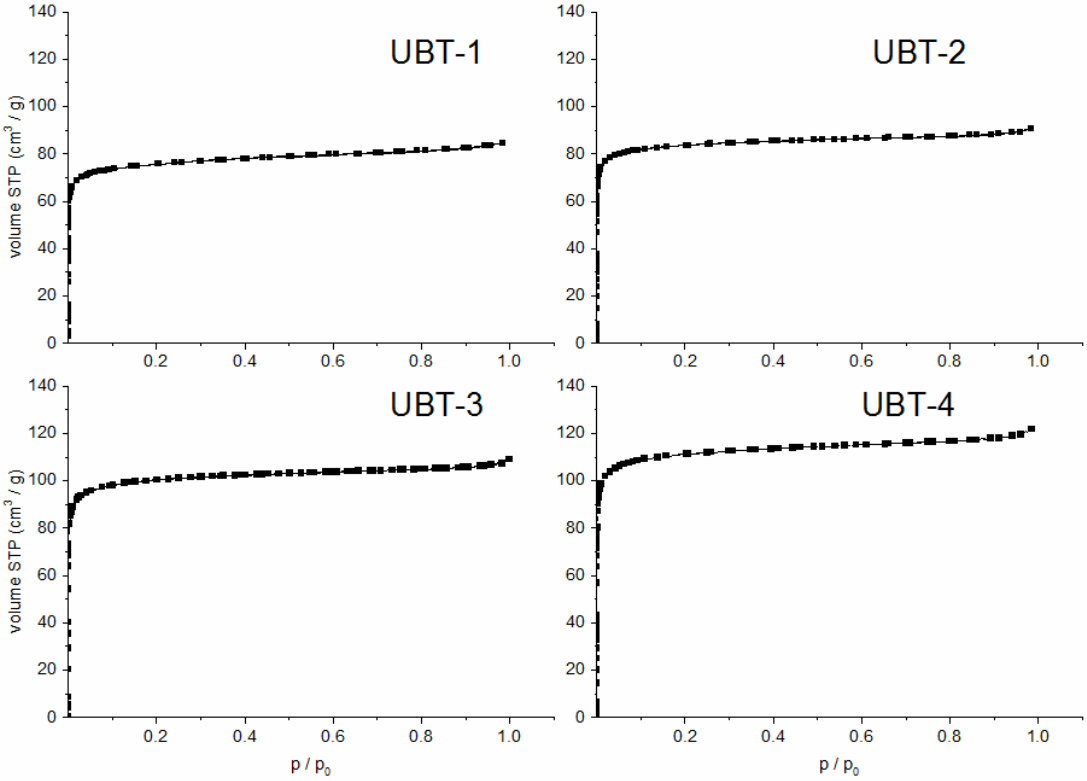

Fig. S2. Physisorption isotherms Ar/Ar(l) at 87.35 K for UBT-1 to UBT-4 (linear scale).

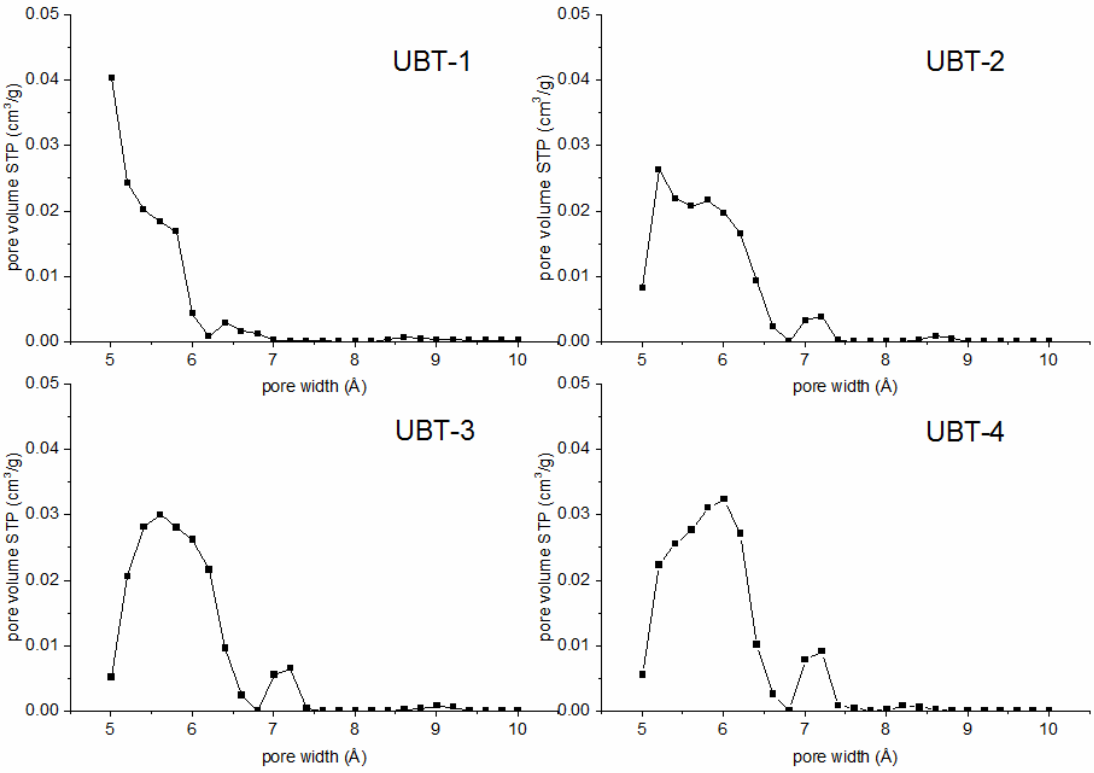

Fig. S3. Pore size distribution upon reducing the layer charge of UBT-1 to UBT-4.

Table S1. Measured values for Figure 4: Uptake of (±)-but-3-yn-2-ol by hectorites pillared with (+)-Co(sep) (UBT-1 to UBT-4) and enantiomeric excess.

	(±)-but-3-yn-2-ol (µL / 10 mg MOPS)	(*S*)-but-3-yn-2-ol (µL / 10 mg MOPS)	(*R*)-but-3-yn-2-ol (µL / 10 mg MOPS)	Enantiomeric excess (%)
UBT-1	1.733±0.014	0.797±0.012	0.937±0.017	7.45±0.45
UBT-2	2.243±0.019	1.109±0.020	1.134±0.018	0.54±0.31
UBT-3	2.459±0.049	1.223±0.050	1.236±0.048	-0.05±0.43
UBT-4	2.362±0.019	1.178±0.019	1.185±0.019	-0.31±0.31

Table S2: Measured values for Figure 4: Uptake of (±)-but-3-yn-2-ol by hectorites pillared with (-)-Co(sep) (UBT-5 to UBT-8) and enantiomeric excess.

	(±)-but-3-yn-2-ol (µL / 10 mg MOPS)	(*S*)-but-3-yn-2-ol (µL / 10 mg MOPS)	(*R*)-but-3-yn-2-ol (µL / 10 mg MOPS)	Enantiomeric excess (%)
UBT-5	1.689±0.044	0.919±0.046	0.770±0.041	8.24±0.48
UBT-6	2.088±0.016	1.062±0.015	1.026±0.017	1.10±0.44
UBT-7	2.279±0.044	1.152±0.044	1.126±0.044	0.55±0.37
UBT-8	2.272±0.046	1.143±0.046	1.128±0.047	0.05±0.38

Table S3: Measured values for Figure 4: Uptake of (±)-but-3-yn-2-ol and 2-methyl-but-3-yn-2-ol by UBT-1 to UBT-4.

	(±)-but-3-yn-2-ol (µL / 10 mg MOPS)	2-methyl-but-3-yn-2-ol (µL / 10 mg MOPS)	Molar Ratio *(rac)*-but-3-yn-2-ol / 2-methyl-but-3-yn-2-ol (%)
UBT-1	1.242±0.048	0.552±0.057	73.7±0.5 / 26.3±0.5
UBT-2	1.550±0.026	0.891±0.025	68.4±0.2 / 31.6±0.2
UBT-3	1.497±0.022	0.932±0.037	66.7±0.3 / 33.3±0.3
UBT-4	1.382±0.015	0.986±0.032	63.5±0.4 / 36.5±0.4
Gas Phase Composition			48.7±1.1 / 51.3±3.1

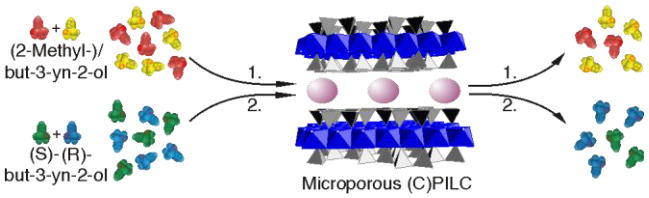

TOC

Appendix 5

Gate Opening in 2-D-ordered Microporous Organically Pillared Layered Silicates (MOPS) upon CO Adsorption

Markus M. Herling[1], Hiroshi Sato[2], Liangchun Li[2], Hussein Kalo[1], Ryotaro Matsuda[2,*], Susumu Kitagawa[2,*] and Josef Breu[1,*]

[1]Lehrstuhl für Anorganische Chemie I, Universität Bayreuth, Universitätsstr. 30, 95440 Bayreuth, Germany

[2]Institute for Integrated Cell-Material Sciences (WPI-iCeMs), Kyoto University, Kyoto 615-8510, Japan

*e-mail: rmatsuda@icems.kyoto-u.ac.jp, kitagawa@icems.kyoto-u.ac.jp, josef.breu@uni-bayreuth.de

To be submitted.

Gate Opening in 2-D-ordered Microporous Organically Pillared Layered Silicates (MOPS) upon CO Adsorption

Markus M. Herling[1], Hiroshi Sato[2], Liangchun Li[2], Hussein Kalo[1], Ryotaro Matsuda[2]*, Susumu Kitagawa[2]* and Josef Breu[1]*

[1]Chair of Inorganic Chemistry I, Universität Bayreuth, Universitätsstr. 30, 95440 Bayreuth, Germany

[2]Institute for Integrated Cell-Material Sciences (WPI-iCeMs), Kyoto University, Kyoto 615-8510, Japan

*e-mail: rmatsuda@icems.kyoto-u.ac.jp, kitagawa@icems.kyoto-u.ac.jp, josef.breu@uni-bayreuth.de

Abstract

By introducing the ellipsoidally shaped Me_2DABCO^{2+} molecule into the interlayer space of a layered silicate a two dimensional microporous network with narrow pore size distribution is generated. The regular arrangement of the pillar molecules in UBT-9 was confirmed by the occurrence of a *10*-band of hexagonal superstructure of pillar molecules in the interlamellar space. Upon CO adsorption, at a certain gate pressure the height of the interlayer space of UBT-9 is expanded and by this the pore volume is extended allowing for accommodation of additional gas molecules. The selective nature of the gate opening may be used for separation of CO and N_2 by pressure swing adsorption.

Keywords: microporous material, rational synthesis, gate opening, microporous network, CO adsorption, gas separation

Introduction

The class of microporous materials was initially prevailed by zeolites with purely inorganic frameworks. Zeolites exhibit narrow pore size distributions and large surface areas concomitantly with superb stabilities in respect to temperature and hydrolysis.[1-5] The class of microporous hybrid materials in turn was dominated by porous coordination polymers (PCPs) while more recently it was supplemented by the largely unnoticed class of microporous organically pillared layered silicates (MOPS).[6-12]

Their framework and pore systems topology renders PCPs highly interesting for a variety of potential applications.[13-20] While for both zeolites and PCPs the framework is built by covalent bond, there is no rigid linkage between the sheets of the 2:1 layered silicates in MOPS and the pillars are rather held in place by non-directional electrostatic interactions.[21] For this reason the charge density of the host must be homogenous to obtain narrow pore size distributions. Given this requirement is met, in turn the two-dimensional pore system of MOPS can be fine tuned by adjusting the layer charge of the layered silicate host and the charge, size and shape of the pillar resulting in a microporous material with a narrow pore size distribution.[6;8;22] MOPS are thermally and hydrolytically stable as the stability is only limited by the stability of the pillars and is typically above 250 °C.

Three-dimensional frameworks constructed by interpenetration and interdigitation are characteristic of PCPs and render the framework dynamic. Adsorption of guest molecules gives rise to structural transformations through slipping motions of the interpenetrated layers. The breathing and gate opening motions are observed at characteristic pressures for different gases and allow for gas separation.

In this respect separation of carbon monoxide and nitrogen is industrially important. In many large scale industrial oxidation processes CO is produced, which has to be separated from N_2 for chemical processing. This separation process is demanding due to the similar physical properties of both gases. CO is mainly used for the synthesis of different carbon-based products like plastics, medicines and carbon fibers.[23-26] For separation of CO a highly selective but nevertheless reversible adsorption is needed. To date CO is mostly separated by chemisorption on transition metal ions like Cu^+ that, however, requires a cost intensive, high temperature release of CO.[27] Sato *et al*. recently reported a self-accelerating CO sorption in a soft nanoporous material with selective CO adsorption on a Cu^{2+}-PCP.[28] The high selectivity was attributed to a synergetic effect of local bonding interaction between CO and accessible metal sites and a global transformation of the framework.

The electrostatic attraction between negative silicate host and positively charged pillars in the interlayer space will in any case thrive to minimize the basal spacing.[29] Ellipsoidal pillars will

therefore arrange with their longer principal axis oriented in the plane of the interlayer space. Upon adsorption of gases into MOPS the pillars might erect resembling the responsive transformation in PCP's.[30-36]

We present herein a MOPS (UBT-9) that has been pillared with Me_2DABCO^{2+} to yield a reversibly expandable pore system towards CO uptake. Upon CO adsorption, at a certain gate pressure the height of the interlayer space of UBT-9 is expanded and by this the pore volume is extended allowing for accommodation of additional gas molecules. The selective nature of the gate opening may be used for separation of CO and N_2 by pressure swing adsorption.

Results & Discussion

A synthetic sodium hectorite with a homogeneous charge density ($Na_{0.94(6)}[Mg_{5.18(10)}Li_{0.34(6)}]Si_8O_{20}F_4$)[22] was pillared with 1,4-Dimethly-1,4-diazabicyclo [2.2.2]octane (Me_2DABCO^{2+}) to obtain the microporous hybrid material (MOPS) UBT-9 with a narrow pore size distribution and micropores between 4-6 Å (Figure S2, S3). The X-ray diffraction pattern of UBT-9 shows a rational *00l*-series with a d-value of 13.9(1) Å indicating a strictly uniform height of the interlamellar space. Aside the *00l* series a superstructure reflex at 9.1 Å (*10*-hk band) is observed (Figure 1, S1). The λ-shape is typical for two-dimensional interference[10;37] and can be indexed with a hexagonal cell of a = 10.49 Å (Figure 1, inset). The occurrence of the *10*-band is indicative of a two dimensional long range ordering of pillars in the plane of the interlayer space. The hexagonal arrangement of the pillar molecules arises from cation-cation repulsion that maximizes the inter-pillar distance. Adjacent interlayers have no fixed phase relationship limiting the interference to two dimensions. The uniform height in combination with a two-dimensional long range order of the pillars assures the well defined micropore space resulting in a narrow pore size distribution as determined by Ar physisorption analysis (Figure S2).

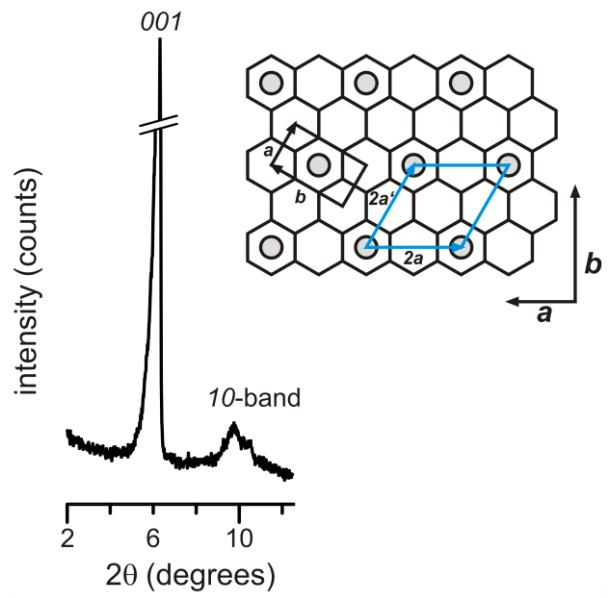

Figure 1. X-ray diffraction pattern of dry UBT-9 with the *001*-reflection and the *10*-band of the superlattice of pillars. Inset: Scheme of the *2a* × *2a'* superlattice of the pillars.

Given unit cell dimensions of the host material of $a \times b = 47.65$ Å^2 [38] and a layer charge of 0.94, a charge density of 50.70 Å^2/+ can be calculated. This is in very good agreement of the charge density of the hexagonal cell of the pillars of 47.62 Å^2/+.

The electrostatic attraction between the negative host and positive interlayer space tends to minimize the basal spacing.[29] Me_2DABCO^{2+} is a slightly ellipsoidal pillar that therefore initially will arrange with its longer principal axis oriented in the plane of the interlayer space resulting in a d-value of 13.9(1)Å. While the hectorite applied here to make UBT-9 shows planar defects that do not allow for a structure refinement, for a related, better ordered, mica-derived material an angle of 24° of the pillar relative to the host layer could be determined.[6] The height of the interlayer is obtained as 4.3 Å by substracting the thickness of the silicate layer of 9.6 Å from the basal spacing.[39] With this interlayer height and the inter-pillar distance fixed by the charge density of the host, an amount of 38 ml (STP) g^{-1} of CO is adsorbed at low partial pressures (Fig. 2). At this point the initial pore volume of UBT-9 is filled and the adsorption isotherm reaches a first plateau.

With increasing CO partial pressure at a certain threshold pressure, the adsorption enthalpy becomes large enough to render the free energy of adsorption again negative. At this point, the subtle balance of a positive term related to the expansion of the interlayer space against the Coulomb attraction and the negative adsorption term is shifted in favour of additional incorporation of CO in the microporous interlayer space.

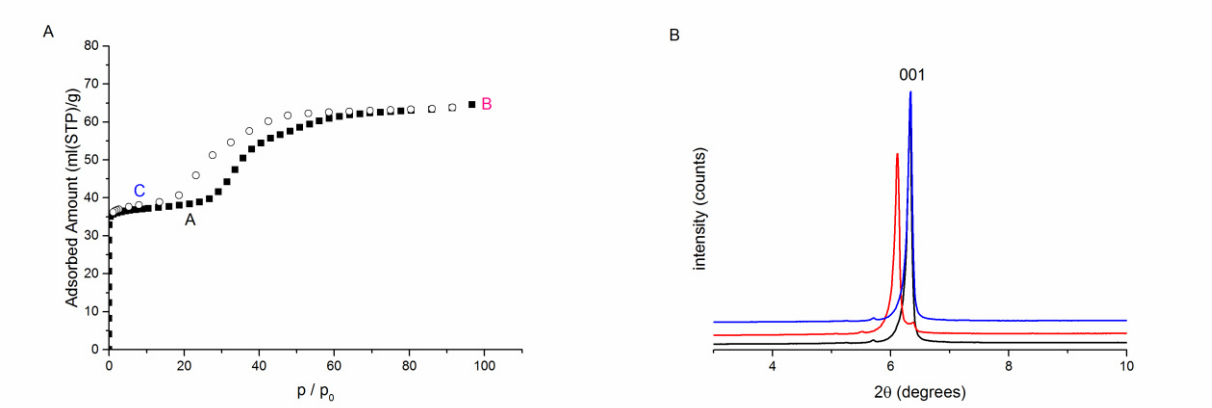

Figure 2. A) CO physisorption isotherm of UBT-9 at 82 K. Points A, B and C are correlated to the X-ray diffraction measurements. **B)** In-situ X-ray diffraction pattern of UBT-9 upon CO adsorption in the ranges of 3-10° 2θ.

In-situ X-ray diffraction measurements at point **A** to **B** of the isotherm showed an increase of the initial d_{001}-value of 13.95(10) Å to 14.44(10) Å upon the additional CO adsorption (Fig 2 B). The breathing of the interlayer space from 4.3 Å to 4.9 Å is fully reversible upon desorption (compare diffractograms recorded at point **B** to **C,** Figure 2 B, S4)). Although the stacking disorder does not allow to present experimental evidence, a concomitant reorientation of the ellipsoidal shaped Me_2DABCO^{2+} molecule inside the interlayer space appears most likely.

The volume increase per unit cell area is 47.65 $Å^2$ × 0.5(1) Å = 23.83 $Å^3$. Assuming that the packing density in the interlayer space does not change upon breathing and that the density of intercalated CO is comparable to solid CO. Experimentally, the adsorption capacity upon breathing increases by 70 % from 38 ml (STP) g^{-1} to 65 cm^3 (STP) g^{-1}.

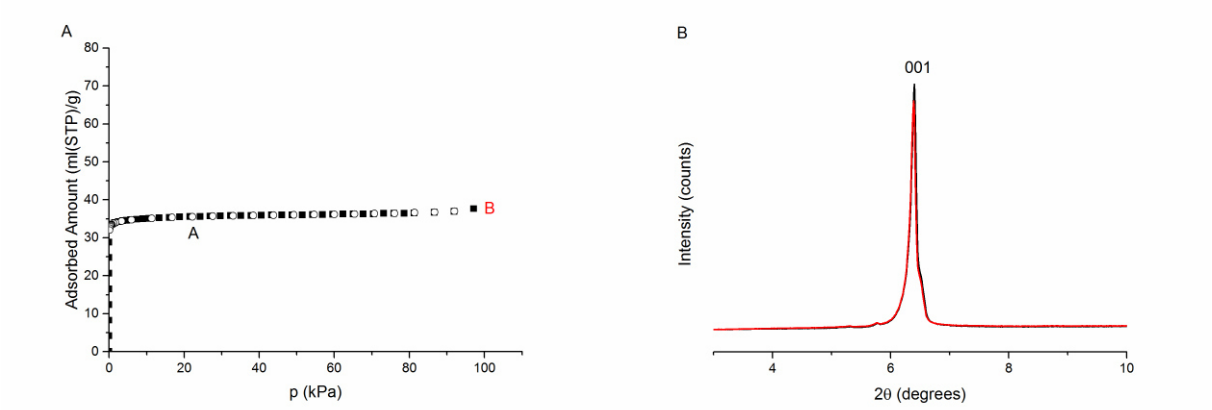

Figure 3. A) N_2 physisorption isotherm of UBT-9 at 77 K. Points A and B are correlated to the X-ray diffraction patterns. **B)** In-situ X-ray diffraction pattern of UBT-9 upon N_2 adsorption in the ranges of 3-10° 2θ.

Contrary to CO, the N_2 adsorption isotherm is exhibiting a normal type I adsorption behaviour (Figure 3, S5) and a total adsorbed amount of 38 cm^3 ml (STP) g^{-1}. Adsorption of N_2 is limited to filling the initial micropores but no gate opening is observed. This would suggest that in the pressure range studied the adsorption enthalpy of N_2 is insufficient to overcome the Coulomb

attraction. While for Cu^{2+}-PCP[28] the selectivity was attributed to a synergetic effect of local bonding interactions between CO and accessible metal sites and a global transformation of the framework, for UBT a synergism between non-directional Coulomb attraction between silicate layer and pillar and framework expansion would have to be postulated. In any case, the distinct adsorption behaviour can potentially be utilized for the separation of CO and N_2 by pressure swing adsorption.

Conclusion

Much similar to PCP frameworks constructed by interpenetration and interdigitation, the new class of microporous hybrid materials called MOPS shows breathing structures and gate opening effects. Moreover, gate opening is only observed for selected gases allowing for gas separation. The highly modular character of constructing MOPS should allow for fine-tuning the distinct adsorption isotherms by optimizing the charge density of the layered silicate and the shape anisotropy of the pillar. Pillaring itself is straight forward. Unfortunately, the required homogeneity of the charge density of the layered silicates asks for melt synthesis which might represent a certain barrier to the research field but the authors will be happy to provide synthetic hectorites on request.

Materials & Methods

Synthesis of UBT-9

The fluorohectorite $[Na_{0.47(3)}]^{inter}[Mg_{2.59(5)}Li_{0.17(3)}]^{oct}[Si_4]^{tet}O_{10}F_2$ used was synthesized via melt synthesis.[10, 40, 41] The high purity reagents (in total ~45 g) of SiO_2 (Merck, fine granular, calcined), MgF_2 (Chempur, 99.99%), MgO (Alfa Aesar 99.95%), Li_2SiO_3 (Alfa Aesar 99.95%), and Na_2O–$2SiO_2$-glass were weighed into a molybdenum crucible in an Ar atmosphere in accordance with a stoichiometric composition of $[Na_{0.6}]^{inter}[Mg_{2.6}Li_{0.2}\square]^{oct}[Si_4]^{tet}O_{10}F_2$ (target composition). Na_2O–$2SiO_2$-glass was produced by melting Na_2CO_3 (Aldrich, 99.9%) and SiO_2 (Merck, fine granular, calcined) in a 1:2 molar ratio at 1050 °C for 10 h to ensure complete release of carbon dioxide. The molybdenum crucible was sealed so as to be gas-tight using the procedure described elsewhere.[39] The crucible was heated in a graphite furnace (Graphit HT-1900, Linn High Therm) for the synthesis. To prevent inhomogeneity of the product owing to gravity segregation in the melt, the crucible was positioned horizontally in the furnace and rotated at 50 rpm. The crucible was heated from room temperature (RT) to 1750 °C (20 °C min^{-1}), left at 1750 °C for 1 h, then cooled to 1300 °C with a cooling rate of 50 °C min^{-1}, followed by a cooling rate of 10 °C min^{-1} from 1300 °C to 1050 °C, and finally it was quenched by switching off the power. The crucible was opened under an Ar atmosphere and the synthetic Sodium fluorohectorite was stored in a Glovebox.[42]

For pillaring, the hectorite (100 mg) was treated hydrothermally four times for 12 h at 120 °C using 30 mg of $Me_2DABCOCl_2$ in 15 mL H_2O.

X-ray diffraction measurements

Powder X-Ray Diffraction patterns (PXRD) of dry samples were recorded with a STOE Stadi P powder diffractometer (transmission geometry, $CuK_{\alpha 1}$ radiation ($\lambda = 1.54056$ Å), Ge monochromator, MYTHEN 1K detector) in a sealed capillary (Hilgenberg, diameter 0.5 mm).The samples were dried for 24 h at 120 °C in high vacuum (10^{-6} mbar).

Argon phyisorption measurements

Argon adsorption measurements were performed using a Quantachrome Autosorb 1 at Ar(l) temperature (87.35 K) with Ar employing samples dried for 24 h at 100 °C in high vacuum. The pore sizes and volumes were calculated using a non-local DFT model (software version 2.11, Ar on zeolite/silica, cylindrical pores, equilibrium model).

In-situ physisorption and X-ray diffraction measurements

The sorption isotherm measurements for N_2 (99.9999%) and CO (99.996%) were performed using an automatic volumetric adsorption apparatus (BELSORP-18PLUS or BELSORP-max; Bel Japan, Inc.) connected to a cryostat system. Those apparatuses were synchronized with each other and each PXRD pattern was obtained at each equilibrium point of the sorption isotherms.

A known weight (~100 mg) of the as-synthesized UBT-9 was placed on a copper plate, then, the sample was dried under high vacuum (below 10^{-2}Pa) at 120 °C for 12 h to remove the guest molecules.

Acknowledgements

This work was supported by the German Research Foundation (SFB 840).

References

[1] W. Schmidt, *ChemCatChem.* **2009**, *1*, 53-67.

[2] F. Schüth, *Annual Review of Materials Research* **2005**, *35*, 209-238.

[3] J. Weitkamp, *Solid State Ionics* **2000**, *131*, 175-188.

[4] S. Zones, *Microporous and Mesoporous Materials* **2011**, *144*, 1-8.

[5] A. Corma, *Journal of Catalysis* **2003**, *216*, 298-312.

[6] A. Baumgartner, K. Sattler, J.Thun, J. Breu, *Angewandte Chemie-International Edition* **2008**, *47*, 1640-1644.

[7] M. Stöcker, W. Seidl, J. Breu, *Zeitschrift für Anorganische und Allgemeine Chemie* **2006**, *632*, 2140.

[8] M. M. Herling, H. Kalo, S. Seibt, R. Schobert, J. Breu, *Langmuir* **2012**, *28*, 14713-14719.

[9] W. Seidl, J. Breu, *Zeitschrift für Kristallographie* **2005**, *220*, 169-176.

[10] M. Stöcker, L. Seyfarth, D. Hirsemann, J. Senker, J. Breu, *Applied Clay Science* **2010**, *48*, 146-153.

[11] M.Stöcker, W. Seidl, L.Seyfarth, J. Senker, J.Breu, *Chemical Communicatinos* **2008**, 629-631.

[12] M. M. Herling, J. Breu, *Zeitschrift für Anorganische und allgemeine Chemie* **2014**, *640*, 547-560.

[13] S. Kitagawa, R. Kitaura, S. Noro, *Angewandte Chemie – International Edition* **2004**, *43*, 2334-2375.

[14] O. M. Yaghi, M. O'Keeffe, N. W. Ockwig, H. K. Chae, M. Eddaoudi, J. Kim, *Nature* **2003**, *423*, 705-714.

[15] A. U. Czaja, N. Trukhan, U. Müller, *Chemical Society Reviews* **2009**, *38*, 1284-1293.

[16] J. R. Li, R. J. Kuppler, H. C. Zhou, *Chemical Society Reviews* **2009**, *38*, 1477-1504.

[17] L. Ma, C. Abney, W. Lin, *Chemical Society Reviews* **2009**, *38*, 1248- 1256.

[18] Y. Liu, W. Xuan, Y. Cui, *Adv. Mater.* **2010**, *22*, 4112-4135.

[19] S. Kitagawa, M. Kondo, *Bulletin of the Chemical Society of Japan* **1998**, *71*, 1739-1753.

[20] G. Ferey, C. Serre, *Chemical Society Reviews* **2009**, *38*, 1380-1399.

[21] M. Stöter, D. A. Kunz, M. Schmidt, D. Hirsemann, H. Kalo, B. Putz, J. Senker, J. Breu, *Langmuir* **2013**, *29*, 1280-1285.

[22] A. Baumgartner, F. E. Wagner, M. Herling, J. Breu, *Microporous and Mesoporous Materials* **2009**, *123*, 253-259.

[23] K. Weissermehl, H.-J. Arpe, *Industrial Organic Chemistry*, 5ed. Wiley-VCH, Weinheim **2008**.

[24] A. Haynes, *Advances in Catalysis* **2010**, *53*, 1-45.

[25] K. C. Waugh, *Catalysis Today* **1992**, *15*, 51-75.

[26] F. E. Paulik and J. F. Roth, *Chemical Communications* **1968**, 1578.

[27] J. A. Hogendoorn, W. P. M. Vanswaaij, G. F. Versteeg, *Chemical Engineering Journal and the Biochemical Engineering Journal* **1995**, *59*, 243-252.

[28] H. Sato, W. Kosaka, R. Matsuda, A. Hori, Y. Hijikata, R. V. Belosludov, S. Sakaki, M. Takata, S. Kitagawa, *Science* **2014**, *343*, 167-170.

[29] J. Breu, C. R. A. Catlow, *Inorganic Chemistry* **1995**, *34*, 4504-4510.

[30] L. C. Tabares, J. A. R. Navarro, J. M. Salas, *J. Am. Chem. Soc.* **2001**, *123*, 383-387.

[31] G. J. Halder, C. J. Kepert, B. Moubaraki, K. S. Murray, J. D. Cashion, *Science* **2002**, *298*, 1762-1765.

[32] R. Kitaura, K. Seki, G. Akiyama, S. Kitagawa, *Angewandte Chemie – International Edition* **2003**, *42*, 428-431.

[33] C. Serre, C. Mellot-Draznieks, S. Surble, N. Audebrand, Y. Filinchuk, G. Ferey, *Science* **2007**, *315*, 1828-1831.

[34] D. Bradshaw, J. E. Warren, M. J. Rosseinsky, *Science* **2007**, *315*, 977-980.

[35] B. D. Chandler, G. D. Enright, K. A. Udachin, S. Pawsey, J. A. Ripmeester, D. T. Cramb, G. K. Shimizu, *Nature Materials* **2008**, *7*, 229-235.

[36] J. Rabone, Y. Yue, S. Chong, K. Stylianou, J. Bacsa, D. Bradshaw, G. Darling, N. Berry, Y. Khimyak, A. Ganin, P. Wiper, J. Claridge, M. Rosseinsky, *Science* **2010**, *329*, 1053-1057.

[37] J. Breu, A. Stoll, K. G. Lange, T. Probst, *Physical Chemistry Chemical Physics* **2001**, *3*, 1232-1235.

[38] H. Kalo, W. Milius, J. Breu, RSC Advances 2012, 2, 8452-8459.

[39] J. Breu, W. Seidl, A. J. Stoll, K. G. Lange, T. U. Probst, *Chem. Mater.* **2001**, *13*, 4213-4220.

[40] H. Kalo, M. W. Möller, M. Ziadeh, D. Dolej, J. Breu, *Appl. Clay Sci.* **2010**, *48*, 39-45.

[41] K. Kitajama, F. Koyama, N. Takusagawa, *Bull. Chem. Soc. Jpn.* **1985**, *58*, 1325-1326.

[42] M. M. Herling, M. Schwedes, S. Seibt, H. Kalo, U. Lacher, R. Schobert, J. Breu, *submitted* **2014**.

Supporting Information

Gate Opening in 2-D-ordered Microporous Organically Pillared Layered Silicates (MOPS) upon CO Adsorption

Markus M. Herling[1], Hiroshi Sato[2], Liangchun Li[2], Hussein Kalo[1], Ryotaro Matsuda[2]*, Susumu Kitagawa[2]* and Josef Breu[1]*

[1]Chair of Inorganic Chemistry I, Universität Bayreuth, Universitätsstr. 30, 95440 Bayreuth, Germany

[2]Institute for Integrated Cell-Material Sciences (WPI-iCeMs), Kyoto University, Kyoto 615-8510, Japan

*e-mail: rmatsuda@icems.kyoto-u.ac.jp, kitagawa@icems.kyoto-u.ac.jp, josef.breu@uni-bayreuth.de

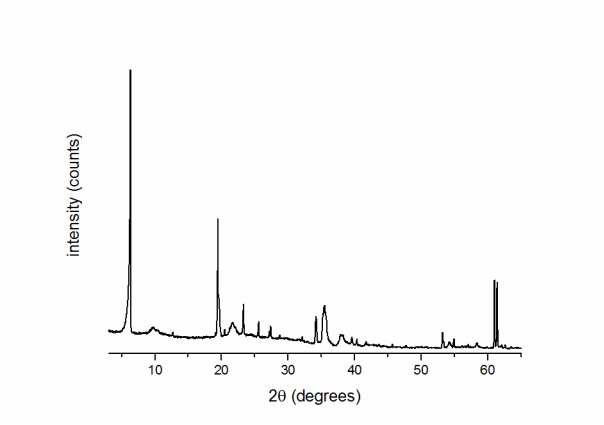

Figure S1. X-ray diffraction pattern of dry UBT-9.

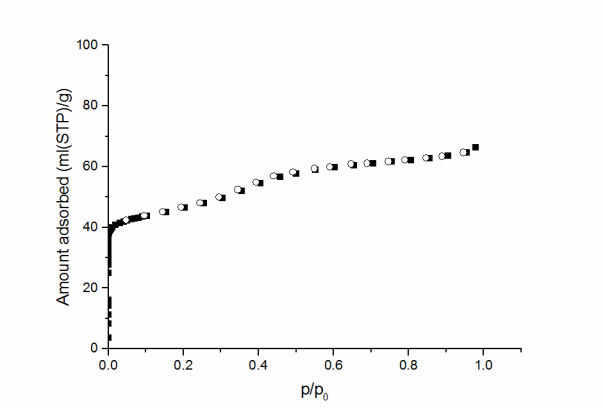

Figure S2: Ar physisorption isotherm of UBT-9 at 87.3K.

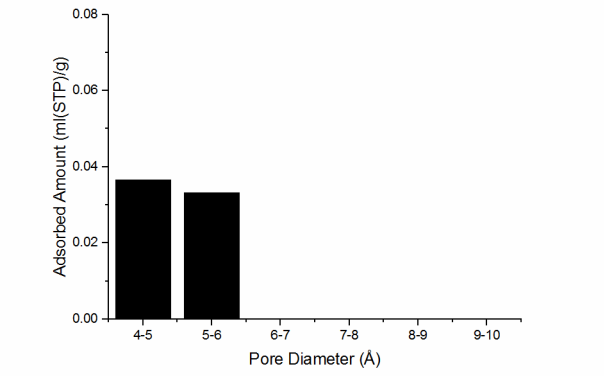

Figure S3: Pore size histogram of UBT-9.

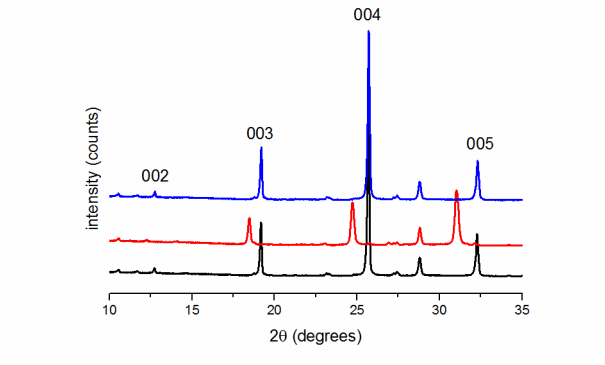

Figure S4. In-situ X-ray diffraction patter of UBT-9 upon CO adsorption in the ranges of 10-35° 2θ showing the *00l*-series at point A (black), B (red) and C (blue).

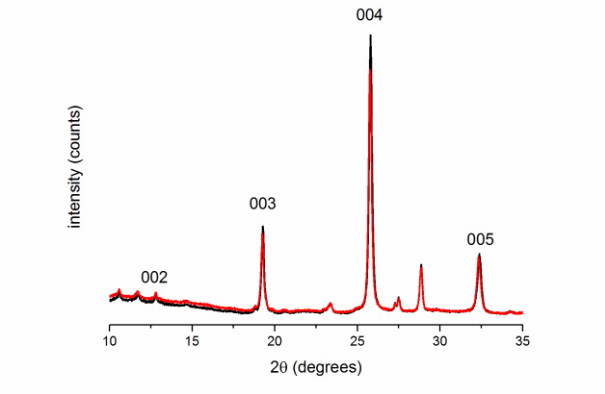

Figure S5. In-situ X-ray diffraction pattern of UBT-9 upon N_2 adsorption in the ranges of 10-35° 2θ showing the *00l*-series at point A (black) and B (red).

7. Manuskripte und Konferenzbeiträge

Manuskripte

- "Gate Opening in 2D-ordered Microporous Organically Pillared Layered Silicates (MOPS) upon CO Adsorption

  Markus M. Herling, Hiroshi Sato, Liangchun Li, Hussein Kalo, Ryotaro Matsuda, Susumu Kitagawa, Josef Breu, *to be submitted*.

- "MOPS – A New Class of Stereo and Size Selective Class of Microporous Hybrid Materials"

  Markus M. Herling, Mathias Schwedes, Sebastian Seibt, Hussein Kalo, Ulrike Lacher, Rainer Schobert, Josef Breu, *to be submitted*.

- "Biomimetic Morphological Polymer Analogs of Natural Sponges

  Gaigai Duan, Shaohua Jiang, Amir Fathi, Jacqueline Uhm Volker Altstädt, **Markus Herling**, Josef Breu, Valerie Jerome, Ruth Freitag, Joachim H. Wendorff, Seema Agarwal, Andreas Greiner, *submitted*.

- "The Largely Unknown Class of Microporous Hybrid Materials: Clays Pillared by Molecules"

  Markus M. Herling, Josef Breu; *Zeitschrift für anorganische und allgemeine Chemie* **2013**, accepted for publication.

- "Porosity of Pillared Clays Studied by Hyperpolarized ^{129}Xe NMR Spectroscopy and Xe Adsorption Isotherms"

  Caroline D. Keenan, **Markus M. Herling**, Renee Seigel, Ernst A. Rössler, Josef Breu, Jürgen Senker; *Langmuir* **2013**, 29, 642-652.

- "Tailoring the Pore Sizes of Microporous Pillared Interlayered Clays through Layer Charge Reduction"

  Markus M. Herling, Hussein Kalo, Sebastian Seibt, Rainer Schobert, Josef Breu; *Langmuir* **2012**, 28, 14713-14719.

- "Towards a tunable pore size utilizing oxidative pillaring of the mica ferrous tainiolite"

  Alexander Baumgartner, Fritz E. Wagner, **Markus Herling**, Josef Breu; *Microporous and Mesoporous Materials* **2009**, 123, 253-259.

Konferenzen

- "MOPS – A New Class of Functional Hybrid Materials" - **Poster**

  Markus M. Herling, Mathias Schwedes, Rainer Schobert, Josef Breu;

  17. Vortragstagung Fachgruppe Festkörperchemie und Materialforschung der GDCh **2014**, Dresden.

- "Adjusting the pore sizes of PILCs" - **Poster**

  Markus M. Herling, Hussein Kalo, Sebastian Seibt, Rainer Schobert, Josef Breu;

  16. Vortragstagung Fachgruppe Festkörperchemie und Materialforschung der GDCh **2012**, Darmstadt.

- "Gas Sensitivity of Pillared and Non-pillared Layered Silicates" - **Poster**

  Markus Herling, Gunter Hagen, Ralf Moos, Josef Breu;

  15. Vortragstagung Fachgruppe Festkörperchemie und Materialforschung der GDCh **2010**, Berlin.

8. Danksagung

Am Ende meiner Dissertation und meiner Zeit in Bayreuth möchte ich mich bei allen bedanken, die einen wertvollen Beitrag zum Erfolg meiner Arbeit geleistet und mich stets unterstützt haben.

Mein besonderer Dank gilt meinem Doktorvater und Betreuer Prof. Dr. Josef Breu für die Bereitstellung des sehr interessanten Themas und das in mich gesetzte Vertrauen. Er unterstütze mich bei auftretenden Fragestellungen, die gemeinsamen intensiv und lösungsorientiert diskutiert wurden. Ich möchte mich bei Ihm auch sehr für die Möglichkeiten des Auslandsaufenthaltes an der Kyoto University in Japan, die Teilnahme an verschiedenen Tagungen und die schöne und prägende Zeit am Lehrstuhl bedanken.

An dieser Stelle möchte ich mich auch bei Prof. Dr. Jürgen Senker und Prof. Dr. Rainer Schobert für die gute Zusammenarbeit und aufschlussreichen Diskussionen bedanken. Auch Dr. Yamini Avadhut und Dr. Ulrike Lacher möchte ich für die Zusammenarbeit danken.

Mein Dank gilt auch Prof. Dr. Susumu Kitagawa, Dr. Ryotaro Matsuda und Dr. Hiroshi Sato für Ihre Gastfreundlichkeit und Hilfsbereitschaft während meines Auslandsaufenthaltes. Auch vielen Dank an Dr. Hyung Joon Jeon, Dr. Prakash Kanoo, Dr. Liangchun Li, Dr. Yongtai Zheng, Dr. Maw Lin Foo und Kiyo Yamashita für die schöne und interessante Zeit in Kyoto.

Weiterhin möchte ich mich bei allen Kollegen und Freunden des Lehrstuhls AC I, AC III und OC I für die schöne Zeit bedanken. Besonders danke ich meinen Laborkollegen Sebastian Koch, Beate Bojer, Sonja Lutschinger und Bernd Putz für die sehr gute und amüsante Atmosphäre im Labor. Ein herzlicher Dank gilt auch Herrn. Dr. Wolfgang Milius für das stets offene Ohr und seine Unterstützung bei Fragen aller Art.

Vielen Dank auch an alle meine Praktikanten und meinen Bachelorstudenten Martin Riess für die erfolgreiche Zusammenarbeit.

Mein Dank gilt auch Lena Geiling und Nadine Popp für die gegenseitige Unterstützung bei der Planung und Durchführung der Physisorptionsmessungen. Auch den Sekretärinnen Petra Seidl, Iris Raithel und Sieglinde Hörath danke ich für die Unterstützung bei bürokratischen Problemen und das Ausfüllen unendlicher Formulare.

Hubert Schulze und Detlef Krauße möchte ich für die Vorbereitung der WDX-Proben und deren Messung danken.

Mein Dank gilt auch meinen Mitstreitern und Freunden aus dem Studium für die unvergessliche und tolle Zeit in Bayreuth.

Ich möchte mich auch bei den Gründungsmitgliedern des JCF Bayreuth bedanken, ohne die es nicht möglich gewesen wäre so etwas auf die Beine zu stellen. Vielen Dank für das Vertrauen und die schönen, gemeinsamen Events. Macht weiter so!!

Auch möchte ich mich beim CSG e.V. für das entgegengebrachte Vertrauen das Amt des Kassenwarts zu übernehmen, den sehr guten Zusammenhalt und die zahlreichen und gelungenen Events bedanken.

Ich bedanke mich bei meinen Eltern Willi und Christel und meiner Schwester Anja für das in mich gesetzte Vertrauen und die Unterstützung während meiner Ausbildung.

Von ganzen Herzen danke ich meiner Freundin Aniela für die Unterstützung bei allen Höhen und Tiefen der letzten 5 Jahre.

Erklärung des Verfassers

(§ 8 S. 2 Nr. 6 PromO)

Hiermit erkläre ich mich damit einverstanden, dass die elektronische Fassung meiner Dissertation unter der Wahrung meiner Urheberrechte und des Datenschutzes einer gesonderten Überprüfung hinsichtlich der eigenständigen Anfertigung der Dissertation unterzogen werden kann

(§ 8 S. 2 Nr. 8 PromO)

Hiermit erkläre ich eidesstattlich, dass ich die Dissertation selbstständig verfasst und keine anderen als die von mir angegebenen Quellen und Hilfsmittel benutzt habe.

(§ 8 S. 2 Nr. 9 PromO)

Ich habe die Dissertation nicht bereits zur Erlangung eines akademischen Grades anderweitig eingereicht und habe auch nicht bereits diese oder eine gleichartige Doktorprüfung endgültig nicht bestanden.

(§ 8 S. 2 Nr. 10)

Hiermit erkläre ich, dass ich keine Hilfe von gewerblichen Promotionsberatern bzw. –vermittlern in Anspruch genommen habe und auch künftig nicht nehmen werde.

_____

Ort, Datum Markus M. Herling